Fabrication and Properties Evaluation of VGCFs/Mg-Al-Ca Composites

(VGCFs/Mg-Al-Ca 複合材料の作製及び特性評価)

July 2017

姚　友強

Department of Mechanical Science and Engineering
Graduate School of Engineering
Hiroshima University, Japan

Fabrication and Properties Evaluation of VGCFs/Mg-Al-Ca Composites

（VGCFs/Mg-Al-Ca 複合材料の作製及び特性評価）

July 2017

Youqiang Yao

CONTENTS

List of Figures

List of Tables

Chapter 1

Background and Objective

1.1 Introduction

Magnesium, one of the most promising lightweight materials, offers a very high specific strength among conventional engineering alloys and possess excellent castability, superior machinability, and good damping capacity. Magnesium alloys have made significant inroads in automotive interior and other room- or near-room-temperature applications in the last decade. The most visible magnesium applications have been instrument panel beams, transfer cases, valve/cam covers, steering components, and various housings and brackets. However, compared to other structural metals, magnesium alloys have a relatively limited high strength, especially at elevated temperatures, and flammability, which limited their wide range of applications. To cover the deficiencies in mechanical properties of magnesium, efforts have been made to develop flame resisting magnesium alloys, and magnesium matrix composites are prospecting candidates due to their promising superior properties.

Magnesium matrix composites refer to a kind of material consisting of reinforcement and magnesium matrix, which combine metallic properties of magnesium (low density, ductility, and damping capacity) with characteristics of reinforcement (high strength, high modulus, and wear resistance), leading to greater strength and higher service temperature capabilities. Thus, magnesium matrix composites exhibit multiple properties, and became attractive candidates for structural and functional materials.

Mg-Al-Ca alloys have been developed as flame resistant magnesium alloys. Calcium addition significantly improves the high temperature strength, creep resistance and oxidation resistances. Vapor grown carbon fibers (VGCFs) possess attractive mechanical, electrical, and thermal properties with similar carbon structure to carbon nanotubes. VGCFs have attracted much attention in various fields, and have been particularly considered as an ideal candidate for reinforcement in multifunctional composites and engineering applications. Therefore, VGCFs reinforced Mg-Al-Ca alloy composites are supposed to possess satisfactory mechanical properties at both room and elevated temperature.

1.2 Development of magnesium alloys

The compelling need for lightweight, energy-efficient, environmentally benign engineering systems is driving the development of a wide range of structural and functional materials for energy generation, energy storage, propulsion, and transportation [1]. Magnesium is attractive for lightweight structural systems and, most notably, automotive systems [2, 3]. With the lowest density of all metallic constructional materials, magnesium alloys possess high specific strength, good castability, superior machinability and good damping capacity. Compared with polymeric materials, they have better mechanical properties, ageing resistance and recyclability. However, the disadvantages of magnesium have limited its wide range of applications [1, 4], such as flammability, low temperature plasticity, limited high strength and creep resistance at elevated temperatures and limited corrosion resistance in some applications. Recently, the demand for lightweight, energy-efficient materials has promoted the development of magnesium alloys. Fig. 1-1 shows the different trends in alloy development depending on the main requirement [4].

Currently, the most widely used magnesium alloys are based on the Mg-Al system, such as, AZ91 and AM60 [5, 6]. The Mg–Al alloys are readily castable, particularly by high-pressure die casting, and exhibit good mechanical properties at room temperature and adequate corrosion resistance. Ternary alloys with zinc, manganese, silicon, calcium, and rare-earth elements in addition to aluminum are used to obtain improved mechanical properties. Fig. 1-1 shows further development of Mg–Al. Zinc is added to improve the room temperature strength and fluidity. Addition of manganese is required to control the corrosion behavior, and magnesium alloys with aluminum and manganese (AM60) are commonly used for components where good ductility and impact strength are required. Silicon, calcium, and rare-earth elements are added to improve the creep strength of the alloys by forming intermetallic compounds on the grain boundaries. Mg–Li–X is a development of super light alloys. Addition of Li causes a useful phase change to bcc, which decreases strength but increases ductility.

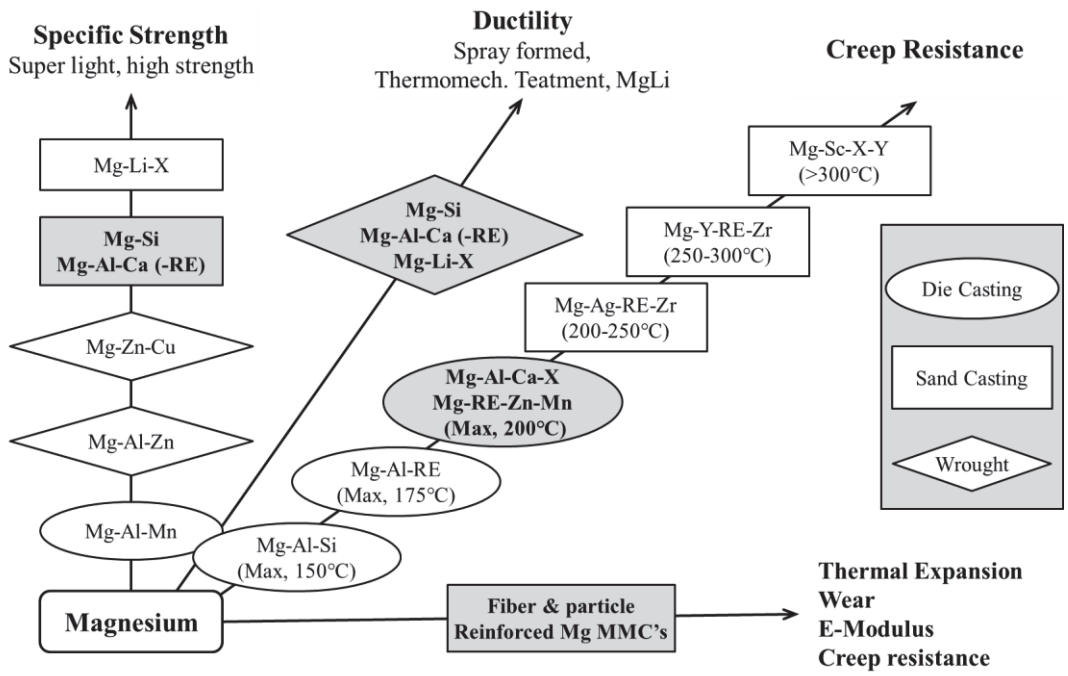

Fig. 1-1 Directions of magnesium alloy development [4].

1.2.1 Creep-resistant magnesium alloys

At temperatures above 125 ℃, Mg-Al alloys undergo excessive creep deformation even at moderate stress levels, which makes them not suitable for use at elevated temperatures [7, 8]. Both diffusion controlled dislocation climb and grain boundary sliding are reported mechanisms for creep in magnesium alloys, depending upon the alloy system, microstructure, and stress and temperature regimes [9]. The poor creep resistance of Mg-Al alloys is generally considered to be associated with the formation of the $Mg_{17}Al_{12}$ phase. The poor thermal stability of $Mg_{17}Al_{12}$ phase and its discontinuous precipitation can result in substantial grain boundary sliding at elevated temperatures. The accelerated diffusion of aluminum solute in magnesium matrix and the self-diffusion of magnesium at elevated temperature can also contribute to creep deformation in Mg-Al based alloys. Possible approaches to improving creep resistance in magnesium alloys include: suppressing the formation of $Mg_{17}Al_{12}$ phase; pinning grain boundary sliding; and slowing diffusion in the magnesium matrix.

There have been considerable efforts directed toward improving the creep resistance

of Mg-Al alloys based on the above principles. A number of special alloys have therefore been developed such as Mg-Al-Ca [10], Mg-Re-Zn-Mn [11] and Mg-Y-Re-Zr [12] alloys. These alloys have additional alloying elements that form either high melting point intermetallic compounds with Al to suppress the formation of $Mg_{17}Al_{12}$ (elements such as Ca, RE, and Sr), or high melting point intermetallic compounds with Mg (elements including RE, Si, and Sn), or strengthening precipitates (elements such as Ca and Nd). Rare earth elements such as yttrium, lanthanum, cerium, and neodymium can improve the structure and properties of cast Mg alloys but substantially increase alloy cost. With additions of Al and Ca to magnesium, an intermetallic C36 Laves-type phase forms during solidification. The unusual combination of mechanical and physical properties resulting from the low-cost Ca additions make the Mg-Al-Ca alloys promising for a variety of lightweight, high-temperature automotive powertrain components produced by die casting.

1.2.2 Mg-Al-Ca alloys

The developed magnesium alloys which contain calcium, strontium, RE, and silicon offer varying degrees of improvement in creep resistance and different combinations of other properties. Calcium is a promising elemental addition to develop Mg–Al alloys for high-temperature applications. Flame-resistant and noncombustible Mg alloys have also been developed by adding Ca to Mg alloys, and these materials have received flame-resistance and noncombustion certifications in the rail, aerospace, and construction sectors.

The Calcium addition encourages the formation of Ca-containing thermally stable intermetallic compounds and suppresses the formation of unstable β-$Mg_{17}Al_{12}$, which improves the flame resistance, high temperature strength, creep resistance, and oxidation resistances. [10, 13-15] Die-sticking and hot cracking were problems that prevented practical use of Ca-containing based alloys. Since then, several investigations have been directed to develop new Ca-containing magnesium alloys for elevated-temperature applications. Ninomiya et al.[13] found out that, for the Ca/Al ratios of less than 0.8, Al_2Ca is the only phase that would be formed in the Mg–Al alloys after Ca additions. Higher values of Ca, would lead to the formation of both Mg_2Ca and Al_2Ca

in the microstructure. Another research by Luo et al. [10] on the microstructure and creep properties of die-cast Mg–5Al–2Ca and Mg–5Al–3Ca showed that the second phase $(Mg, Al)_2Ca$ can be formed, even though the Ca/Al ratio is lower than 0.8. The study of solidification path in the Mg–Al–Ca ternary system indicates that in most of the commercially available Mg–Al–Ca alloys, the second phase $(Mg, Al)_2Ca$ with C36 structure is formed [16]. It has been further shown that this phase, after prolonged exposures to elevated temperatures, would transform to Al_2Ca with C15 structure through a shear-assisted transformation. Computational thermodynamics and experimental investigations have shown that Al_2Ca with a C15 structure is stable in the equilibrium condition.

Some studies have been focus on the tensile property and creep resistance of Mg-Al-Ca-based alloys. The mechanical properties of Mg–Al–Ca alloys are summarized and listed in Tab. 1-1. Luo et al. [9, 10] indicated that compared with the baseline AM50 alloy, the tensile strength and creep strength of Mg-Al-Ca alloys are significantly improved, which is due to the strengthening effect of $(Mg, Al)_2Ca$ phase in the microstructure. The tensile yield strength of Mg–Al–Ca alloys increases with increasing Ca content at room and elevated temperatures (175°C) due to solute and grain boundary strengthening. The studies by Terada et al. [17] on the creep properties of AM50 alloy with Ca additions have shown that the high melting point and eutectic temperatures along with semi-coherent interface of the second phases with Mg grains in these Ca-containing Mg–Al alloys are the main reasons for their enhanced thermal stability and creep resistance. With the Ca addition, the tensile strength and elongation of AZ91magnesium alloy at ambient temperature are reduced, whereas Ca addition confers elevated temperature strengthening on AZ91 magnesium alloy. The tensile strength at 150 °C increases with increasing Ca content. The impact toughness of AZ91magnesium alloy increases, and then declines as the Ca content increases [18]. The tendency of the alloy to form hot tearing substantially increased with Ca content rise from 0 to 1 wt.%. The ultimate tensile strength and relative elongation worsened, while the yield strength improved. The grain refinement of AZD91 alloy with Ca additions could be explained by the restriction of the grain growth induced by Ca aggregations on the boundaries. From the other side, the thermally stable phase Al_2Ca can lead to a

higher brittleness of the alloy [19]. Masoumi et al. [20] reveal that the presence of (Al, Mg)$_2$Ca phase are the main cause of the intergranular fracture for squeeze cast magnesium Mg–Al–Ca alloy. The coarse (Mg, Al)$_2$Ca compound is more brittle and easily broken than the fine Mg$_2$Ca compound [15]. By hot extrusion, Mg–Al–Ca alloys show high UTS and elongation. Application of hot extrusion has a significant effect on refining grain size, cracking secondary phase and improving their distribution. The large secondary phases along grain boundaries in the as-cast alloys disappear, which are instead by the fine spherical secondary phases dispersedly distributed along the extrusion direction. The UTS, elongation and strain hardening rate of the as-extruded alloys increased with higher Ca addition. [21] Watanabe et al. [22] found out that, by hot extrusion, the ductility of Mg-6Al-2Ca alloy at room temperature was high compared with other magnesium alloys containing Ca. The ductility was enhanced at elevated temperature, and climb controlled dislocation creep could be a dominant deformation process. Jing et al. [23] indicated that hot extrusion results in significant increase of tensile properties for AJC421 (Mg–4Al–2Sr–1Ca) alloy at ambient and elevated temperature of 175 °C. However, the creep resistance is obviously deteriorated after extrusion deformation. The steady-state creep rate of as-extruded AJC421 at 175 °C/70 MPa is about three orders of magnitude higher than that of their corresponding as-cast samples. In order to increase applications of these magnesium alloys in the automotive industry, sufficient high temperature strength, creep resistance and inexpensive production for magnesium alloys are required.

Tab. 1-1 Tensile properties at room temperature and 150°C, 175°C, the creep strength at 175°C (stress to produce 0.1 creep strain in 100 hours), and the secondary creep rate at 175°C, 70 MPa of Mg–Al–Ca alloys.

Material	Tensile property			Creep strength, (175), MPa	Secondary creep rate, d (s^{-1})
	YS (MPa)	UTS (MPa)	δ(%)		
AM50 Die-cast [9]	116(RT) 90(175)	-	-	12	-
Mg-5Al-0.8Ca, Die-cast [9]	128(RT) 102(175)	192(RT) 161(175)	7(RT) 7(175)	55	-
Mg-5Al-2Ca, Die-cast [9]	161(RT) 133(175)	228(RT) 171(175)	13(RT) 23(175)	75	0.695×10^{-9}
Mg-5Al-3Ca, Die-cast [9]	186(RT) 151(175)	250(RT) 196(175)	9(RT) 15(175)	74	0.864×10^{-9}
AZ91, Cast [18]	-	162(RT) 102(150)	2.1(RT) 7.8(150)	-	-
AZ91 + 1Ca, Cast [18]	-	152(RT) 110(150)	1.8(RT) 7.0(150)	-	-
AZ91 + 2Ca, Cast [18]	-	147(RT) 112(150)	1.7(RT) 6.8(150)	-	-
AZ91 + 1Ca, Cast [19]	87(RT)	140(RT)	1(RT)	-	-
AM60, As-extruded [22]	130(RT)	282(RT)	30(RT)	-	-
Mg–6Al–2Ca, As-extruded [22]	152(RT)	269(RT)	13(RT)	-	-
AZ31 + 2Ca, Rolled [24]	185(RT)	275(RT)	7(RT)	-	-
AJ42, As-cast [23]	114(RT) 97(175)	162(RT) 136(175)	5.1(RT) 9.8(175)	-	5.6×10^{-9}
AJC42 + 1Ca, As-cast [23]	88(RT) 91(175)	131(RT) 121(175)	1.2(RT) 1.6(175)	-	3.5×10^{-9}
AJ42, As-extruded [23]	262(RT) 144(175)	296(RT) 169(175)	6.2(RT) 19(175)	-	1.9×10^{-6}
AJ42 + 1Ca, As-extruded [23]	299(RT) 168(175)	326(RT) 205(175)	3.6(RT) 10(175)	-	3.3×10^{-7}

1.3 Development of magnesium matrix composites

Metal matrix composites (MMCs) offer a unique balance of physical and mechanical properties. Additional functionalities can be designed into some MMCs through appropriate selection of constituents. The increasing demand for lightweight and high performance materials is likely to increase the need for magnesium matrix composites. For the high-performance magnesium materials, the formation of a composite is an effective approach to strengthening some magnesium alloys. The incorporation of thermally stable reinforcements into composite materials makes them preferable for high temperature applications. The potential applications of magnesium matrix composites in the automotive industry include their use in: disk rotors, piston ring grooves, gears, gearbox bearings, connecting rods, and shift forks.

1.3.1 Manufacturing processes of magnesium matrix composites

The development of new processing techniques is attracting interest in composite materials. A key challenge in the processing of composites is to homogeneously distribute the reinforcement phases to achieve a defect-free microstructure. Many fabrication processes for MMCs have been investigated to obtain high performance composites through the efficient fabrication route. The fabrication process is mainly divided into two routes: solid-state process and liquid-state process. Fig. 1-2 represents the manufacturing processes for MMCs [25, 26]. Due to the similar melting temperatures of magnesium and aluminum alloys, the processing of a magnesium matrix composite is similar to that of an aluminum matrix composite. For example, the reinforcing phases (powders/fibers/whiskers) in magnesium matrix composites are incorporated into a magnesium alloy mostly by conventional methods such as stir casting, squeeze casting and powder metallurgy.

Stir casting and squeeze casting are generally viewed as liquid-state process. The casting process has been an attractive process for the MMCs fabrication, especially for low melting point metal.

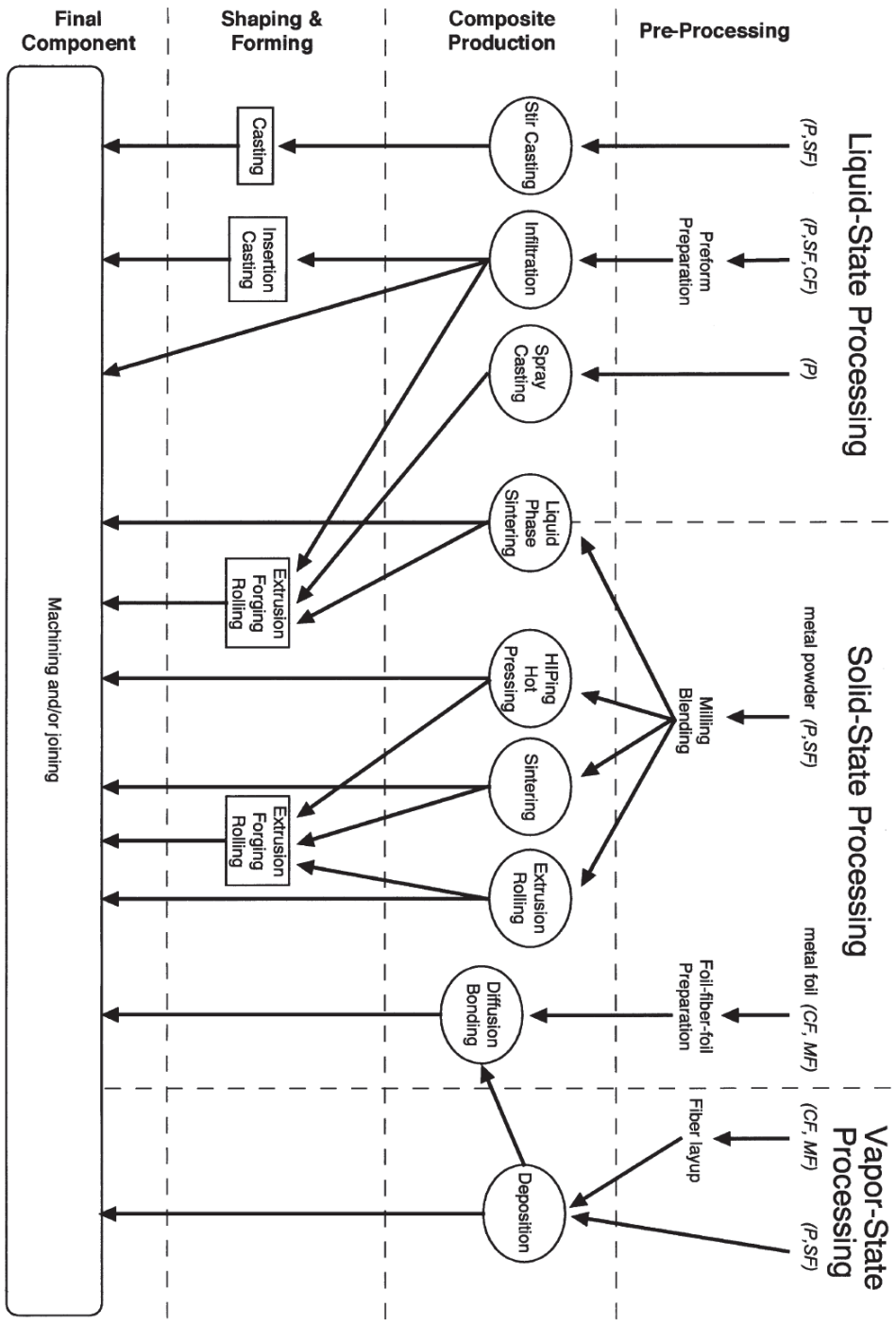

Fig.1-2 Manufacturing steps and different processes for the production of metal matrix parts.

Stir casting is one of the simple methods for the fabrication of MMCs: The reinforcements as the particles or short fibers are added into the molten metal and distributed by mechanical stirring. Mechanical stirring in the furnace is a key element of this process. Then, the resultant molten alloy can be used for die casting, permanent mold casting, or sand casting. Stir casting allows for the use of conventional metal processing methods with the addition of an appropriate stirring system such as mechanical stirring; ultrasonic or electromagnetic stirring; or centrifugal force stirring [27]. Stir casting is easily adaptable and economically viable. Its advantages lie in its simplicity, flexibility and applicability to large quantity production. This method has been adopted for wide applications such as automotive and other industrial fields due to the cost-effective fabrication [28, 29]. Magnesium composites with various matrix compositions, such as pure magnesium [30], AM60[31], Z6 [32], and AZ91 [33-39], have been produced using this method. Stir casting is suitable for manufacturing composites with up to 30% volume fractions of reinforcement [40]. The cast composites are sometimes further extruded to reduce porosity, refine the microstructure, and homogenize the distribution of the reinforcement. The major merit of stir casting is its applicability to large quantity production. Among all the well-established metal matrix composite fabrication methods, stir casting is the most economical (Compared to other methods, stir casting costs as little as one third to one tenth for mass production [41]). For that reason, stir casting is currently the most popular commercial method of producing aluminum based composites. But, no commercial use of stir casting has been reported on magnesium matrix composites. Stir casting also has some disadvantages, such as high foundry and casting equipment cost, low ductility of the final product due to the agglomerated reinforcement in the matrix and lack of design information for use as engineered materials.

Squeeze casting is recognized as typical high pressure-assisted casting method. During squeeze casting, the reinforcement (either powders or fibers/whiskers) is usually made into a preform and placed into a casting mold. The molten magnesium alloy is then poured into the mold and solidified under high pressure. Numerous magnesium matrix composites such as SiCw/Mg [42], SiCw/AZ91 [43, 44], SiCp/AZ91[45], Mg_2Si/ZK51A [46], have been produced using this technology. Squeeze casting allows

for the incorporation of higher volume fractions (up to 40–50%) of reinforcement into the magnesium alloys [47]. The use of high pressure also introduces effective compensation for the solidification contraction. Under high pressure, the shrinkage in a solidifying ingot can be filled. The inherent castability of the alloy becomes less important under high pressure. In addition, squeeze casting is a near-shape process with little or no need for subsequent machining. However, the excessively high pressure can also damage the reinforcement in a composite material and reduce the mechanical properties of the composites [48]. The shortcomings of the squeeze casting process lie mainly in the constraints on the processing imposed by the casting shape, its dimensions, and its low suitability for large quantity automatic production.

Powder metallurgy (PM) is well known for the solid-state process. In the PM process, reinforcement and metal powders are mixed, pressed, and sintered at a certain temperature under a controlled atmosphere or in a vacuum. The PM process is suitable for the matrix of high melting point alloys which is difficult to use for the liquid-state process [49]. The advantages of this processing method include the capability of incorporating a relatively high volume fraction of reinforcement or a too low volume fraction of reinforcements to make preform by liquid state process, the uniform dispersion of reinforcements in matrix by uniform blending of reinforcements and matrix powders before sintering, and fabrication of composites with matrix alloy and reinforcement systems that are otherwise immiscible by liquid casting. A variety of magnesium matrix composites have been fabricated through powder metallurgy such as SiC/Mg [50-52], B_4C/Mg [53], CNT/Mg [54], and CNT/AZ31B [54]. However, this method requires alloy powders that are generally more expensive than bulk material, involves complicated processes during the material fabrication, and is not feasible for net-shape fabrication [55]. Thus, powder metallurgy may not be an ideal processing technique for mass production.

The fabrication methods described above are well established and embody the mainstream of the manufacturing routes for magnesium matrix composites. A comparative evaluation of these three traditional metal matrix composite processing techniques is provided in Table 1-2 [56].

Table 1-2 Comparison of stir casting, squeeze casting, and powder metallurgy [56].

Method	Working range	Metal yield	Reinforcement fraction (vol%)	Damage to reinforcement	Fabrication cost
Stir casting	Wide range of shape, larger size (up to 500 kg)	Very high, >90%	~30	No damage	Least expensive
Squeeze casting	Limited by preform shape (up to 20 cm height)	Low	~45	Severe damage	Moderately expensive
Powder metallurgy	Wide range, restricted size	High	-	Fracture	Expensive

1.3.2 Mechanical properties of magnesium matrix composites

While the performance gains of discontinuously reinforced MMCs were more modest than continuously reinforced MMCs, these systems provided credible pathways to improved affordability and processability and represented an area of opportunity for commercial applications. As a lightest metal structural material, magnesium matrix composites exhibit many advantages over monolithic magnesium or magnesium alloys, such as high elastic modulus, high strength, superior creep and wear resistances at elevated temperatures. The desired properties can be achieved by a judicious selection of the type and size of the reinforcing particles. The reinforcements should be stable in the given working temperature and non-reactive too. Discontinuous micro-scale reinforcements such as particles, short fibers, or whiskers, have been used to produce magnesium MMCs.

Silicon carbide (SiC) increases the strength and wear resistance of Mg alloys. Lan et al. [57] indicated that the microhardness of 5 wt.% SiC nanoparticle reinforced

magnesium composites increased 75% compared to that of AZ91D. Lim et al. [58] reveal that the SiCp reinforced magnesium matrix composites exhibit slightly superior wear resistance under the low load. Sajuri et al. [59] reveal that the mechanical properties i.e. hardness and tensile strength of SiC particulates reinforced magnesium composites prepared by spark plasma sintering increased with increasing of SiC content up to 10 wt.%. Further increase of SiC content gives rise to the tensile strength decrease due to the agglomeration of SiC particles. Nie et al. [60] found that, by hot extrusion, the ultimate tensile strength, yield strength and elongation to fracture of the SiC nanoparticles reinforced magnesium matrix composites were simultaneously improved. The tensile strength and ductility value of the composite increases in comparison to the unreinforced and extruded AZ91 alloy.

Titanium Carbide (TiC) particulates play a vital role on damping behavior of magnesium composites. Reinforcement of TiC particles lead in improvement of yield strength, tensile strength, and elastic modulus significantly, while the ductility is reduced to some extent. Zhang et al. [61] revealed that the tensile strength and damping capacity of the TiC particulates reinforced magnesium matrix composites were improved compared to AZ91 magnesium alloy.

The reinforcement of Aluminum Oxide (Al_2O_3) induces good creep resistance, compressive strength. Hassan et al. [62] reveal that the incorporation of nano and submicron size Al_2O_3 particulates in magnesium matrix led to a simultaneous increase in hardness, yield strength, UTS, and ductility of pure magnesium.

Boron Carbide (B_4C) is one of known hardest element. It has high elastic modulus and fracture toughness. The addition of B_4C in magnesium matrix increases the flexural strength of hybrid composite, hardness, and wear resistance [53, 63, 64].

Fibers are the important class of reinforcements which effect on the directional strength and stability of the composites. They transfer the strength to the matrix constituent influencing and enhancing their properties as desired. Zhang et al. [65] investigated the tensile behavior of AM60 based composites reinforced with alumina (Al_2O_3) fiber at a pressure of 90 MPa. The results showed that with the addition of fibers, the tensile properties improved significantly, but the ductility was reduced compare to the unreinforced matrix alloy. Localized damages, like fibers damage and

cracking, matrix fracture, and interface debonding were consistent with the tensile property. Sklenicka et al. [66] conducted a study on constant stress tensile creep behavior of AZ91 magnesium based composite reinforced with 20 vol.% Al_2O_3. The creep resistance of the reinforced material was considerably improved in comparison to the matrix alloy. The creep strengthening arises due to the effective load transfer between plastic flow in the matrix and fibers. Tian et al. [67] studied the creep behavior of aluminum silicate short-fiber-reinforced magnesium matrix composite. They found that both the matrix and fiber have the same true stress exponent and true activation energy for creep. The composites creep behavior is mainly controlled by controlling of the viscous slip of dislocation and the controlling of grain boundary slippage as a supplement.

1.3.3 Carbon nanotube reinforced magnesium matrix composites

Carbon nanotubes (CNTs) have attracted the attention of many scientists worldwide since their discovery in 1991 [68]. CNT possess the excellent mechanical, electrical, thermal, and optical properties. Their extraordinary strength (up to 150 GPa) and Young's modulus (up to 1 TPa) [37] make them ideal candidates as reinforcements for high strength, light weight and high performance composites. Consequently, the studies on CNT reinforced polymer and metal matrix composites were also carried out by many researchers.

Recently, much work has been devoted to investigate the mechanical properties of Mg-based composites reinforced with carbon nanotubes. Tab. 1-3 lists the tensile properties of magnesium composites reinforced with carbon nanotubes prepared by liquid melt processing and powder metallurgy routes. [69] Liu et al. employed both mechanical stirring and high-intensity ultrasonic processing to fabricate MWNT/Mg nanocomposite [39]. They reported that the addition of 1.5 wt% MWNT to Mg improves its tensile strength, yield strength and elongation. Zeng et al. introduced MWNT performs into molten AZ31 under manual stirring [70]. They reported that by adding 1 wt% MWNT, the microhardness, tensile strength, Young's modulus and elongation of magnesium improve significantly. With more MWNT concentration, the tensile properties degrade somewhat due to the agglomeration of MWNTs. By taking the

advantage of low cost CNFs, Honma et al. [71] fabricated AZ91D composites reinforced with Si-coated CNF using compo-casting, squeeze casting and extrusion. The yield stress and tensile strength of AZ91D increases from 244 to 342 MPa by adding 1.5 wt% CNF. The strengthening effect of CNFs can be attributed to the improved wettability of CNFs by coating with silicon. However, the tensile elongation of CNF/AZ91D nanocomposites decreases sharply by adding CNFs. Goh et al. used the disintegrated melt deposition and extrusion processes to fabricate MWNT/Mg nanocomposites [72]. The yield strength, ultimate strength and tensile elongation of magnesium can be improved by adding 0.3 and 1.3 wt% MWNT. At 1.6 and 2 wt% MWNT, the yield stress, tensile strength and ductility reduce considerably due to the agglomeration of nanotubes. In another study, they prepared MWNT/Mg composites containing 0.06–0.3 wt% MWNT by mixing nanotubes with Mg powders in a blender followed by sintering and hot extrusion [73]. The yield strength and ductility of the composites improve with increasing nanotube content. However, carbon nanotube additions have little effect in enhancing ultimate tensile strength of the composites. Carreno-Morelli et al. [74] produced multiwall carbon nanotube/pure magnesium composites by a powder metallurgical method. The Young's modulus was about 9% higher compared to pure Mg metal by adding 2 wt% CNTs.

To enhance dispersion of MWNTs in the matrix, Shimizu et al. used ball milling, hot pressing and extrusion processes to fabricate MWNT/AZ91D nanocomposites [75]. The composite with 1 wt% MWNT was found to exhibit the about 23% highest yield stress and ultimate tensile strength. Kondoh et al. fabricated MWNTs reinforced Mg/AZ31B composites by SPS and hot extrusion treatments [54]. The yield stress of extruded Mg increases from 178 MPa to 253 MPa by adding 1.1 vol% MWNT, i.e. 42% increment in yield strength. Similarly, there is nearly 27% increment in the yield stress of the AZ31B by adding 0.95 vol% MWNT. Sun et al. mixed the in situ synthesized MWNT/Mg powders by ball milling [76]. followed by sintering and hot extrusion. With increasing MWNT content up to 2.4 wt%, the tensile strength of Mg increases to 285 MPa, which is about 45% higher than that of pure Mg. When the MWNT reaches 3 wt%, the tensile strength decreases due to the formation of nanotube clusters.

Tab. 1-3 Tensile properties of magnesium composites reinforced with carbon nanotubes prepared by liquid melt processing and powder metallurgy routes. [69]

Matrix material	MWNT content, wt%	Processing methods	Young's modulus, GPa	Yield strength, MPa	Tensile strength, MPa	Fracture strain, %
AZ91D[39]	0	Melt stirring, high-intensity ultrasonic processing and casting	44.3	86	128	0.90
	1.5		64.3	104	157	1.28
AZ31[70]	0	Ball milling MWNT preform, melt infiltration and casting	60	–	160	3.74
	1		90	–	210	8.56
	1.5		98.9	–	190	7.15
Mg[72]	0	Melt stirring, disintegrated melt deposition and hot extrusion	–	126	192	8.0
	0.3		–	128	194	12.7
	1.3		–	140	210	13.5
	1.6		–	121	200	12.2
	2		–	122	198	7.7
AZ31[77]	0	Melt stirring, disintegrated melt deposition and hot extrusion	–	172	263	10.4
	1		–	190	307	17.5
Mg[73]	0	Powder mixing for 10 h, cold compaction, sintering and extrusion	–	127	205	9
	0.06		–	133	203	12
	0.18		–	139	206	11
	0.3		–	146	210	8
AZ91D[75]	0	Ball milling, hot pressing, and extrusion	40	232	315	14
	0.5		43	281	383	6
	1		49	295	388	5
	3		51	284	361	3
	5		51	277	307	1
Mg[54]	0	Wet mixing, SPS and hot extrusion	–	178	–	9.4
	1.1		–	253	–	1.2
AZ31B[54]	0		–	279	–	10.8
	0.9		–	355	–	5
Mg[76]	0	In-situ synthesized MWNT/Mg powders, ball milling and extrusion	–	–	220	2.14
	1.8		–	–	252	1.61
	2.4		–	–	285	1.87
	3		–	–	258	1.35

1.3.4 Strengthening mechanism of CNT/Mg composites

The understanding of strengthening mechanism of carbon nanotubes in metal matrix composite is important to predict the strength and improve fabrication process. The research on carbon nanotubes reinforced metal matrix composites mainly focused on the preparation methods and mechanical properties. There is little research focused on the strengthening mechanism. Literature review summarized some works on the strengthening mechanism of CNTs in metal matrix composites [69].

1.3.4.1 Micromechanical models

The strengthening effects of CNTs depends greatly on the achievement of effective stress-transfer across the metal matrix-filler interface during mechanical tests. The aspect ratio, homogenous dispersion of CNTs in the matrix, and the formation of interfacial products also govern the load transfer efficiency of CNTs. Based on several micromechanical models for conventional fiber-reinforced composites, the reinforcing mechanisms of nanofillers was elucidated by analyzing the discrepancies between experimental and predicted results.

1.3.4.2 Metallurgical factors

Metallurgical factors such as Hall–Petch effect due to grain size refining, Orowan looping and dislocation generation resulting from thermal mismatch between the matrix and carbon nanomaterials also contribute to the strengthening effect [37].

Hall–Petch effect: The uniform distributed CNTs in metal matrix composites can prevent grain growth, since the CNTs with relatively small size pin on the grain boundary, and prevent the grain boundary from migrating. Decrease of grain size is beneficial to the enhancement of mechanical properties of the composites, which can be explained by the Halle-Petch relation.

Orowan looping: CNTs may act as impenetrable obstacles similar to non-shearable precipitates and increase the yield stress through an Orowan mechanism. Orowan strengthening is not significant in the microsized particulate-reinforced MMCs [78], because the reinforcement particles are coarse and the interparticle spacing is large. For

nanofillers with uniform distribution, it is necessary to take into consideration the Orowan strengthening.

Thermal mismatch: There is a significant mismatch in coefficient of thermal expansion between CNT and the matrix, and this might be accommodated by extensive dislocation nucleation around CNT which then leads to hardening of the metal matrix.

1.3.4.3 Ductility

Increased ductility has been found in CNT reinforced Mg composites before by Goh [79]. The improvement in tensile ductility of composites with MWNT content is attributed to the high activity of basal slip system and the activation of prismatic slip by adding CNTs. It implicates a minimum of five independent slip systems which are required to deform a polycrystalline metal plastically (von Mises criterion), therefore resulting in a much higher ductility of the composites.

1.4 Problem and Objective of this study

Mg-Al-Ca alloys have been developed for elevated temperature applications. The addition of calcium significantly improves their flame resistance, high-temperature strength, creep resistance, and oxidation resistances. To enhance the strength and rigidity of the matrix, carbon nanofibers can be used to reinforce Mg-Al-Ca alloy, which are supposed to give them satisfactory mechanical properties at both room and elevated temperatures.

The main problem for CNT reinforced metal matrix composites is to obtain a homogenous dispersion in the matrix materials. CNTs have larger surface area and much higher aspect ratio than traditional fillers. It is difficult to disaggregate CNTs due to their attractive Van der Waals interactions. The investigation of metal matrix composites reinforced with CNTs has many challenges: uniform dispersion of CNTs in the metal matrix; fabrication technique suitable for up-scaling and commercial production; control of the interfacial reaction between CNTs and the metal matrix; high preparation cost for CNT limits its commercial application. Compared to CNTs, vapor grown nano-carbon fibers (VGCNFs) have received less research attention because CNTs have better mechanical properties and smaller diameter than VGCNFs. However, because of their availability and relatively low price, VGCNFs are an excellent alternative for CNTs. In addition, VGCNFs possess good mechanical, electrical and thermal properties with same structure to carbon structure of CNTs. With a larger diameter than CNTs, VGCFs have smaller surface area. Thus, VGCFs are relatively easy to disperse in the metal matrix.

The cost-effective processing of composite materials is an essential element for expanding their applications. Among the variety of manufacturing processes available for discontinuous metal matrix composites, stir casting is easily adaptable and economically viable. Its advantages lie in its simplicity, flexibility, and applicability to large quantity production. However, there are some problems associated with stir casting of metal matrix composites such as: poor wettability and heterogeneous distribution of the reinforcement material.

The poor wettability of the reinforcement in the melt prevents the reinforcement from infiltrating the molten matrix, with the result that it simply floats on the melt surface.

This is due to the surface tension, very large specific surface area, and high interfacial energy of the reinforcements, along with the presence of oxide films on the melt surface. Compo-casting is a liquid state process in which the infiltration of reinforcement into a semi-solid metal (SSM) can be facilitated by means of agitation.

The uniform distribution of the reinforcement within the matrix and its bond strength with the matrix are essential structural requirements for a stronger metal matrix composite. The wettability and distribution of the reinforcement are difficult because of the small size of VGCFs. This is due to the large surface area and surface energy of the particles, which cause an increasing tendency for agglomeration. Thus, an intermediate layer of nickel is coated on the carbon fibers to facilitate the wetting. Prior to fabricate the VGCF-reinforced magnesium-calcium alloy composites, the effect of nickel coating on the wettability of magnesium with carbon fiber was investigated.

Table 1-4 Measured properties of carbon nanotube and carbon nanofiber.

Material	Single-walled carbon nanotube (SWCNT)	Multi-walled carbon nanotubes (MWCNT)	Vapor grown carbon fiber (VGCF)
Diameter, nm	1–2	5–50	50-200
Density (g/cm^3)	1.3	1.75	2.1
Specific surface area, (m^2/g)	-	1000	13
Aspect ratio	100-10000	100-10000	10～500
E (GPa)	1000 [80]	270–950 [81]	240 [82]
UTS (GPa)	50-500 [83]	10-60 [83]	2.92 [82]
Thermal conductivity, (W/mK)	3500	500–2069	1200

In this study, the effect of nickel coating on wetting behavior of magnesium alloys and graphite sheet was investigated. Ni-coated VGCFs reinforced Mg-Al-Ca alloy composites are fabricated by compo-casting process. The effects of Ni-coated VGCFs

on the microstructure and mechanical properties of magnesium alloy are investigated, and the strengthening mechanism of Ni-coated VGCFs reinforced Mg-Al-Ca alloy composites is discussed.

1.5 Outline of this thesis

In Chapter 1, the trend of applications and the development status of the magnesium alloys for elevated temperature applications and magnesium matrix composites are reviewed. Moreover, from the problems of the previous studied magnesium matrix composites, the direction of newly developing MMCs, VGCF-reinforced magnesium-calcium alloy composite is proposed.

Prior to fabricate the VGCF-reinforced magnesium-calcium alloy composite, the wettability of magnesium with carbon fiber was investigated in Chapter 2. In this chapter, wetting behavior of magnesium alloys on graphite sheet, pure nickel, and nickel coated graphite sheet were investigated using sessile drop method.

In Chapter 3, fabrication of VGCF reinforced magnesium matrix composites was carried out by low pressure infiltration. Porous VGCF preforms with nickel coating were fully infiltrated. The applied infiltration pressure to the VGCF preform was compared with the threshold pressure estimated with the measured contact angle.

In Chapter 4, the fabrication of the VGCF-reinforced magnesium-calcium alloy composite by stir casting process was presented. Especially, the effects of Ni-coated VGCFs on the microstructure of magnesium alloys were investigated.

The characterization of mechanical properties on the VGCF-reinforced magnesium-calcium alloy composites were investigated in Chapter 5. The influences of Ni-coated VGCFs on the mechanical properties of magnesium alloys were studied. In addition, the tensile properties at elevated temperature of the composites were investigated.

The results from above mentioned investigation are summarized in Chapter 6.

References

1) T. M.Pollock: Science **328** (2010) 986.
2) J. F Nie: Metall. Mater. Trans. A **43** (2012) 3891-3939.
3) A. A. Luo, R. K. Mishra, B. R. Powell, and A. K. Sachdev: Mater. Sci. Forum **706-709** (2012) 69-82.
4) B. L. Mordike: Mater. Sci. Eng., A **40** (2001) 691-701.
5) M. K. Kulekci: The International Journal of Advanced Manufacturing Technology **39** (2008) 851-865.
6) A. K. Dahle, Y. C. Lee, M. D. Nave, P. L. Schaffer, and D. H. StJohn: Journal of Light Metals **1** (2001) 61-72.
7) A. A.Luo: Mater. Sci. Forum **419** (2003) 57-66.
8) M. K. Kulekci: The International Journal of Advanced Manufacturing Technology **39** (2008) 851-865.
9) A. A. Luo: Int. Mater. Rev. 49 (2004) 13-30.
10) A. A. Luo: Metall. Mater. Trans. A **33A** (2002) 567-574.
11) J. Wang, P. F. Song, S. Huang, and F. S. Pan: Mater. Lett. **93** (2013) 415-418.
12) G. Ben-Hamu, D. Eliezer, K. S. Shin, and S. Cohen: J. Alloys Compd. **431** (2007) 269-276.
13) R. Ninomiya, T. Ojiro, and K. Kubota: Acta Metall. Mater. **43**(1995) 669-674.
14) L. Han, H. Hu, and D. O. Northwood: Mater. Lett. **62**(2008): 381-384.
15) S. W. Xu, N. Matsumoto, K. Yamamoto, S. Kamado, T. Honma, and Y. Kojima: Mater. Sci. Eng., A **509** (2009) 105-110.
16) A. Suzuki, N. D. Saddock, J. W. Jones, and T. M. Pollock: Acta Mater. **53** (2005) 2823-2834.
17) Y. Terada, R. Sota, N. Ishimatsu, T. Sato, and K. Ohori: Metall. Mater. Trans. A **35**(2004): 3029-3032.
18) Q. D. Wang, W. Z. Chen, X. Q. Zeng, Y. Z. Lu, W. J. Ding, Y. P Zhu, X. P. Xu, and M. Mabuchi: J. Mater. Sci. **36** (2001) 3035-3040.
19) P. Li, B. Tang, and E.G. Kandalova: Mater. Lett. **59** (2005) 671-675.
20) M. Masoumi, and H. Hu: Mater. Sci. Eng., A **528** (2011) 3589-3593.
21) L. Zhang, K. K. Deng, K. B. Nie, F. J. Xu, K. Su, and W. Liang: Mater. Sci.

Eng., A **636** (2015) 279-288.

22) H. Watanabe, M. Yamaguchi, Y. Takigawa, and K. Higashi: Mater. Sci. Eng., A **454-455** (2007) 384-388.

23) J. Bai, Y. S. Sun, F. Xue, S. Xue, J. Qiang, and W. J. Tao: Scr. Mater. **55** (2006) 1163-1166.

24) C. D. Yim, B. S. You, J. S. Lee, and W. C. Kim: Mater. Trans. **45** (2004) 3018-3022.

25) H. P. Degischer, P. Prader, and C. San Marchi: Compos. Appl. Sci. Manuf. **32** (2001) 1161-1166.

26) A. Mortensen, C. San Marchi, and H. Degischer: MMC-Assess Publications, Institute of Materials Science and Testing, Vienna University of Technology, Vienna, Austria (2000).

27) P. Rohatgi: Mod. Cast. **78** (1988) 47-50.

28) N. Barekar, S. Tzamtzis, N. H. Babu, Z. Fan, and B. Dhindaw: Metall. Mater. Trans. A **40** (2009) 691-701.

29) S. Mallik, N. Ekere, C. Best, and R. Bhatti: Appl. Therm. Eng. **31** (2011) 355-362.

30) H. Y. Wang, Q. C. Jiang, Y. Q. Zhao, F. Zhao, B. X. Ma, and Y. Wang: Mater. Sci. Eng., A **372** (2004) 109-114.

31) H. Yan, Y. Rao, and R. He: J. Mater. Process. Technol. **214** (2014) 612-619.

32) C. D. Li, X. J. Wang, W. Q. Liu, K. Wu, H. L. Shi, C. Ding, and M. Y. Zheng: Rare Met. (2015) 1-6.

33) Q. C. Jiang, X. L. Li, and H. Y. Wang: Scripta Mater. **48** (2003) 713-717.

34) P. Poddar, V. C. Srivastava, P. K. De, and K. L. Sahoo: Mater. Sci. Eng., A **460–461** (2007) 357-364.

35) X. J. Wang, K. Wu, W. X. Huang, H. F. Zhang, M. Y. Zheng, and D. L. Peng: Compos. Sci. Technol. **67** (2007) 2253-2260.

36) X. J.Wang, K. Wu, H. F. Zhang, W. X. Huang, H. Chang, W. M. Gan, M. Y. Zheng, and D. L. Peng: Mater. Sci. Eng., A **465** (2007) 78-84.

37) Q. Q. Li, A. Viereckl, C. A. Rottmair, and R. F. Singer: Compos. Sci. Technol. **69** (2009) 1193-1199.

38) K. K. Deng, K. Wu, Y. W. Wu, K. B. Nie, and M. Y. Zheng: J. Alloys Compd. **504** (2010) 542-547.

39) S. Y. Liu, F. P. Gao, Q. Y. Zhang, X. Zhu, and W. Z. Li: Trans. Nonferrous Met. Soc. China **20** (2010) 1222-1227.

40) R. Saravanan, and M. Surappa: Mater. Sci. Eng., A **276** (2000) 108-116.

41) M. Surappa: J. Mater. Process. Technol. **63** (1997) 325-333.

42) S. Y. Chang, H. Tezuka, and A. Kamio: Mater. Trans. **38** (1997) 18-27.

43) M. Zheng, K. Wu, and C. Yao: Mater. Sci. Eng., A **318** (2001) 50-56.

44) M. Y. Zheng, K. Wu, S. Kamado, and Y. Kojima: Mater. Sci. Eng., A **348** (2003) 67-75.

45) A. R. Vaidya, and J.J. Lewandowski: Mater. Sci. Eng., A **220** (1996) 85-92.

46) H. Lianxi, and W. Erde: Mater. Sci. Eng., A **278** (2000) 267-271.

47) A. A. Luo: J. Magn. Alloy. **1** (2013) 2-22.

48) K. S. Sohn, K. Euh, S. Lee, and I. Park: Metall. Mater. Trans. A **29** (1998) 2543-2554.

49) E. Delannay, C. Colin, Y. Marchal, L. Tao, F. Boland, P. Cobzaru, B. Lips, and M. Dellis: J. Phys. IV **3** (1993) 1675-1684.

50) G. Garcés, P. Pérez, and P. Adeva: Scr. Mater. **52** (2005) 615-619.

51) B. W. Chua, L. Lu, and M.O. Lai: Compos. Struct. **47** (1999) 595-601.

52) J. Gu, X. N. Zhang, Y. F. Qiu, and M. Y. Gu: Compos. Sci. Technol. **65** (2005) 1736-1742.

53) Q. C. Jiang, H. Y. Wang, B. X. Ma, Y. Wang, and F. Zhao: J. Alloys Compd. **386** (2005) 177-181.

54) K. Kondoh, H. Fukuda, J. Umeda, H. Imai, B. Fugetsu, and M. Endo: Mater. Sci. Eng., A **527** (2010) 4103-4108.

55) Y. Liu, S. Lim, L. Lu, and M. Lai: J. Mater. Sci. **29** (1994) 1999-2007.

56) H. Z. Ye, and X.Y. Liu: J. Mater. Sci. **39** (2004) 6153-6171.

57) J. Lan, Y. Yang, and X. Li: Mater. Sci. Eng., A **386** (2004) 284-290.

58) C. Y. H. Lim, S.C. Lim, and M. Gupta: Wear **255** (2003) 629-637.

59) W. Muhammad, Z. Sajuri, Y. Mutoh, and Y. Miyashita: J. Alloys Compd. **509** (2011) 6021-6029.

60) K. B. Nie, X. J. Wang, L. Xu, K. Wu, X. S. Hu, and M. Y. Zheng: J. Alloys Compd. **512** (2012) 355-360.

61) X. Q. Zhang, H. W. Wang, L. H. Liao, and N. H. Ma: Compos. Sci. Technol. **67** (2007) 720-727.

62) S. F. Hassan, and M. Gupta: J. Alloys Compd. **457** (2008) 244-250.

63) S. C. Sharma, B. Anand, and M. Krishna: Wear **241** (2000) 33-40.

64) C. Nie, J. Gu, J. L. Liu, and D. Zhang: J. Alloys Compd. **454** (2008) 118-122.

65) X. Zhang, Q. Zhang, and H. Hu: Mater. Sci. Eng., A **607** (2014) 269-276.

66) V. Sklenička, M. Svoboda, M. Pahutová, K. Kuchařová, and T. G. Langdon: Mater. Sci. Eng., A **319–321** (2001) 741-745.

67) J. Tian, and Z. Q. Shi: Trans. Nonferrous Met. Soc. China **24** (2014) 632-640.

68) S. Iijima: Nature **354** (1991) 56.

69) S. C. Tjong: Mater. Sci. Eng., R **74** (2013) 281-350.

70) X. Zeng, G. H. Zhou, Q. Xu, Y. J. Xiong, C. Luo, and J. C. Wu: Mater. Sci. Eng., A **527** (2010) 5335-5340.

71) T. Honma, K. Nagai, A. Katou, K. Arai, M. Suganuma, and S. Kamado: Scripta Mater. **60** (2009) 451-454.

72) C. S. Goh, J. Wei, L. C. Lee, and M. Gupta: Mater. Sci. Eng., A **423** (2006) 153-156.

73) C. S. Goh, J. Wei, L. C. Lee, and M. Gupta: Nanotechnology **17** (2006) 7-12.

74) E. Carreno-Morelli, J. Yang, E. Couteau, K. Hernadi, J. W. Seo, C. Bonjour, L. Forro, and R. Schaller: Phys. Status Solidi A **201** (2004) R53-R55.

75) Y. Shimizu, S. Miki, T. Soga, I. Itoh, H. Todoroki, T. Hosono, K. Sakaki, T. Hayashi, Y. A. Kim, M. Endo, S. Morimoto, and A. Koide: Scripta Mater. **58** (2008) 267-270.

76) F. J. Sun, C. S. Shi, K. Y. Rhee, and N. Q. Zhao: J. Alloys Compd. **551** (2013) 496-501.

77) M. Paramsothy, S. F. Hassan, N. Srikanth, and M. Gupta: J. Nanosci. Nanotechnol. **10** (2010) 956-964.

78) T. Clyne, and P. Withers, An introduction to metal matrix composites. 1995: Cambridge university press.

79) C. S. Goh, J. Wei, L. C. Lee, and M. Gupta: Compos. Sci. Technol. **68** (2008) 1432-1439.

80) M. F. Yu, B. S. Files, S. Arepalli, and R. S. Ruoff: Phys. Rev. Lett. **84** (2000) 5552-5555.

81) M. F. Yu, O. Lourie, M. J. Dyer, K. Moloni, T. F. Kelly, and R. S. Ruoff: Science **287** (2000) 637.

82) T. Ozkan, M. Naraghi, and I. Chasiotis: Carbon **48** (2010) 239-244.

83) M. H. Al-Saleh, U. Sundararaj: Composites Part A, **42** (2011) 2126-2142.

Chapter 2

Nickel Formation on Graphite Sheet Surface for Improving Wettability with Magnesium Alloy

2.1 Introduction

Magnesium alloys offer a very high specific strength among conventional engineering alloys and possess excellent castability, superior machinability, and good damping capacity. They have gained widespread attention in scientific research and commercial application.[1, 2] To cover the deficiencies in mechanical properties of magnesium, especially at elevated temperatures, efforts have been made to develop creep resistant magnesium alloys, and magnesium matrix composites are prospecting candidates due to their promising superior properties. Calcium is a promising elemental addition to develop Mg–Al alloys for high-temperature applications. The Calcium addition encourages the formation of Ca-containing thermally stable intermetallic compounds and suppresses the formation of unstable β-$Mg_{17}Al_{12}$. Thus, Calcium addition significantly improves the high temperature strength, creep resistance and also oxidation resistances.[3-6] Carbon fibers possess excellent mechanical, thermal properties and low density.[7] Carbon fiber reinforced magnesium matrix composites can offer significant gains in terms of specific strength and modulus, and also they have the inherent environmental stability of metallic systems.[8-10] Among various short carbon fibers, vapor-grown carbon fibers (VGCFs) are increasingly used in various composites owing to their excellent properties and low cost.[11-13] The magnesium-calcium alloy-based composites reinforced with VGCFs are supposed to possess satisfactory high-temperature properties.

However, poor wettability of magnesium on carbon fiber was a technical problem encountered in making magnesium alloy–carbon fiber composites. Shi et al. reported that the contact angle of molten magnesium on porous graphite at 973K was 74° in magnesium vapor environment.[14] But on graphite surface, the contact angle of molten magnesium was about 125° at 973K.[15] On basal plane of graphite, the contact angle was 120° at 1189K.[16] Thus, Poor wettability makes it difficult to impregnate the fiber with the molten magnesium, and results in inadequate bonding between them.

Several methods have been found to overcome the wetting problem. The usual method is forcing liquid metal into the space of fiber/particle by the vacuum or pressure during low-pressure infiltration or squeeze casting methods.[17, 18] Another one is decreasing the critical infiltration pressure between the liquid metal and reinforcements.

By control of chemical composition, the wettability of the alloys can be improved. Yoshida et al. reported that the contact angles of aluminum alloys on prismatic plane decreased from 155º at 2.0 mass% Mg to 125º at 2.9 mass% Mg.[19] In addition, the intermediate layer approach is also an effective way to facilitate the wetting. Nickel is known to be wetted with metal. An intermediate layer of nickel on carbon fibers had been considered to facilitate the wetting. Ip et al. found that with nickel coating on graphite sheet, the contact angle of pure aluminum decreased from 140° to 4°.[20] Rams et al. and Ryu et al. fabricated aluminum matrix composites reinforced with nickel coated fibers.[21, 22] Coatings improved the wetting behavior of carbon fibers by molten aluminum because of the formation of a transient Al–Ni intermetallic compound at the matrix–fiber interface, limiting fiber segregation to obtain a homogeneous reinforcement distribution. Nickel coating also reduced the trend to form aluminum carbide.[21-23] By incorporating nickel coated graphite particles into molten aluminum, a wear resistant aluminum matrix composite was produced.[24, 25] While the graphite particles provided lubrication against wear, the aluminum–nickel intermetallic compound formed improved the strength of the aluminum matrix. However, there have been rarely research studies on the wetting between magnesium alloys and nickel coated carbon fiber.

This study aims to improve the wettability of magnesium alloys with carbon fiber. Since the basal plane of graphite sheet is same with the surface of VGCF, the wetting behavior of Mg-Al alloy and Mg-Al-Ca alloys on graphite sheet was investigated. The wetting of Mg-Al-Ca alloys on pure nickel was investigated to explain the mechanism of wetting behavior between Mg-Al-Ca alloys and nickel coated graphite sheet.

2.2 Experimental methods

2.2.1 Materials

Wettability measurements were conducted by two kinds of magnesium alloys, Mg-5Al and Mg-5Al-3Ca alloys. Magnesium alloys were cast by Permanent Mold (PM) with chemical compositions (mass %) shown in Table 2-1. Melting was carried out in an electrical furnace covering with argon gas to prevent molten magnesium from oxidation. High purity magnesium, aluminum and calcium were added in a mild steel crucible as the desired compositions. After the alloying elements were completely dissolved at 973 K, the melt was stirred mechanically for 2 min with a stainless-steel rod, and then poured into a mild steel mould which had been preheated to 573 K. The size of ingot was 14mm × 14 mm × 120 mm.

Table 2-1 Chemical composition of Mg-5Al and Mg-5Al-3Ca alloys.

Nominal composition	Analyzed contents (mass %)		
	Al	Ca	Mg
Mg-5Al	4.4	-	Bal.
Mg-5Al-3Ca	4.6	3.0	Bal.

Microstructures of magnesium alloys were observed by optical microscopy (OM, Nikon Optiphot) and electron probe micro-analyzer (EPMA, JXA-8900RL). Wavelength dispersive spectroscopy (WDS) analysis was performed to reveal the concentration of alloying elements. X-ray diffraction (XRD, M03XHF 22) analysis was carried out to identify the existing phases, and polished samples were exposed to Cu-Kα radiation (λ=0.15418 nm) with a scanning speed of 1°/min.

2.2.2 Substrate materials

Wettability of magnesium alloys was tested on three different kinds of substrate materials, graphite sheet (Gr), nickel plate (Pure Ni) and nickel coated graphite sheet (Gr-Ni).

Surface of graphite sheet had the basal plane of (002) same with that of VGCFs, which was confirmed with XRD, as shown in Fig. 2-1.

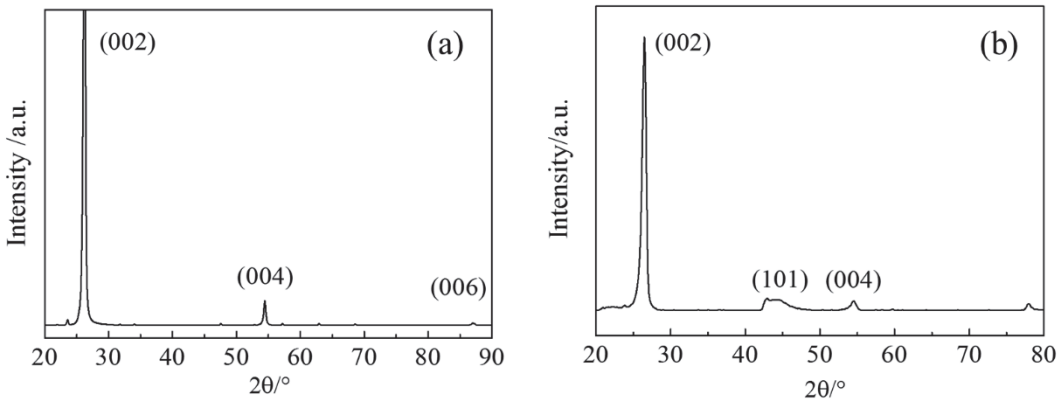

Fig. 2-1 X-ray diffraction profiles of (a) VGCFs and (b) basal plane of graphite sheet.

Nickel plate was electrolytic grade with a minimum purity of 99% Ni and polished to a mirror finish.

Nickel coating on graphite sheet was prepared by vacuum evaporation method with the same quality of nickel described above. Fig. 2-2 shows illustration of vacuum evaporation device. Graphite sheet was located under the heat source in vacuum. Current of the nickel heat source was about 30 A to reach the point where the nickel efficiently evaporates. Nickel atoms transferred to the surface of graphite sheet to grow films. Fig. 2-3 shows the SEM micrograph and WDS mapping of top surface and cross section of nickel coated graphite sheet. With about 0.01g nickel evaporated, the nickel coating on graphite sheet was uniform with thickness of about 2 μm.

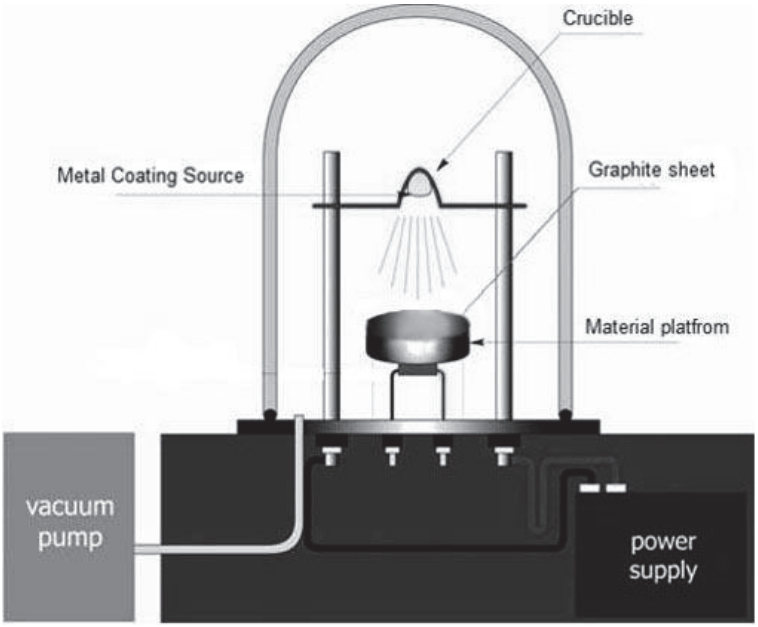

Fig. 2-2 Illustration of vacuum evaporation device.

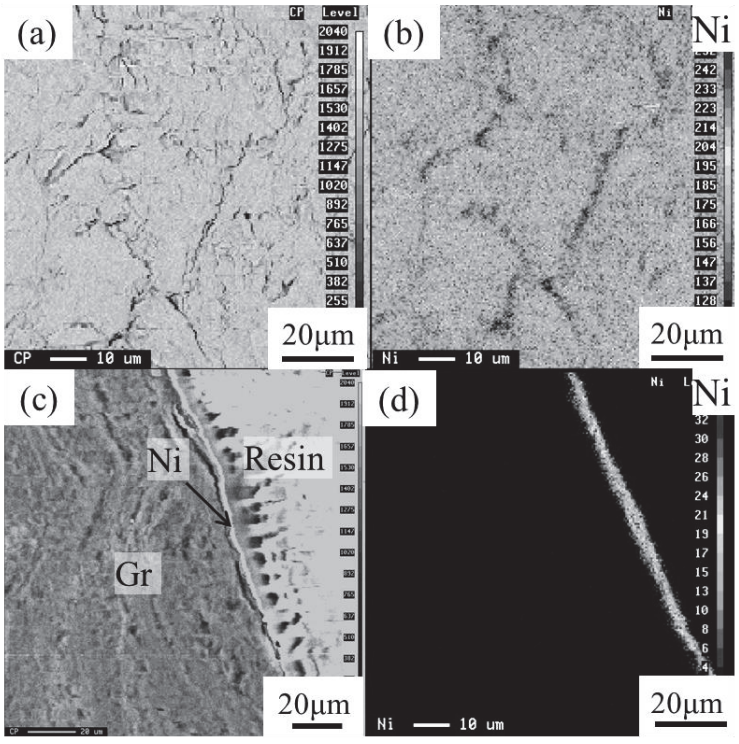

Fig. 2-3 SEM micrograph and WDS mapping of top surface (a), (b) and cross section (c), (d) of nickel coated graphite sheet.

2.2.3 Wettability tests

Wettability tests were carried out using sessile drop method. Contact angle (θ) made between magnesium alloy and the substrate was used to determine the wettability. Wetting relates to the contact between a liquid and a solid surface. It describes the ability of a liquid to spread over a solid surface. The extent of wetting is controlled by the thermodynamic tendency in order to minimize surface free energy. For a liquid droplet on a solid surface (Fig. 4a), the surface energy (tension) of different components can be expressed by:

$$\gamma_{SV} = \gamma_{SL} + \gamma_{LV} \cos\theta \quad (1)$$

where θ is the contact angle, γ_{SV}, γ_{SL} and γ_{LV} are the surface tensions of solid–vapor, solid–liquid and liquid–vapor, respectively. For $\theta = 0°$, the liquid droplet spreads over entire solid surface. At $\theta < 90°$, the liquid droplet wets the solid. The liquid does not wet solid for K > 908, especially $\theta = 180°$. Thus, a liquid can wet a solid when cos $\theta >$ 0, or $\gamma_{SV} > \gamma_{SL}$.

Geometry of droplet is shown in Fig. 2-4b. Taken the droplet as a sphere, the contact angle (θ) was calculated by

$$\theta = 2\arctan(h/r) \quad (2)$$

where h is the height of the droplet, and r is the width of contact interface of the droplet on the substrates. Then the contact angle was verified by the value measured directly by the images.

Fig. 2-5 shows the sessile drop device.[19] The system was composed of a sealed chamber, a bottle of Ar + 3 vol.% H_2 inert gas, a set of vacuum pumps, dropping tube and a CCD video camera or a high-speed video camera. The level of the substrate was confirmed by using steel ball after the substrate was set on a stand under the dropping tube. The dropping tube has Φ1.0 mm aperture at the bottom to drop molten metal. The Chamber was evacuated to 1.5×10^{-3} Pa and then heated to 1003 K with Ar + 3 vol% H_2 shielding gas at the rate of 1.67×10^{-5} m^3/s up to 1.0×10^5 Pa. The chamber was evacuated one more time in the middle of the heating process in order to avoid contamination. The specimen was moved to the bottom of dropping tube. After 180 s, the chamber was evacuated. Molten metal was dropped by means of a pressure difference between the chamber and the dropping tube. The droplet was observed with

a CCD camera for 600 s after dropping.

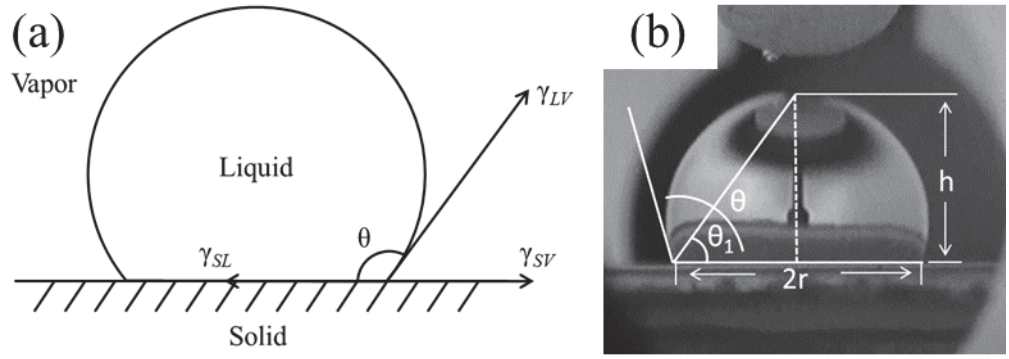

Fig. 2-4 Geometry of droplet.

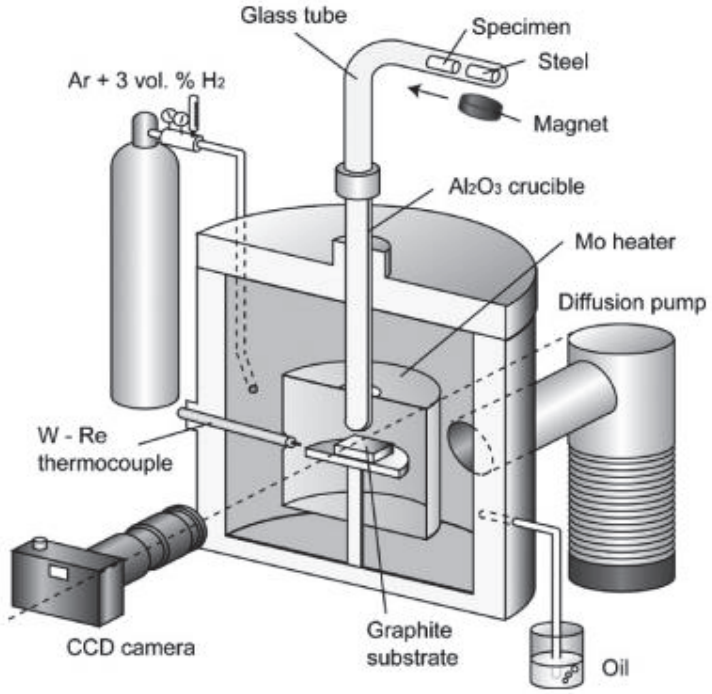

Fig. 2-5 Illustration of sessile drop device.

2.3 Results and discussion

2.3.1 Microstructure of magnesium-calcium alloys

Figure 2-6 shows the microstructures of the Mg-5Al and Mg-5Al-3Ca alloys. Morphology of Mg-5Al alloy was composed of α-Mg and irregular β-$Mg_{17}Al_{12}$ intermetallic compound along grain boundaries (Fig. 2-6(a)). In the case of containing calcium to the Mg-5Al alloy (Fig. 2-6(b)), the magnesium alloy exhibited a dendritic microstructure with Ca-containing phase along grain boundaries. WDS mapping images as shown in Fig. 2-6(c), show that aluminum existed at the same place of calcium as well as some magnesium. The existence of the $(Mg, Al)_2Ca$ phase in Mg-Al-Ca alloy have been widely recognized recently.[4-6, 26, 27] The phase was identified as a new Laves phase with a dihexagonal C36 crystal structure that was different from Mg_2Ca (C14, hexagonal) and Al_2Ca (C15, cubic). Amerioun et al.[28] indicated that with increasing Mg content x, the Laves phase structures of compounds $CaAl_{2-x}Mg_x$ were C15 ($0 \leq x < 0.24$), C36 ($0.66 < x < 1.07$), and C14 ($1.51 < x \leq 2.0$). Due to their similarity of crystal structures, it is difficult to distinguish $(Mg, Al)_2Ca$ phase from Mg_2Ca and Al_2Ca phases by X-ray diffraction analysis. Fig. 2-7 shows the results of XRD analysis. Ca-containing phases were contained in Mg-5Al-3Ca alloy, instead of β-$Mg_{17}Al_{12}$ phases in Mg-5Al alloy. Calcium addition caused decreasing of the β-$Mg_{17}Al_{12}$ phase because aluminum atoms were consumed by the formation of Ca-containing phase.

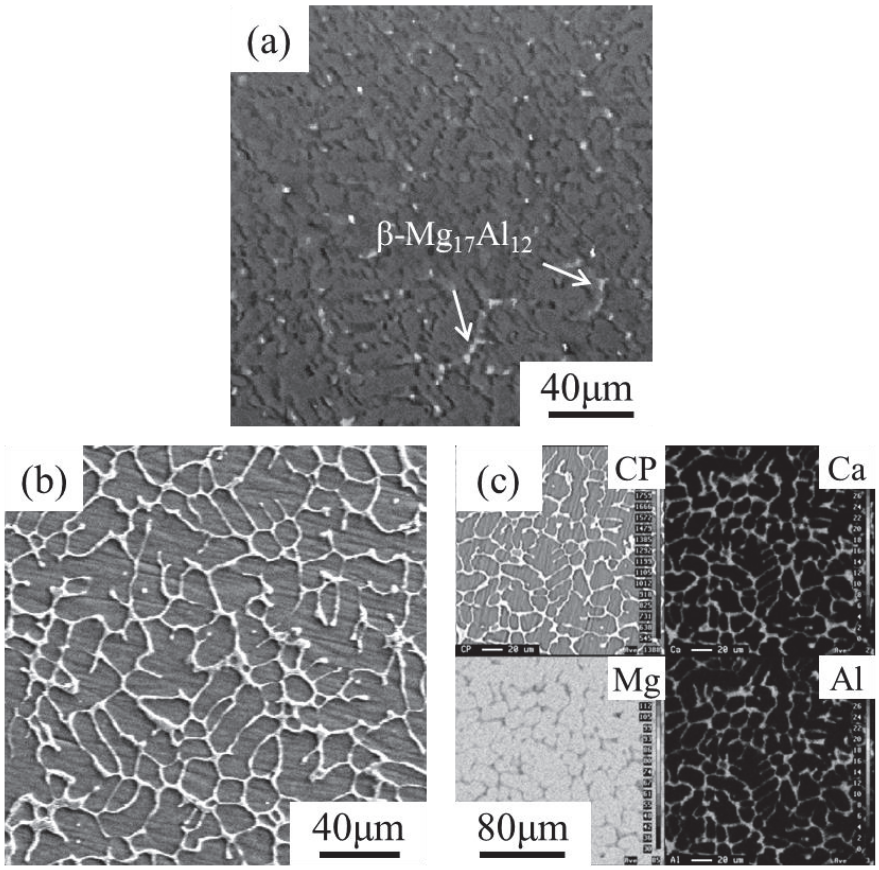

Fig. 2-6 Typical microstructure at the as-cast condition, showing of (a) SEM micrograph of Mg-5Al alloy, (b) SEM micrograph and (c) WDS mapping of Mg-5Al-3Ca alloy.

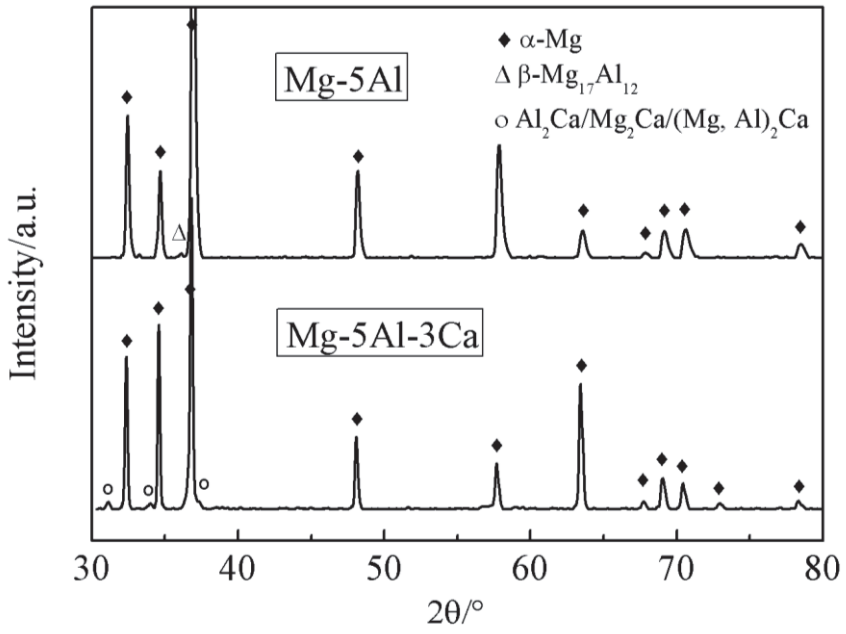

Fig. 2-7 X-ray diffraction profile of Mg-5Al and Mg-5Al-3Ca alloys.

2.3.2 Contact angle of magnesium alloys on various substrates

Figure 2-8 shows the droplets of the Mg-5Al and Mg-5Al-3Ca alloys on various substrates during contacting about 10 min at 1003K. Images of the droplets show that both the oxidation and evaporation problem of the melt encountered in previous study[17, 21] were successfully avoided during 10 min. Fig. 2-8(a) represents the Mg-5Al alloy droplet on graphite sheet. Mg-5Al alloy did not wet the graphite substrate and thus formed a spherical ball on the graphite surface.

Contact angle between the Mg-5Al alloy and the base plate of Gr was 120°. Uozumi et al. 18) reported that the contact angle between magnesium and graphite was about 120° at 1189K, and our result reasonably agreed with them. Fig. 2-8(b) shows the Mg-5Al alloy droplet on Gr-Ni. The wetting of Mg-5Al alloy on the nickel coated surface was improved slightly in comparison with that on graphite sheet surface with the contact angle decreasing to 107°. Experiments of magnesium alloys on Pure Ni showed a different behavior, as shown in Fig. 2-8(c, d). Contact angles of both Mg-5Al and Mg-5Al-3Ca alloys decreased rapidly as contact time increasing.

Figure 2-9 shows the contact angle measurements of Mg-5Al and Mg-5Al-3Ca alloys on various substrates as a function of holding time. On base plate of Gr, contact angles of Mg-5Al and Mg-5Al-3Ca alloys were similar, with the value of 120° and 119°, respectively. They showed similar tendencies with increasing of holding time. Contact angles remained stable over a period of 10 min. Calcium addition showed little effect on the wetting of magnesium alloys on Gr. Contact angle of Mg-5Al-3Ca alloy on Gr-Ni was about 110°. It also showed some improvement, although it was slightly larger than that of Mg-5Al alloy (107°). Contact angles of magnesium alloys with Gr-Ni showed slightly variation. On Pure Ni, initial contact angles of Mg-5Al and Mg-5Al-3Ca alloys were similar and relatively large in range of 92-95°. However, the contact angle of the Mg-5Al alloy stabilized at 30° after about 10 min contact, while that of Mg-5Al-3Ca alloy stabilized at 43°. Calcium addition showed negative effect on the wetting of magnesium alloys on Pure Ni. To explore the reasons underlying the differences, the samples after sessile drop test were cut in cross-section for microscopic examination.

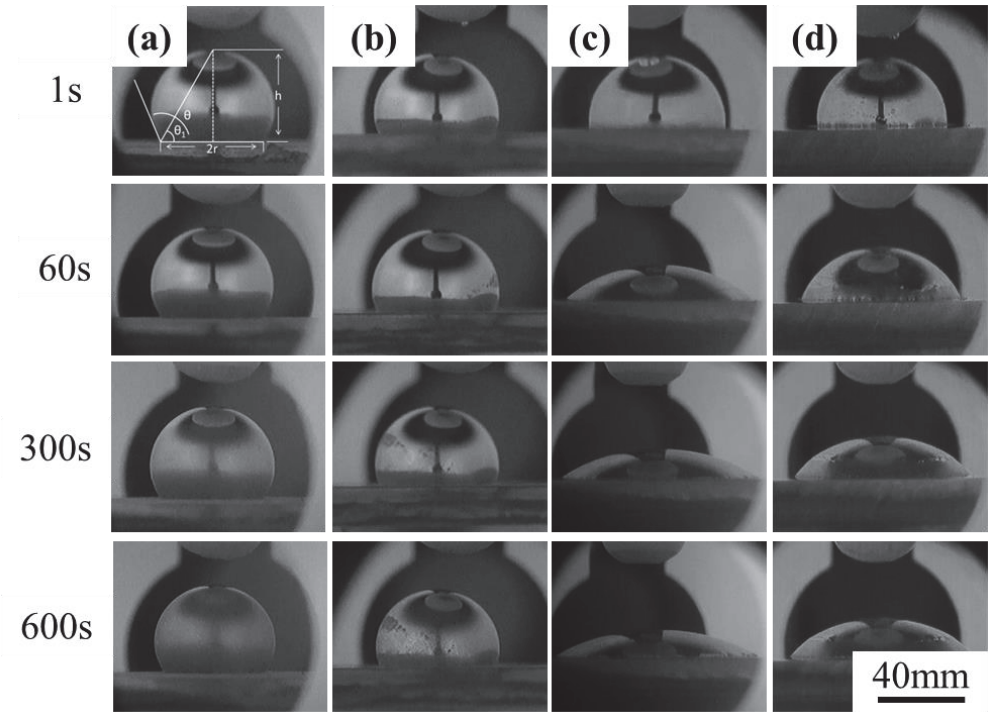

Fig. 2-8 Droplet of Mg-5Al alloy on (a) Gr, (b) Gr-Ni and (c) Pure Ni and (d) Mg-5Al-3Ca alloy on Pure Ni.

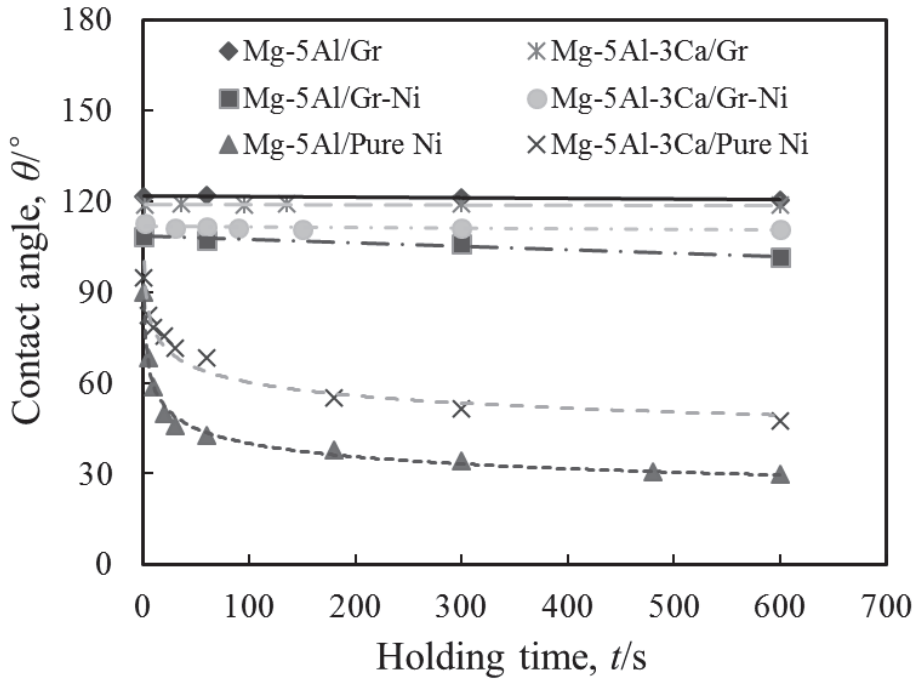

Fig. 2-9 Contact angle of Mg-5Al and Mg-5Al-3Ca alloys on various substrates.

2.3.3 Wetting of magnesium alloys on nickel coated graphite sheet

Microstructures of the droplets of Mg-5Al and Mg-5Al-3Ca alloys on nickel coated graphite sheet are shown in Fig. 2-10. As shown in Fig. 2-10(a, b), the interface between Mg-5Al-3Ca alloy droplet and graphite sheet was occupied by Ca-containing phases, while for Mg-5Al alloy the interface was mainly composed of magnesium. However, those intermetallic compounds were not supposed to affect the wetting behavior, since they all had dissolved before contacting. As shown in Fig. 2-10(c), there was no nickel observed on the surface of graphite sheet. Nickel coating had dissolved into the droplet, and formed intermetallic compounds. Since the quantity of nickel was low, there was no obvious effect observed on microstructure of the droplet of both alloys.

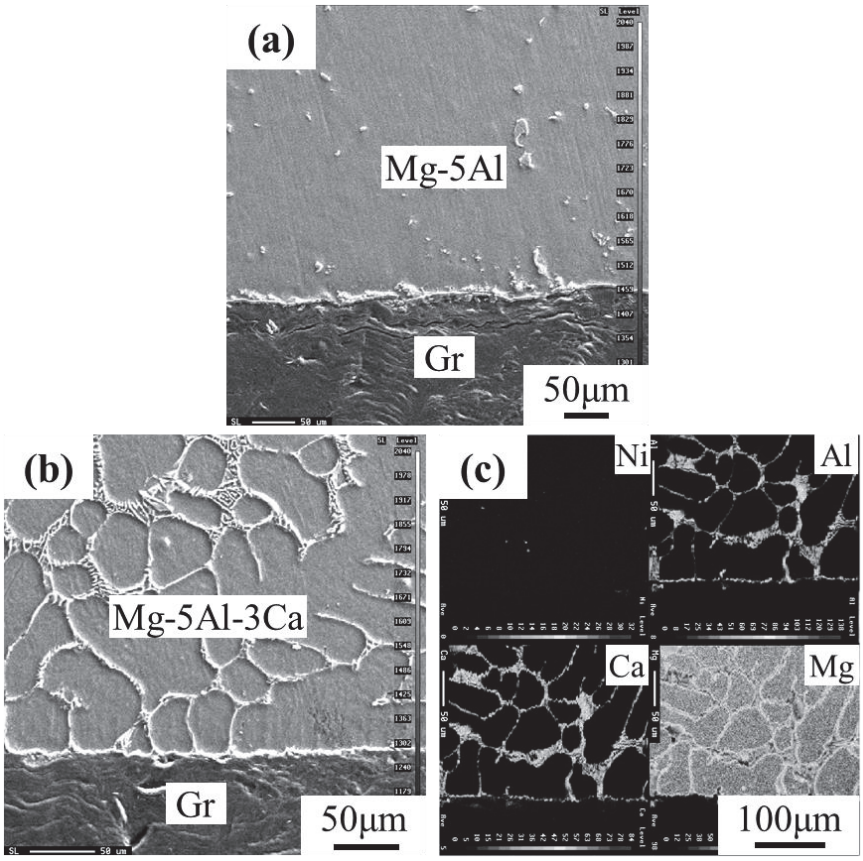

Fig. 2-10 Microstructure of magnesium alloy droplet on Gr-Ni, showing of (a) SEM micrograph of Mg-5Al alloy, (b) SEM micrograph and (c) WDS mapping of Mg-5Al-3Ca alloy.

2.3.4 Wetting behavior of magnesium alloys on nickel plate

By means of wetting behavior of magnesium alloys on pure nickel, we can infer what happened on nickel coated graphite sheet. Fig. 2-11 shows the cross-section of the Mg-5Al alloy droplet on substrate of Pure Ni. Fig. 2-11(a) is the macro metallographic image of the droplet. The white area on the bottom of the micrograph is the nickel substrate. The droplet, occupying the majority of the micrograph, had become a magnesium–nickel alloy. The thickness of nickel diffused into the magnesium alloy droplet was about 0.1mm after holding for 10 min. The coarser, rod-like compounds was identified to be Mg_2Ni phase. WDS analysis shows that those Mg-Ni phases both inside of the droplet and on the boundary were Mg_2Ni, indicated as position 1 and 2 in Fig. 2-11(d). Dark grey like position 3, which is the matrix, also contains flake-like Ni-containing phase. These fine precipitates formed during cooling after the test. In addition, there was an interesting phenomenon that the Al-Ni compounds formed a band, as shown in Fig. 2-11(b) by the arrows.

Based on the observed results, schematic of the wetting behavior of magnesium alloys on pure nickel is shown in Fig. 2-12. The wetting between magnesium alloy and nickel under chemical non-equilibrium condition occurs. Non-equilibrium develops because both the solid and liquid phases are unsaturated with respect to each other. During the non-equilibrium dynamic conditions, an interfacial reaction or diffusion of a component from one bulk phase to the other results in the lowering of the corresponding interfacial tensions.[29] Therefore, when the magnesium alloy is contacted with the nickel, nickel atoms diffuse into the melt of magnesium alloy, and then the melt turns to an Mg-Al-Ni ternary system. Nickel transfer across the interface results in a decrease in the interfacial free energy and the interfacial tension. Thus, the contact angle of the droplet on nickel plate decreases continuously until the system reaches a state of chemical equilibrium. According to the magnesium-nickel phase diagram, at 1003K, nickel becomes saturated in magnesium when the dissolved concentration of nickel rises to about 24 at. %. When nickel saturation occurs, the interfacial tension gradually increases toward their static values. Then, spreading of the droplet stops, while Mg_2Ni intermetallic compound begins to form. In addition, Al_3Ni intermetallic compounds forms at first which has a higher eutectic temperature of 1003K according

to Mg-Al-Ni ternary phase diagram. But the reason to form a band should be studied more in the future.

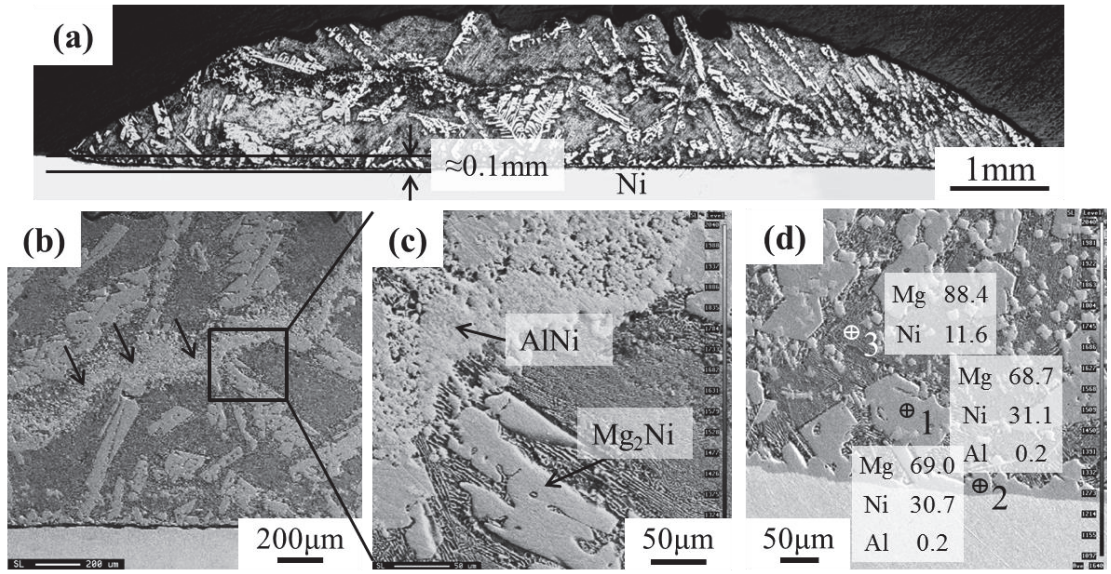

Fig. 2-11 Microstructure of Mg-5Al alloy droplet on Pure Ni. (a) overall view, (b), (c) SEM micrograph and d) WDS analysis (Atom (%)) showing chemical composition of various phases in droplet.

a. Initial contact

b. Nickel diffuse; Interfacial tension decrease; Droplet spread; Contact angel decrease.

c. Spreading stop; Nickel saturation; Mg_2Ni precipitate.

Fig. 2-12 Schematic of the wetting behavior of magnesium alloys on pure nickel.

2.3.5 Effect of calcium addition on wetting behavior of magnesium alloys

Microstructure of the Mg-5Al-3Ca alloy droplet on Pure Ni was similar to that of Mg-5Al alloy, as shown in Fig. 2-13. Coarser Mg_2Ni compounds were major components. WDS quantitative analysis of position 2 in Fig. 2-13(b) shows that calcium elements mainly distributed in the matrix of the droplet, and fine Ca-containing precipitates were possibly formed. Calcium addition showed little effect on the initial contact angle of magnesium alloy on Pure Ni, while it showed a negative effect after contacting for several minutes. Initial contact angle can be considered as a non-reactive wetting. The interfacial areas for the system are associated only with the interfacial tension. It seems that calcium addition has little influence on the non-reactive wetting of magnesium alloys on Pure Ni. During contacting, existence of calcium may hinder the diffusion rate of nickel, and reduce the solubility of nickel in magnesium alloy. Thus, the calcium addition shows negative effects on the wetting of magnesium alloy on Pure Ni. Calcium addition also hinders the spread of magnesium alloy droplet on Gr-Ni. The contact angle of Mg-5Al alloy on Gr-Ni increased from 107° to 110° for 3 mass% Calcium additions.

Since initial contact angle is in the case of non-reactive wetting, the contact angle of magnesium alloy on Gr-Ni should have been, at least, equal to the initial contact angle on Pure Ni. But contact angle of Mg-5Al alloy on Gr-Ni (107°) was much larger than that on Pure Ni (30°), even larger than the initial contact angle on Pure Ni (about 94°). In consideration of the transient reaction between the droplet and nickel, there are two possibilities to explain this question. One is that the nickel coating diffuses rapidly into the droplet, thus the wetting of Mg-5Al alloy and Gr-Ni turns to that of Mg-Al-Ni alloy and Gr. The other one is that the measured 94° is the contact angle of Mg-Ni alloy on Pure Ni, and in this case, the actual contact angle at initial contact between Mg-5Al alloy and Pure Ni should be larger than 94°.

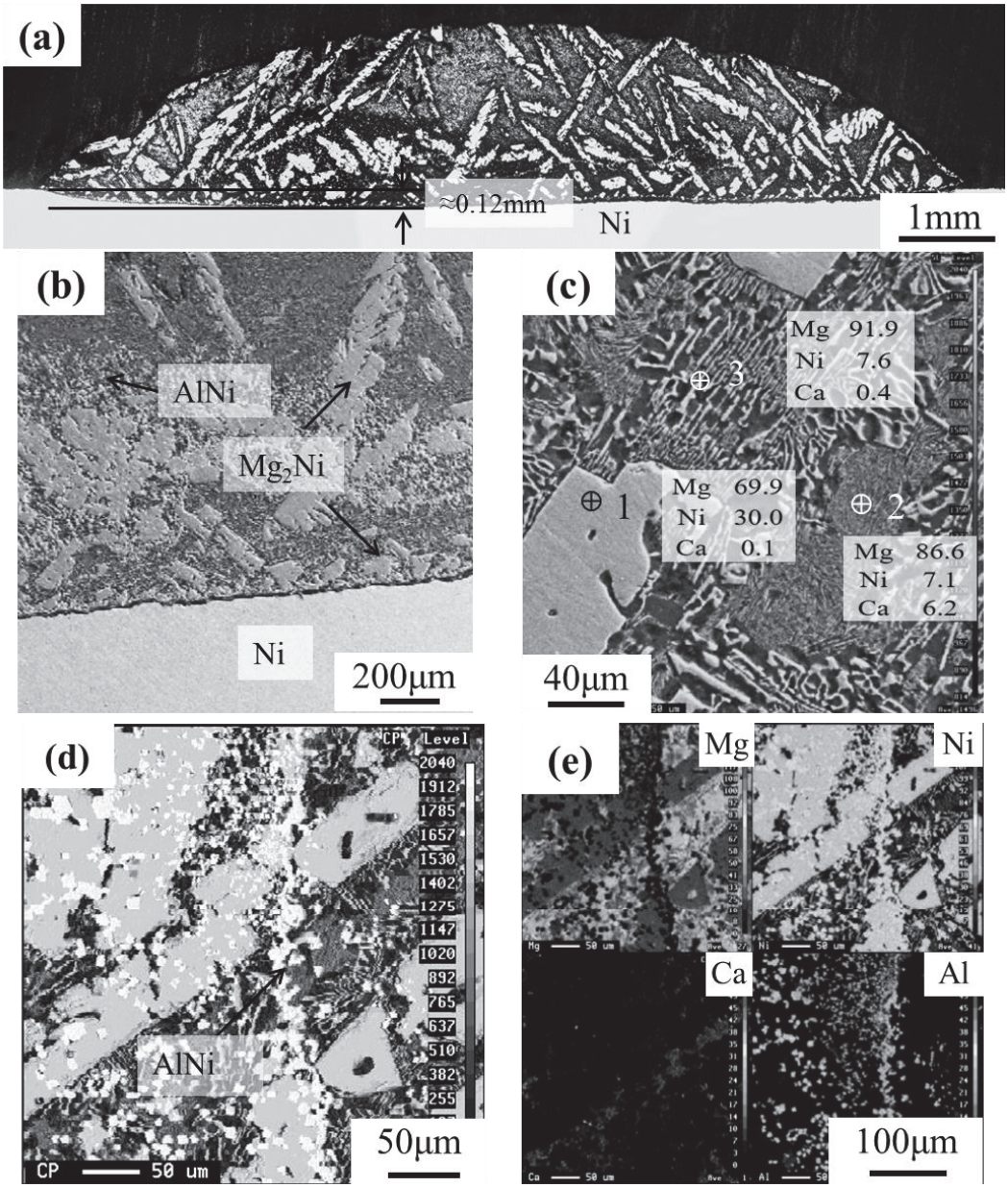

Fig. 2-13 (a) SEM micrograph of Mg-5Al-3Ca alloy droplet on Pure Ni and (b) WDS analysis (Atom (%)) showing chemical composition of various phases in droplet.

2.4 Summary

(1) Microstructure of Mg-5Al alloy consisted of β-$Mg_{17}Al_{12}$ intermetallic phase in the α-Mg matrix. Additions of 3 mass% Calcium suppressed the formation of the β phases, and encouraged the formation of the $(Mg, Al)_2Ca$ phases in the shape of continuous network.

(2) Mg-Al alloys did not wet graphite sheet with the contact angle of about 120°. The droplet of magnesium alloy on Pure Ni spread rapidly. Improvement of wettability of magnesium alloy on Gr-Ni was achieved through the dissolution of nickel into the liquid magnesium alloy at the interface between droplet and substrate.

(3) Mechanism for the wetting behavior between liquid magnesium alloys and solid nickel at 1003 K was proposed. Nickel dissolved into magnesium alloy during contacting. Spreading of the droplet stopped when nickel saturation occurred and Mg_2Ni intermetallic compound began to form.

(4) Calcium addition had no effect on the wetting of magnesium alloy on Gr, while it showed negative effect on the Pure Ni, and slightly hindered the spread of magnesium alloy droplet on Gr-Ni.

References

1) R. Brown: International magnesium association 55th annual world conference, (Light Metal Age, Chicago, 1998) pp. 86-93.
2) B.L. Mordike and T. Ebert: Mater. Sci. Eng. A **302** (2001) 37-45.
3) R. Ninomiya, T. Ojiro and K. Kubota: Acta Metall. Mater. **43** (1995) 669-674
4) A.A. Luo, M.P. Balogh and B.R. Powell: Metall. Mater. Trans. A **33** (2002) 567-574.
5) L. Han, H. Hu and D.O. Northwood: Mater. Lett. **62** (2008) 381-384.
6) S.W. Xu, N. Matsxumoto and K. Yamamoto: Mater. Sci. Eng. A **509** (2009) 105-110.
7) L. H. Peebles: Carbon Fibers: Formation, Structure, and Properties, (CRC Press, Boca Raton, 1995).
8) S. Paprocki, D. Kizer and W. Meyerer: Proceedings of the 24th National Symposium and Exhibition, (The Enigma of the Eighties: Environment, Economies Energy, San Francisco, California, 1979) pp.1451-1457.
9) Y. Kagawa and E. Nakata: J. Mater. Sci. Lett. **11** (1992) 176-178.
10) S.S. Tompkins, K.E. Ard, R.G. Sharpe, J.T. Hoggett, S.G. Hill and J.C. Johnson: Proceedings of the 18th International SAMPE Technical Conference SAMPE, (Seattle, WA, 1986) pp. 623-637.
11) G. G. Tibbetts, M. L. Lake, K. L. Strong and B. P. Rice: Compos. Sci. Tech. **67** (2007) 1709-1718.
12) E. Hammel, X. Tang, M. Trampert, T. Schmitt, K. Mauthner, A. Eder and P. Pötschke: Carbon **42** (2004) 1153-1158.
13) Z. F. Xu, Y. B. Choi, K. Matsugi, D. C. Li and G. Sasaki: Mater. Trans. **51** (2010) 510-515.
14) W. Shi, M. Kobashi and T. Choh: Mater. Trans. JIM **41**(2000)335-338.
15) N. Shinozaki, J. Morita and K. Wasai: J. Jpn. Inst. Light Met. **55** (2005) 310.
16) H. Uozumi, K. Kobayashi and K. Nakanishi: Mater. Sci. Eng. A **495** (2008) 282-287.
17) G. Sasaki, Y. Hara, Z. F. Xu, K. Sugio, H. Fukushima, Y. B. Choi and K. Matsugi: Mater. Sci. Forum **654-656** (2010) 2692-2695.

18) T. Matsunaga, M. Yoshida, G. Sasaki, J. Pan, T. Fujii, N. Fuyama and H. Fukunaga: Proceedings of the 8th Japan International SAMPE Symposium, (November 2003) pp.773-776.
19) M. Yoshida, T. Matsunaga, K. Ogata, T. Hatayama and K. Shinozaki: Mater. Sci. Forum **539-543** (2007) 877-882.
20) S.W. Ip, R. Sridhar and J.M. Toguri: Mater. Sci. Eng. A **244** (1998) 31-38.
21) J. Rams, A. Urena and M.D. Escalera: Composites **38** (2007) 566-575.
22) Y.M. Ryu, E.P. Yoon and M.H. Rhee: J. Mater. Sci. Lett. **19** (2000) 1103-1105.
23) P.K. Rohatgi, V. Tiwari and N. Gupta: J. Mater. Sci. **41** (2006) 7232-7239.
24) T.F. Stephenson, A.E.M. Warner and S. Wilson: Aluminum Hybrid Composites Containing Nickel-Coated Graphite Particulate, (Processing Properties and Applications of Cast Metal Matrix Composites, 1996) pp 337-351.
25) J.A.E. Bell, T.F. Stephenson and A.E.M. Warner: Physical properties of graphitic silicon carbide aluminum metal matrix composites, (SAE Technical Paper 970788, 1997).
26) A. Suzuki, N.D. Saddock, J.W. Jones and T.M. Pollock, Scr. Mater. **51** (2004) 1005-1010.
27) S.M. Liang, R.S. Chen, and J.J. Blandin: Mater. Sci. Eng. A **480** (2008) 365-372.
28) S. Amerioun, S.I. Simak, U. Häussermann, Inorg. Chem. **42** (2003) 1467-1474.
29) I.A. Aksay, C.H. Hoge and J.A. Pask: J. Phys. Chem. **78** (1974) 1178–1183.

Chapter 3

Fabrication of VGCF-Reinforced Magnesium Matrix Composites by Low Pressure Infiltration

3.1 Introduction

Magnesium matrix composite is one of the lowest density metal matrix composites, and has high specific strength, specific stiffness and excellent mechanical, physical properties [1)]. It has been the focus of metal-matrix composites (MMCs) field, and applied to the field of aerospace, automobile and military industry. Carbon fibers possess excellent mechanical, thermal properties and low density [2)]. Among various short carbon fibers, vapor-grown carbon fibers (VGCFs) are increasingly used in various composites owing to their excellent properties and low cost [3)]. Based on magnesium alloys development for elevated temperature application, the magnesium-calcium alloy-based composites reinforced with VGCFs are supposed to possess satisfactory high-temperature properties.

Liquid-metal impregnation method such as squeeze casting enable highly formable metal-matrix composites (MMCs) to be efficiently fabricated. The high pressure during squeeze casting process can effectively facilitate wetting, and eliminate defects [4)]. However, the squeeze casting process needs complex facilities and is high cost. The high pressure can also cause fiber fracture and/or inhomogeneous fiber distribution. Besides, a preform with high compressive strength is needed. On the other hand, the low pressure infiltration (LPI) process is one of the promising infiltration methods by using low applied pressure [5)]. It was also known that the LPI process for the composite materials enabled relatively simple facilities, cost-effective and complex shape fabrication. Moreover, a porous preform can be used to decrease the infiltration pressure. What is more, nickel coating on graphite can improve the wettability with magnesium alloy [6)].

In the present study, wettability of the basal plane of graphite and nickel coated graphite against molten magnesium alloy was examined. Moreover, by the measured contact angle, the threshold pressure for infiltration molten magnesium alloy into VGCF preform was estimated. The porous VGCF preforms were prepared, and the compression test on the preform was carried out in order to determine the infiltration pressure. Moreover, VGCF reinforced magnesium matrix composites was fabricated by infiltration of magnesium alloy into nickel coated porous preform.

3.2 Experimental methods

3.2.1 Manufacturing of VGCF porous preforms

150-nm-diameter, 10-20-μm-length VGCFs (Showa Denko Co., Japan) and as-received 2-μm diameter mesophase pitch (MP) microparticles (JFE Chemical Co., Japan) were used to fabricate the VGCF preform. MP was used as the crosslinker, and NaCl (180~355μm) was used as the spacer material. Fig. 3-1 shows the schematic illustration of the sintering process and preform specimen. The NaCl, VGCFs and MP powders with the composition of the preforms as shown in Tab. 3-1 were mechanically mixed for 10min. Then the mixture was put into a 10-mm-diameter graphite mold, and pressed at 64 MPa. The molded mixture was then heated at 773K for 1.5h. Sintered compact was then immersed into distilled water to dissolve NaCl, and formed porous VGCF-MP preform.

Tab. 3-1 Composition (wt. %) of the preforms.

	NaCl:Powders	Powders
		VGCF:MP
1	7:3	3:7
2		5:5
3		7:3
4	8:2	3:7
5		5:5
6	9:1	3:7

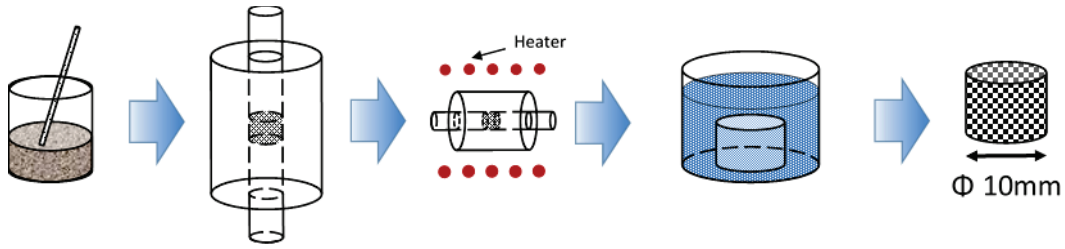

Fig. 3-1 Schematic illustration of the sintering process and preform specimen.

3.2.2 Nickel coating of VGCF preforms

Nickel coating was prepared on the pore walls inside of the preform by an electroless deposition process. Prior to electroless plating, the preform was pre-treated. The preform was degreased rosin with acetone and rinsed with pure water. Then they were etched with 1.69 mol dm^{-3} HNO_3, sensitized with a 5.9×10^{-2} mol dm^{-3} $SnCl_2\cdot2H_2O$ + 0.24 mol dm^{-3} HCl solution, and activated with a 2.3×10^{-3} mol dm^{-3} $PdCl_2$ + 0.48 mol dm^{-3} HCl solution. After filtration and rinsing, the preform was immersed in a nickel electroless plating bath at 363K. Fig. 3-2 shows the illustration of the equipment for electroless deposition. The pH of the bath was adjusted to 6.5 by the addition of NH_3 solution. All the solution was pumped through the preform. After rinsing, electroless plated preform was dried for 60 min at 363K.

Compression test of the porous preform was carried out with the Shimadzu universal testing machine (Autograph DCS-R-5000). The test was performed at room temperature with the crosshead speed of 0.5 mm/min. The compressive strength and compressive behavior can be used to determine the infiltration pressure of the molten Mg. In infiltration process, the buckling strength and elastic modulus of the VGCF preform are important factor to prevent buckle by threshold pressure and minimize compressive deformation of the VGCF preform.

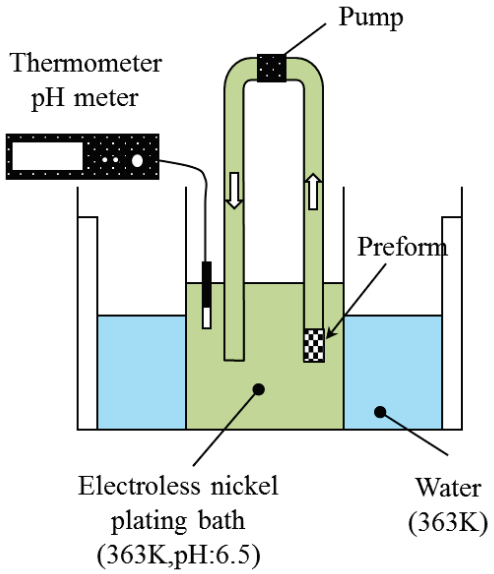

Fig. 3-2 Illustration of the equipment for electroless deposition.

3.2.3 Low pressure infiltration

Magnesium matrix composite was fabricated with infiltrating magnesium alloy into the Ni-coated porous preform by low pressure infiltration method. Fig. 3-3 shows the illustration of the equipment for low pressure infiltration. The alloy and preform were placed in a die, and preheated to 973K to melt the alloy. Then the pressure was applied to infiltrate molten metal into the preform. Low pressure infiltration parameters are shown in Table 3-2.

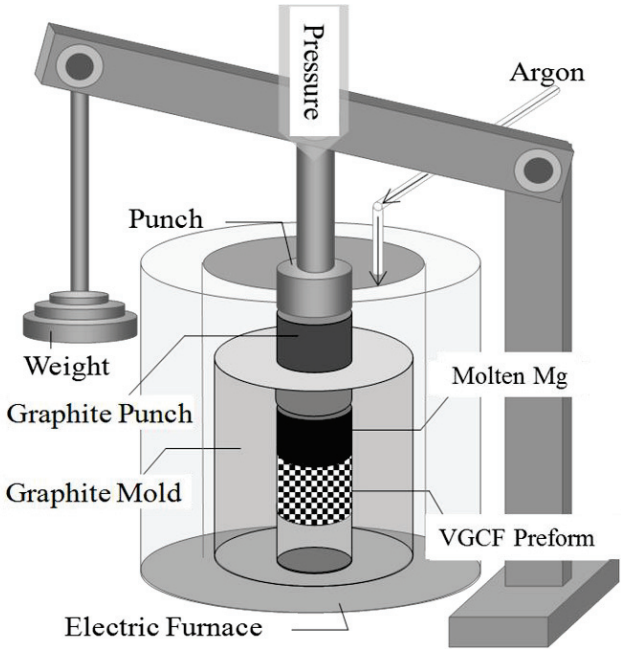

Fig. 3-3 Illustration of the equipment for low pressure infiltration.

Tab. 3-2 Conditions of low pressure infiltration.

	Parameter
Infiltrating temperature (K)	973
Atmosphere	Argon
Pressure (MPa)	1
Pressure time (min)	10
Cooling rate	Furnace cooling

3.2.4 Microstructure and property evaluation

Microstructure of the preform and magnesium matrix composite was observed using scanning electron microscopy (SEM; Hitachi, S-5200, 6-15kV) and electron probe micro-analyzer (EPMA, JXA-8900RL).

3.3 Results and Discussion

3.3.1 Microstructure of VGCF preforms

Figures 3-4 shows the microstructure of the porous VGCF preform with different composition. Pores were generated with the dissolution of NaCl particles. As ahown in Fig. 3-4, the pores were square shape and size of 180-350 μm, same with NaCl particle. With NaCl content increasing, the amount of the pores increased obviously. Accordingly, the porosity of the preform increased. Furthermore, the pores turned to open pores which are connect with other pores.

As shown in Fig. 3-5, when the ratio of VGCF and MP was 3:7, the MP enclosed rather than bridged the VGCFs. It showed some large lumps of MP including VGCFs. the MP bridged the VGCFs which were randomly oriented. The VGCFs could also be bridged together with 30% MP, although the preform was weak. The MP transformed into a liquid crystalline material when heated in the range 623-773 K and thereafter hardened into “coke” [8].

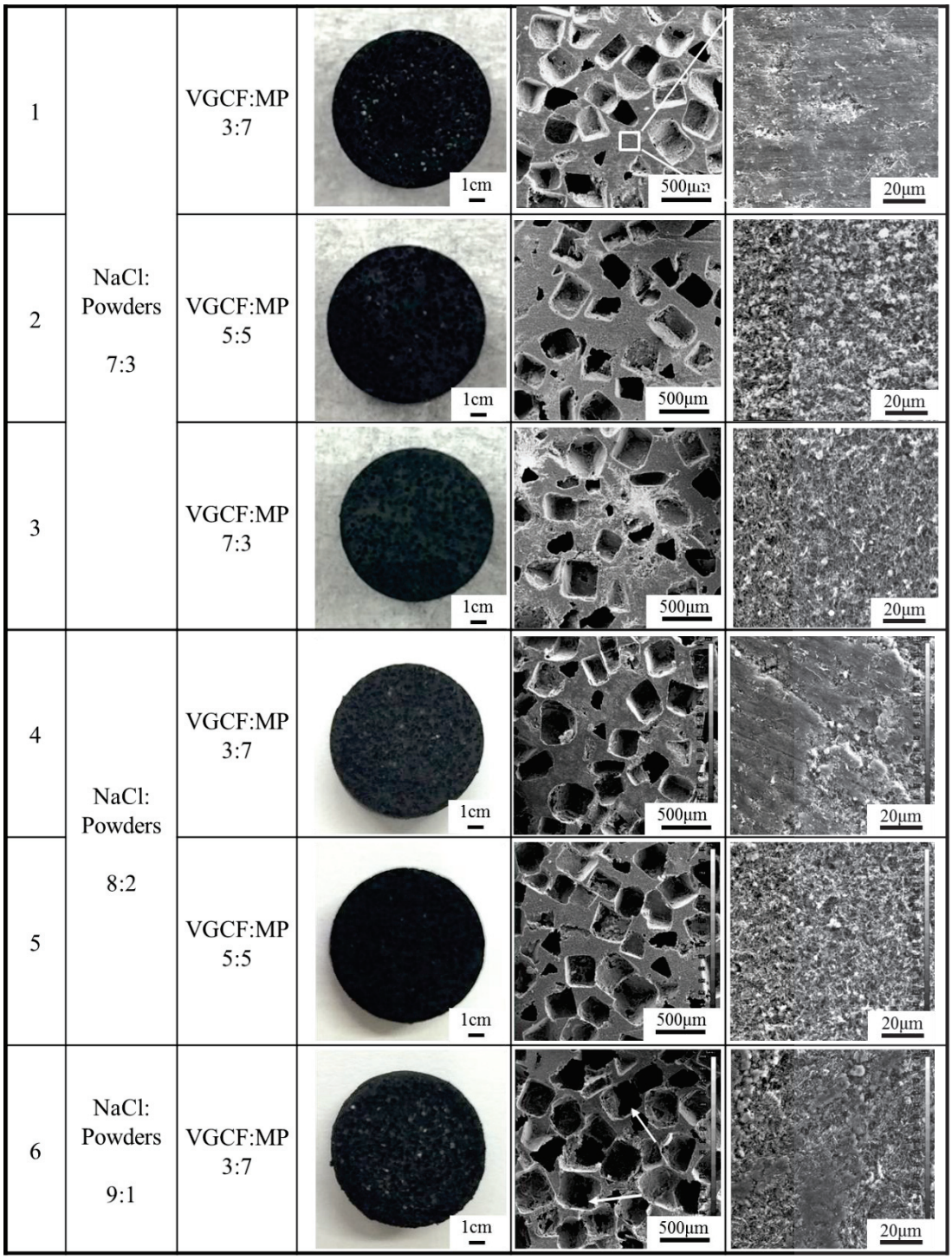

Fig. 3-4 Microstructure of the preform with different composition.

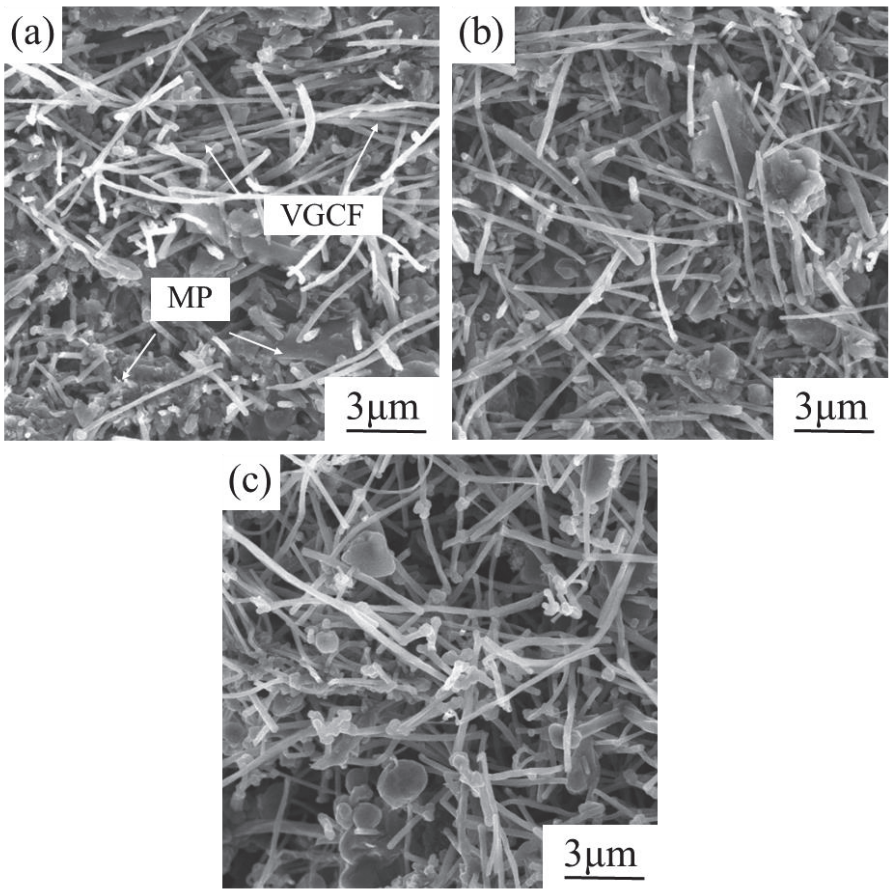

Fig. 3-5 Microstructure of the preform with VGCF:MP of (a) 3:7, (b) 5:5, and (c) 7:3.

3.3.2 Compressive property of VGCF preforms

Figure 3-6 shows the compressive stress-strain curves of the porous preform. In the first elastic deformation region, stress increased linearly with increasing strain. The yield strength of preform with different composition were similar, with the value about 2 MPa. Then a long plateau of plastic deformation with slight stress fluctuation generated. Compression and fracture of the pores started to occur to absorb energy against the applied load, with the presence of some small cracks, as indicated by red circle in Fig. 3-6. When compressive strain developed to about 15%, a final densification region is observed where the stress raised rapidly to a peak value. Then the compressive strength began to decrease, due to the appearance of the penetrating cracks, as indicated by white circle in Fig. 3-6.

Figure 3-7 shows the compressive stress-strain curves of the porous preform with different weight fraction. The maximum stress of preform decreased, with the porosity increasing from 70% to 90%. Even a peak stress was not formed, in the condition of 90% porosity. On the other hand, the preform with the VGCF content of 30% showed similar maximum stress with the 50% VGCF preform, although the bonding area of MP and VGCFs was relatively wide. However, when the VGCF content increase to 70%, small cracks continuously occur from the beginning of the compressive test, combing with little elastic deformation and plastic deformation.

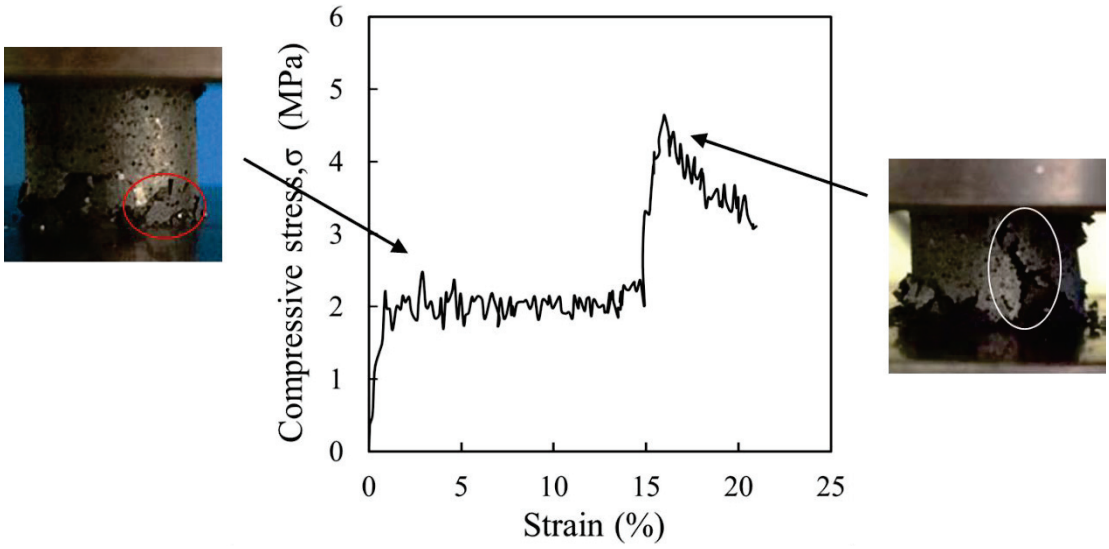

Fig. 3-6 Compressive stress-strain curves of preform with VGCF:MP of 5:5.

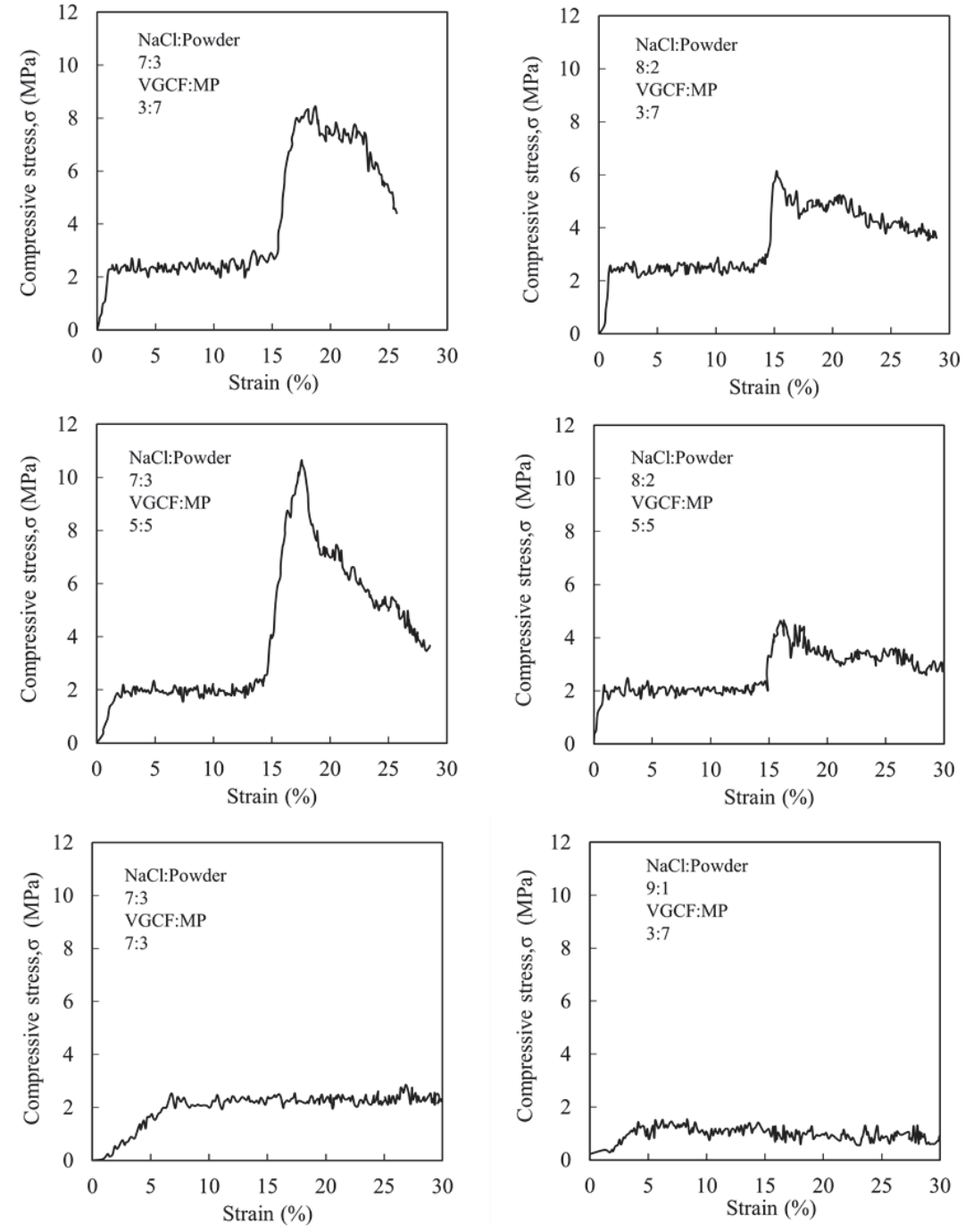

Fig. 3-7 Compressive stress-strain curves of preform with different composition.

3.3.3 Nickel coating in porous VGCF preform

The nickel coated preform is shown in Fig. 3-8. As shown in the cross-section of the preform, almost all of the pores walls were covered with nickel coating. The thickness of the nickel coating was about 1-2 μm.

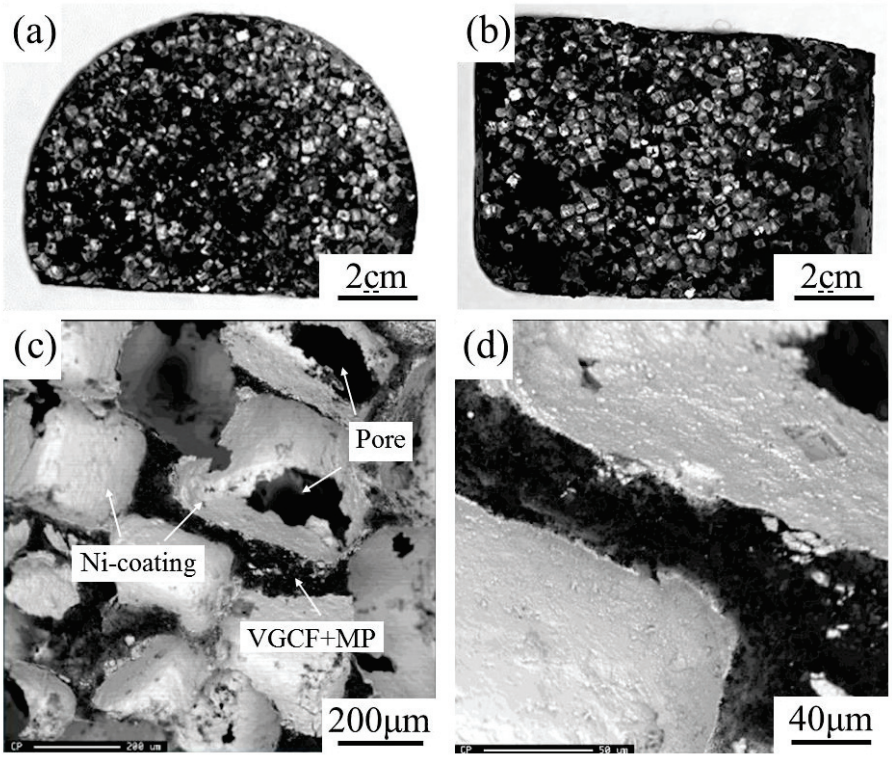

Fig. 3-8 (a) Horizontal section, (b) vertical section, and (c), (d) compo image of the nickel coated preform.

3.3.4 VGCF reinforced magnesium composites

Fig. 3-9 shows the bottom surface of the composites after infiltration. For the preform without Ni-coating (Fig. 3-9a, b), only a part of the preform was infiltrated with the matrices. But for the preform with Ni-coating (Fig. 3-9c, d), it was infiltrated completely. Thus, fabrication of VGCF reinforced magnesium composites by low pressure infiltration was succeeded. These kinds of composites fabricated by low pressure infiltration have not been reported. In addition, the compressive deformation of VGCF preforms was not found in the obtained composites.

Fig. 3-10 shows the microstructure of the composite after infiltration for Ni-coated preform. Nickel coating diffused into the magnesium alloys during infiltration. Al_3Ni intermetallic compounds form and aggregate on the walls of the preform. Along grain boundaries, Mg_2Ni phase forms instead of $(Mg, Al)_2Ca$ phase.

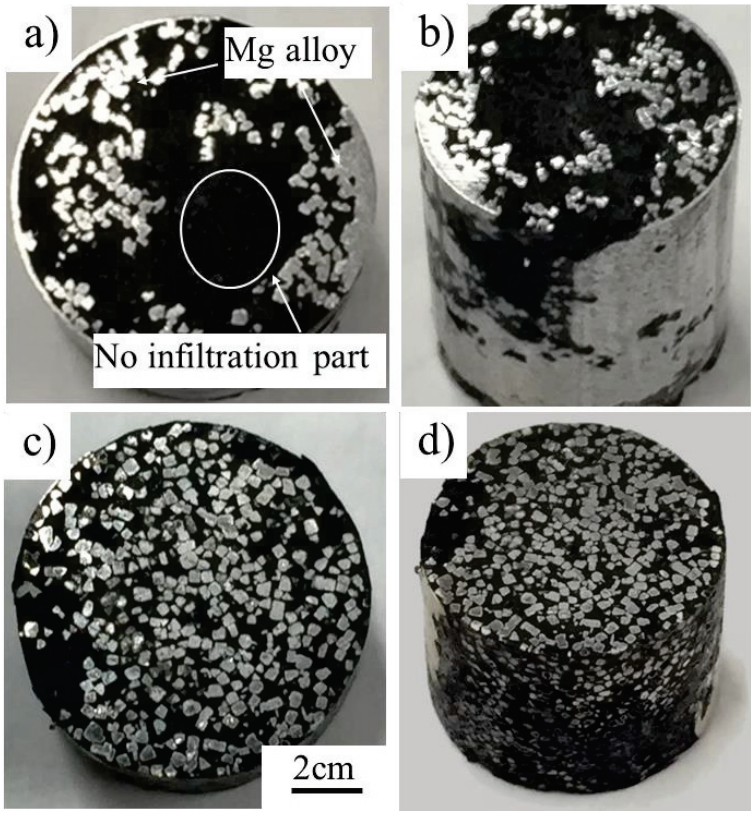

Fig. 3-9 The bottom surface of the composites after infiltration for a) preform without Ni-coating and b) Ni-coated preform.

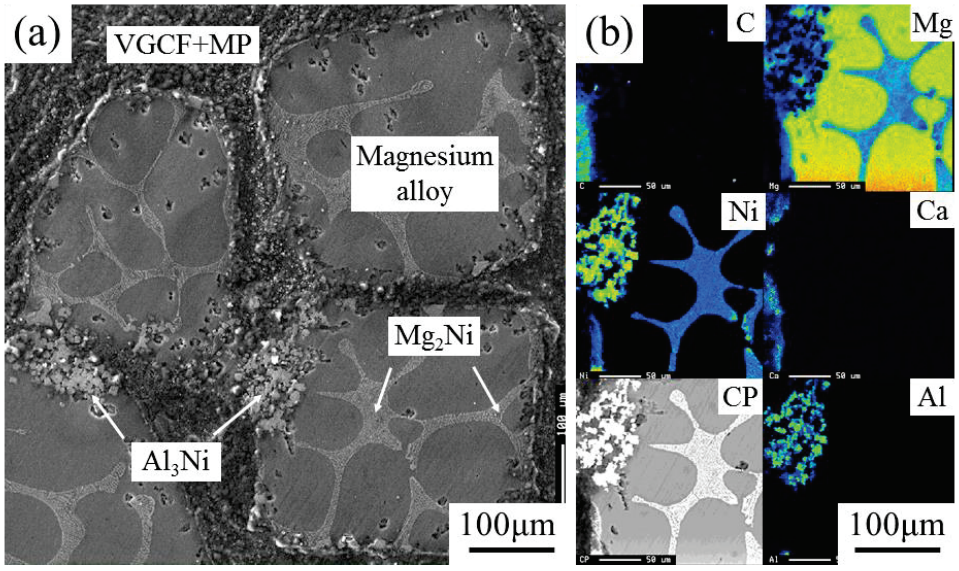

Fig. 3-10 Microstructure of the composite after infiltration for Ni-coated preform.

3.3.5 Calculation of threshold pressure for infiltration

Figure 3-11 shows the droplets of the Mg-5Al-3Ca alloys on various substrates during contacting about 10 min at 1003K. Fig. 3-11a represents the Mg-5Al-3Ca alloy droplets on the base plate of graphite sheet. Mg-5Al-3Ca alloy did not wet the graphite substrate and thus formed a spherical ball on the graphite surface with a contact angle of 119°. Fig. 3-11b shows the Mg-5Al-3Ca alloy droplets on nickel coated graphite sheet. The wetting of Mg-5Al-3Ca alloy on the graphite surface with about 2 μm thick nickel coating was improved slightly with the contact angle decreasing to 110°. Improvement of wettability of magnesium alloy on Gr-Ni was achieved through the dissolution of nickel into the liquid magnesium alloy at the interface between droplet and substrate. When the contact angle is more than 90º, external force is necessary to infiltrate molten metal into carbon fibers. The work of external force per unit area, W, can be estimated by using Young's equation

$$W = \gamma_{SL} - \gamma_{SV} = -\gamma_{LV}\cos\theta$$

where θ (deg.) is contact angle between molten metal and carbon fibers, and γ_{SL}, γ_{SV} and γ_{LV} are solid/liquid, solid/vapor and liquid/vapor interfacial energies, respectively. With nickel coating on graphite sheet, the wettability of magnesium alloy was improved,

and the contact angle became smaller. Thus, the necessary work of external force to infiltrate molten metal into carbon fibers was decreased.

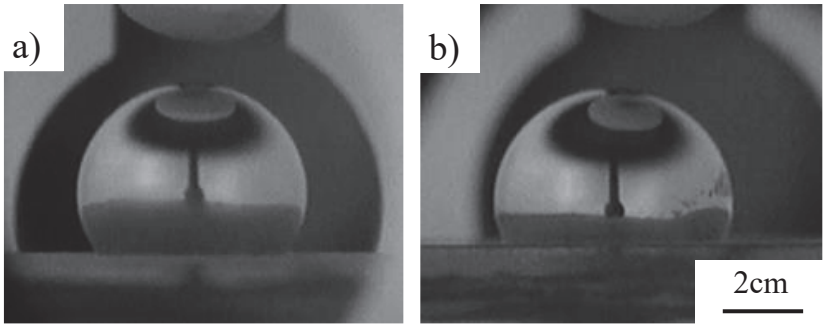

Fig. 3-11 Droplet of Mg-5Al-3Ca alloy on (a) Gr and (b) Gr-Ni.

To compare the threshold pressure with the applied pressure to the VGCF preform, the threshold pressure was estimated. The threshold pressure P_c [9] was described by

$$P_c = -\gamma_{LA} cos\theta * S$$

S is the fiber surface area per unit volume of metal matrix. In the condition of porous preform, S can be taken as the surface area of the pores per unit volume of metal matrix. For the cube pores of edge length a occupying a porosity V_p,

$$S = \frac{6}{a}$$

Thus, the final expression is:

$$P_c = -\frac{6\gamma_{LA} cos\theta}{a}$$

For the surface tension of pure magnesium, 0.559 N/m was used for a first approximation. The minimum size edge length of the NaCl particle 180 μm was used as a. For the contact angle, experimental values of contact angle on the basal plane of Gr and Gr-Ni were used. Taken the contact angle on the basal plane of Gr as 119°, the estimated threshold pressure $P_{c–Gr}$ was 0.010 MPa. This is much smaller than the applied pressure 1MPa. It is because in this model, all pores are taken as perforative pores. Actually, the through-hole between the pores in the preform should be much smaller than 180 μm. So, the actual threshold pressure must be larger than the estimated

value. In addition, even with the shielding gas, oxidation could form on the surface of magnesium alloy. The oxidation could hinder the wetting of magnesium and preform. Thus, under the applied pressure 1MPa, the molten magnesium alloy infiltrated into the preform, but it was difficult to infiltrate the preform completely. With nickel coating, the wettability of magnesium alloy on the preform was improved. For the contact angle on Gr-Ni of 110°, the estimated threshold pressure $P_{c–Gr\text{-}Ni}$ was 0.7 $P_{c–Gr}$. With nickel coating, the preform was infiltrated with the magnesium alloy completely.

3.4 Summary

The effect of nickel coating on infiltration behavior of magnesium alloy into VGCF preform was investigated. Fabrication of VGCF-reinforced magnesium alloy composites was carried out by low pressure infiltration. The result was shown as follow:

(1) Wettability of Mg-5Al-3Ca alloys on graphite sheet was poor with contact angle of about 119°. With nickel coating on graphite sheet, the contact angel decreased to 110°.

(2) Infiltration pressure for magnesium alloy into porous VGCF preform was determined to be 1 MPa, considering with both the estimated threshold pressure and the compression strength of the preform. Magnesium alloy was successfully infiltrated into nickel coated porous preform, while the magnesium alloy was partially infiltrated into the preform without nickel coating.

References

1) R. Oakley, R. F. E. Cochran, and R. Stevens: Key Eng. Mater. **104** (1995) 387-416.
2) Y. Kagawa, and E. Nakata: J. Mater. Sci. Lett. **11** (1992) 176-178.
3) E. Hammel, X. Tang, M. Trampert, T. Schmitt, K. Mauthner, A. Eder, and P. Pötschke: Carbon **42** (2004) 1153-1158.
4) H. Hu. J. Mater. Sci. **33** (1998) 1579-1589.
5) G. Sasaki, Y. Hara, Z. F. Xu, K. Sugio, H. Fukushima, Y. B. Choi, and K. Matsugi: Mater. Sci. Forum. **654** (2010) 2692-2695.
6) Y. Y. Yao, Z. F. Xu, K. Sugio, Y. B. Choi, S. M Kang, R. D. Fu, and G. Sasaki: Mater. Trans. **56** (2015) 1693-1697.
7) H. Uozumi, K. Kobayashi, and K. Nakanishi: Mater. Sci. Eng. A **495** (2008) 282-287.
8) Y. Sato, Y. Kikuchi, T. Nakano, G. Okuno, K. Kobayakawa, T. Kawai, and A. Yokoyama: J. Power Sources **81-82** (1999) 182-186.
9) A. Mortensen, and J. A. Cornie: Metall. Trans. **18A** (1987) 1160-1163.

Chapter 4

Fabrication of VGCF-Reinforced Mg-Al-Ca Alloy Composites by Compo-casting Process

4.1 Introduction

Vapor-grown carbon fibers (VGCFs) possess attractive mechanical, electrical, and thermal properties, with a carbon structure similar to that of carbon nanotubes.[1, 2] VGCFs have attracted much attention in various fields, and have been particularly considered as an ideal candidate for the reinforcement of multifunctional composites and engineering applications. Recent studies on the use of carbon nanofibers in light metal matrix composites have mainly involved the enhancement of the mechanical properties,[3, 4] along with the modification of the electrical conductivity,[5, 6] thermal conductivity and coefficient of thermal expansion.[7, 8]

A magnesium matrix composite has one of the lowest densities of metal matrix composites, has along with a high specific strength and specific stiffness, and excellent mechanical and physical properties. It has been given attention in the metal-matrix composite field, and applied in the aerospace, automotive, and military filed. Mg-Al-Ca alloys have been developed for elevated temperature applications.[9-12] The addition of calcium significantly improves their high-temperature strength, creep resistance, and oxidation resistances. To enhance the strength and rigidity of the matrix, VGCFs can be used to reinforce Mg-Al-Ca alloy, which are supposed to give them satisfactory mechanical properties at both room and elevated temperatures.

Among the variety of manufacturing processes available for discontinuous metal matrix composites, stir casting is easily adaptable and economically viable. Its advantages lie in its simplicity, flexibility, and applicability to large-volume production. However, there are some problems associated with the stir casting of metal matrix composites, including poor wettability and the heterogeneous distribution of the reinforcement material.

The poor wettability of the reinforcement in the melt prevents the reinforcement from infiltrating the molten matrix, with the result that it simply floats on the melt surface. This is due to the surface tension, very large specific surface area, and high interfacial energy of the reinforcements, along with the presence of oxide films on the melt surface. Compo-casting is a liquid state process in which the infiltration of reinforcement into a semi-solid metal (SSM) can be facilitated by means of agitation. In this process, after

the material is completely melted, the melt is cooled to a semi-solid state, and the preheated reinforcements are added and mixed. Then, the slurry is again heated to a fully liquid state and mixed thoroughly. Reduced fluidity can be achieved in the SSM by means of shearing.[13] The primary solid particles already formed in the SSM can mechanically entrap the reinforcing particles, prevent their gravity segregation, and reduce their agglomeration,[14–16] which will result in better distribution of the reinforcement particles.

The uniform distribution of the reinforcement within the matrix and its bond strength with the matrix are essential structural requirements for a stronger metal matrix composite. The wettability and distribution of the reinforcement become more difficult because of the small size of VGCFs. This is due to the large surface area and surface energy of the particles, which cause an increasing tendency for agglomeration. Thus, an intermediate layer of nickel is coated on the carbon fibers to facilitate the wetting. Liquid metals almost always wet solid metals, and the highest wettability is found in the case of mutual solubility or the formation of inter-metallic compounds. Infiltration is thus made easier by the desorption of a metallic coating on the surface of the reinforcing solid.[17] Nickel is frequently used for coating reinforcement particles used with aluminum-based composites.[18-21] It has been found that nickel coatings can improve the wetting behavior of carbon fibers by molten aluminum and limit fiber segregation to obtain a homogeneous reinforcement distribution. Our previous study revealed that an improvement in the wettability of a magnesium alloy on a nickel-coated graphite sheet was achieved through the dissolution of the nickel into the liquid magnesium alloy.[22]

In this study, Ni-coated VGCF-reinforced Mg-Al-Ca alloy composites were fabricated using a compo-casting process. Then, the effects of the Ni-coated VGCFs on the microstructure and mechanical properties of the magnesium alloy were investigated, as well as the strengthening mechanism of the Ni-coated VGCF-reinforced Mg-Al-Ca alloy composites.

4.2 Experimental methods

4.2.1 Materials

Magnesium-calcium alloys are used as the matrix. Some research indicated that when the calcium level was about 1%, casting defects such as cold shuts, hot cracking, and die sticking of Mg-Al-Ca alloys were very severe. However, such problems diminished or significantly reduced when calcium levels were above 2%. Thus, the magnesium alloys used as the matrix alloys are with calcium levels above 2%. The Mg-5Al and Mg-5Al-3Ca (AX53) alloys were fabricated by Permanent Mold casting. The Mg-6Al-2Ca (AZX612) alloy (Gonda Metal Industry Co. Ltd.) is used for comparison. The chemical compositions (mass %) of the magnesium alloys are shown in Table 4-1.

Table 4-1 Chemical composition of magnesium alloys.

Nominal composition	Analyzed contents (mass %)				
	Al	Ca	Zn	Mn	Mg
Mg-5Al	4.4	-	-	-	Bal.
AZX612	6.0	2.0	1.0	0.3	Bal.
AX53	4.6	3.0	-	-	Bal.

The carbon nanofibers used are commercially available VGCFs (Showa Denko Co. Ltd.). These VGCFs were typically 100–200 nm in diameter and 10–20 μm in length. The configurations and physical properties of the VGCFs are listed in Table 4-2.

Table 4-2 Shape and physical properties of VGCF.

	VGCF
Diameter, d/μm	0.15
Fiber length, L/μm	10～20
Aspect ratio	10～500
Specific surface area, Sm/×10^3 $m^2 \cdot kg^{-1}$	13
True density, ρ/×10^3 kg m^{-3}	2

4.2.2 Electroless deposition process

The VGCFs were coated with nickel using an electroless deposition process. Prior to this electroless plating, the VGCFs were pre-treated. To remove any rosin, 10 g dm^{-3} of VGCFs were placed in acetone and subjected to ultrasonic treatment. The VGCFs were dispersed homogeneously in the solution, filtered using a paper filter, and rinsed with pure water. Then, they were etched with 1.69 mol dm^{-3} HNO_3 for 5 min, sensitized with a 5.9×10^{-2} mol dm^{-3} $SnCl_2\cdot2H_2O$ + 0.24 mol dm^{-3} HCl solution for 5 min, and activated with a 2.3×10^{-3} mol dm^{-3} $PdCl_2$ + 0.48 mol dm^{-3} HCl solution for 5 min. After filtration and rinsing, the VGCFs were immersed in a nickel electroless plating bath. The pH of the bath was adjusted to 6.5 by the addition of an NH_3 solution. Electroless plating was performed for 15 min at 385K under ultrasonic treatment. After filtration and rinsing with methanol, the electroless-plated VGCFs were dried for 120 min at 363 K.

The material deposited by the electroless process was then examined using an electron probe micro-analyzer (EPMA, JXA-8900RL) equipped with a wavelength-dispersive spectroscopy (WDS) detector. An X-ray diffraction (XRD) analysis was carried out using Cu-Kα radiation (k = 1.54056 Å) at a scanning speed of 1°/min.

4.2.3 Stir casting process for magnesium alloy

Magnesium alloys were cast by permanent mold (PM) casting. Fig. 4-1 shows the illustration of the melt stirring machine. Melting was carried out in an electrical furnace covering with argon gas to prevent molten magnesium from oxidation. High purity magnesium, aluminum and calcium were added in a mild steel crucible as the desired compositions. After the alloying elements were completely dissolved at 973 K, the melt was stirred mechanically for 2 min with a stainless-steel rod, and then poured into a mild steel mold, as shown in Fig. 4-2, which had been preheated to 573 K. The size of ingot was 14mm × 14 mm × 120 mm.

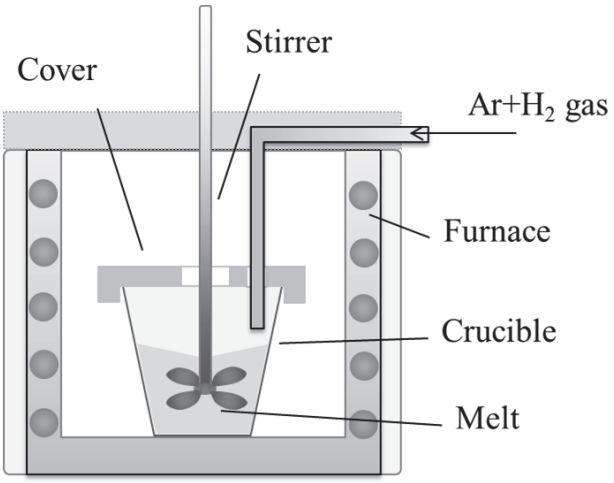

Fig. 4-1 Schematic illustration of the melt stirring equipment.

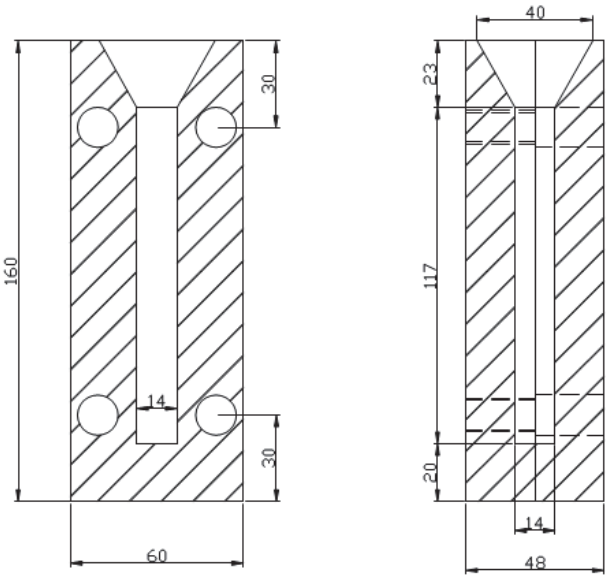

Fig. 4-2 Illustration of the mold.

4.2.4 Compo-casting process for composites

The Ni-coated VGCF-reinforced magnesium-calcium alloy composites were fabricated using a compo-casting process. Compo-casting is a liquid state process in which the infiltration of reinforcement into semi-solid metal (SSM) can be facilitated by means of agitation. In this process, after totally melted, the melt is then cooled down to a semi-solid state. From the phase diagrams, as shown in Fig. 4-3, 4-4, the temperature is determined to be 873K.

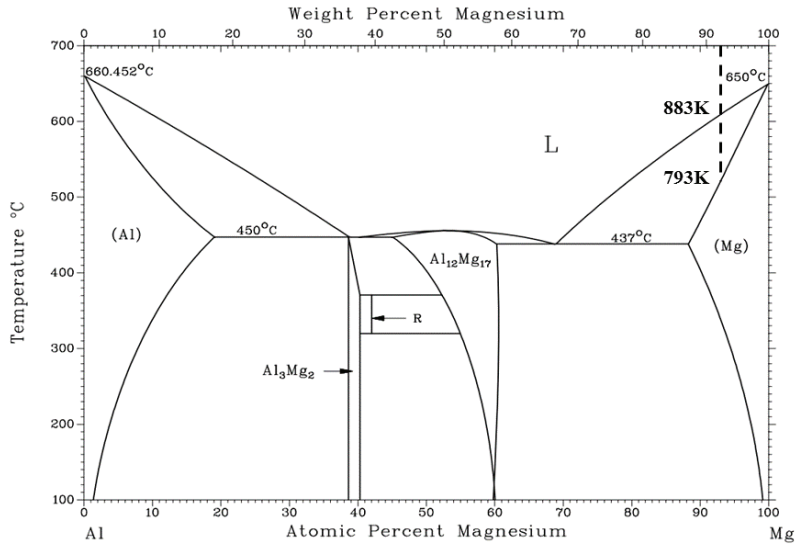

Fig. 4-3 Al-Mg phase diagram.

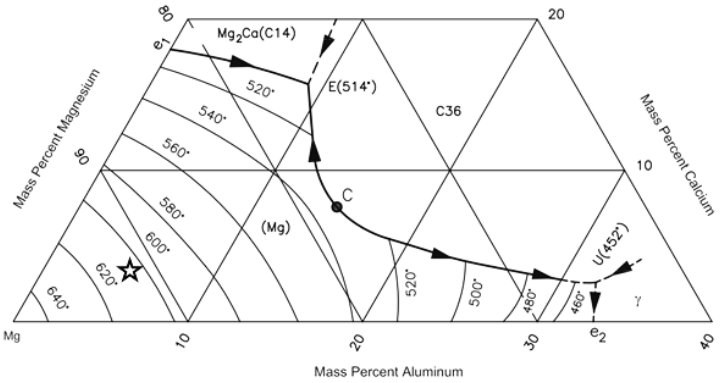

Fig. 4-4 Al-Ca-Mg phase diagram.

Fig. 4-5 shows the process of compo-casting. A charge of 50 g of the magnesium alloy was placed in a mild steel crucible preheated to 673 K in an electric resistance furnace. Argon gas was allowed to pass through the furnace to avoid burning the Mg during melting. The furnace temperature was raised to 973 K and held for about 30 min. The melt was homogenized for 2 min by stirring. Then the temperature was brought down to around 873 K, and Ni-coated VGCFs (0.5, 1.0 wt%) wrapped in Al foil were added to the melt during stirring. After 20 min, the melt was again rapidly heated to 973 K rapidly. The melt was stirred for 20 min after a semi-solid metal achieved. The composite melt was then hold for 10 min and poured into a permanent steel mold to form a 120 mm × 14 mm × 14 mm ingot.

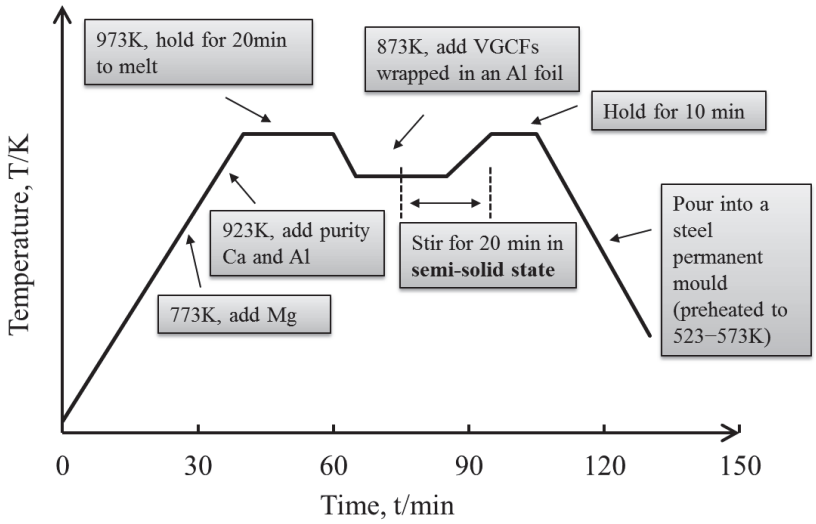

Fig. 4-5 Process of compo-casting.

Table 4-3 Theoretical composition of the composites.

Material	VGCFs	Ni
Mg alloy	0	0
0.5%Ni@VGCFs/Mg alloy	0.5 wt. %	1.7 wt. %
1.0%Ni@VGCFs/ Mg alloy	1.0 wt. %	3.5 wt.%

4.2.5 Microstructure observation

The as-cast magnesium alloys and composites were cut into various specimens for the following analyses. The microstructures of the magnesium alloys and composites were observed using the EPMA and a scanning electron microscope (FEI Siron200 SEM). The specimens of as-cast alloy were etched in a hydrochloric acid solution (5% HCl+95% alcohol). The average grain size was measured using Image-Pro Plus 5.0 software.

4.3 Results and discussion

4.3.1 Characterization of VGCFs and Ni-coated VGCFs

Figure 4-6 shows SEM micrographs of the raw VGCFs and electroless nickel-plated VGCFs. The nickel was homogeneously deposited on the VGCFs, resulting in nickel-coated VGCF powder (Fig. 4-6b) with a larger diameter than the raw VGCFs (Fig. 4-6a). A qualitative analysis using WDS showed the presence of about 70 wt% nickel in the Ni-coated VGCFs. Phosphorus, at about 1–2 wt%, was present in the nickel coatings. Figure 4-7 shows XRD patterns of the VGCFs and Ni-coated VGCFs. The Ni-coated VGCFs exhibit broad humps corresponding to nanocrystals or some amorphous nickel.

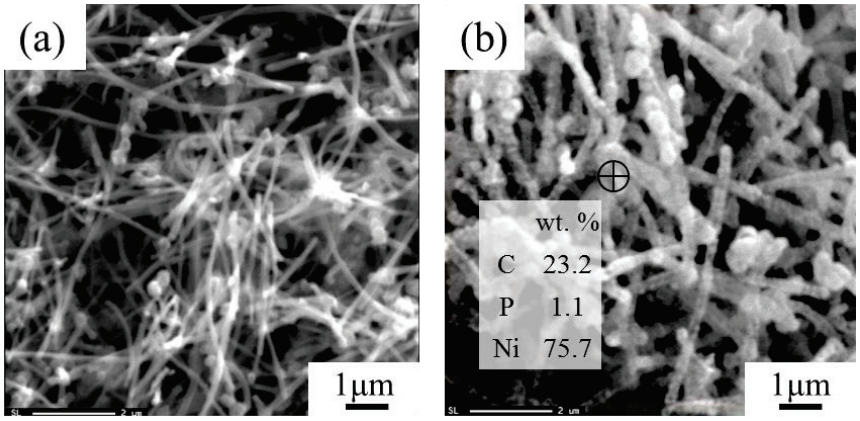

Fig. 4-6 Microstructures of (a) raw VGCFs and (b) Nickel-coated VGCFs obtained by electroless deposition with WDS analysis.

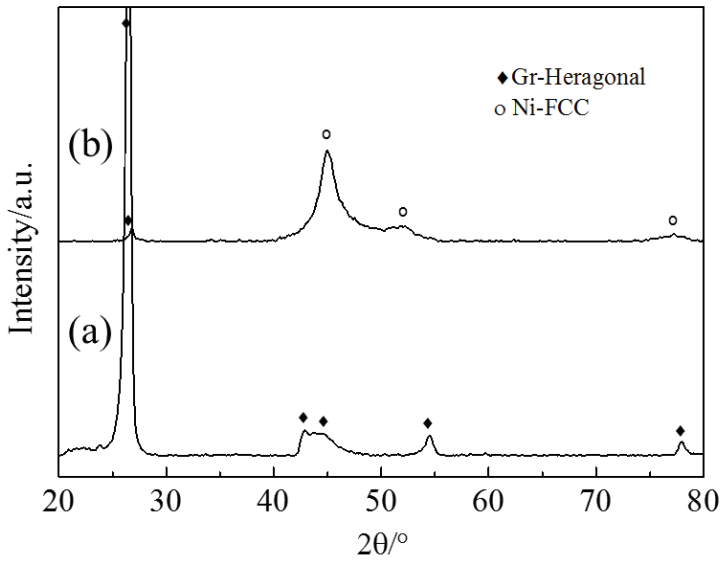

Fig. 4-7 X-ray diffraction pattern of (a) raw VGCFs and (b) nickel-coated VGCFs.

4.3.2 Microstructures of Mg-Al-Ca alloys

Figure 4-8 shows the microstructures of the Mg-5Al, AZX612, and AX53 alloys. Morphology of Mg-5Al alloy was composed of α-Mg and irregular β-$Mg_{17}Al_{12}$ intermetallic compound along grain boundaries, as shown in Fig. 4-8a, b and c. In the case of containing calcium to the Mg-5Al alloy (Fig. 4-8d-i), the magnesium alloy exhibited a dendritic microstructure with Ca-containing phase along grain boundaries. The coarse lamellar phase with bright contrast formed along the grain boundaries instead of the irregular β phase in the Mg-5Al alloy. With the help of Image-Pro Plus 5.0 software, the volume fractions of precipitates in the as-cast AZX612 and AX53 are measured, which are 20.4%, and 24.7%, respectively. It means that the number of secondary phases along grain boundaries increases with increasing Ca/Al ratio. WDS mapping images as shown in Fig. 4-8e and h, show that aluminum existed at the same place of calcium as well as some magnesium. For the as-cast AZX612 alloy, WDS analysis as shown in Fig. 4-8f, shows that the composition of the coarse lamellar secondary phase is 30.6Mg–48.2Al–21.2Ca, which may correspond to $(Mg, Al)_2Ca$. For the as-cast AX53 alloy, the secondary phase shows similar morphology with that in AZX612 alloy. WDS analysis (Fig. 4-8i) shows that the composition is 47.2Mg–34.1Al–18.7Ca, which may correspond to $(Mg, Al)_2Ca$.

The as-cast Mg-Al-Ca alloys exhibit dendritic microstructure. The alloys are prone to segregation due to relatively wide temperature spans between the liquid and the solid curves. Large crystals of α-Mg phase form under nonequilibrium solidification conditions. Al and Ca admixture is pushed away to the front of solid/liquid interface and dendrite clearance until the condition of eutectic solidification was satisfied. Calcium addition caused decreasing of the β-$Mg_{17}Al_{12}$ phase because the formation of Ca-containing phase consumed aluminum atoms. The solidification pathways of Mg–Al–Ca system alloys by thermal analysis confirmed that the category of Ca-containing phase mainly depends on Ca content and Ca/Al ratio. With increasing the Ca/Al ratio, these phases transform from Al_2Ca to $(Mg, Al)_2Ca$ and Mg_2Ca. Ninomiya et al. [9] indicated that, for the Ca/Al ratios of less than 0.8, Al_2Ca is the only phase that would be formed in the Mg–Al alloys after Ca additions. Higher values of Ca, would lead to

the formation of both Mg_2Ca and Al_2Ca in the microstructure. Another research by Luo et al. [10] showed that the second phase $(Mg, Al)_2Ca$ can be formed in the Mg–5Al–2Ca and Mg–5Al–3Ca alloys, even though the Ca/Al ratio is lower than 0.8. The existence of the $(Mg, Al)_2Ca$ phase in Mg-Al-Ca alloy have been widely recognized recently.[10-12] The phase was identified as a ternary Laves phase with a dihexagonal C36 crystal structure that was different from other Laves phases such as Mg_2Ca (C14, hexagonal) and Al_2Ca (C15, cubic). It has been further shown that this phase, after prolonged exposures to elevated temperatures, would transform to Al_2Ca with C15 structure through a shear-assisted transformation without significant change in the morphology of the phases. Computational thermodynamics and experimental investigations have shown that Al_2Ca with a C15 structure is stable in the equilibrium condition. However, for the high cooling rates of the melts it is possible to have $(Mg, Al)_2Ca$ with a C36 structure. According to the solidification paths of Mg-Al-Ca ternary alloys calculated by Luo et al. [10], as shown in Fig. 4-9 and Fig. 4-10, the AX52 alloy has a $L \rightarrow \alpha\text{-Mg} + (Mg, Al)_2Ca + Mg_{17}Al_{12}$ eutectic reaction, while AX53 alloy has a different ternary eutectic reaction $L \rightarrow \alpha\text{-Mg} + (Mg, Al)_2Ca + Mg_2Ca$, where Mg_2Ca is formed instead of the $Mg_{17}Al_{12}$.

Combining with our experimental results, for the AZX612 alloy with an Ca/Al ratio of 0.33, the intermetallic compounds mainly consist of the $(Mg, Al)_2Ca$ phase, and the presence of $Mg_{17}Al_{12}$ can be inferred. For the AX53 alloy (Ca/Al ratio equals 0.6), the intermetallic compounds mainly consist of the $(Mg, Al)_2Ca$ phase with small amount of Mg_2Ca phase.

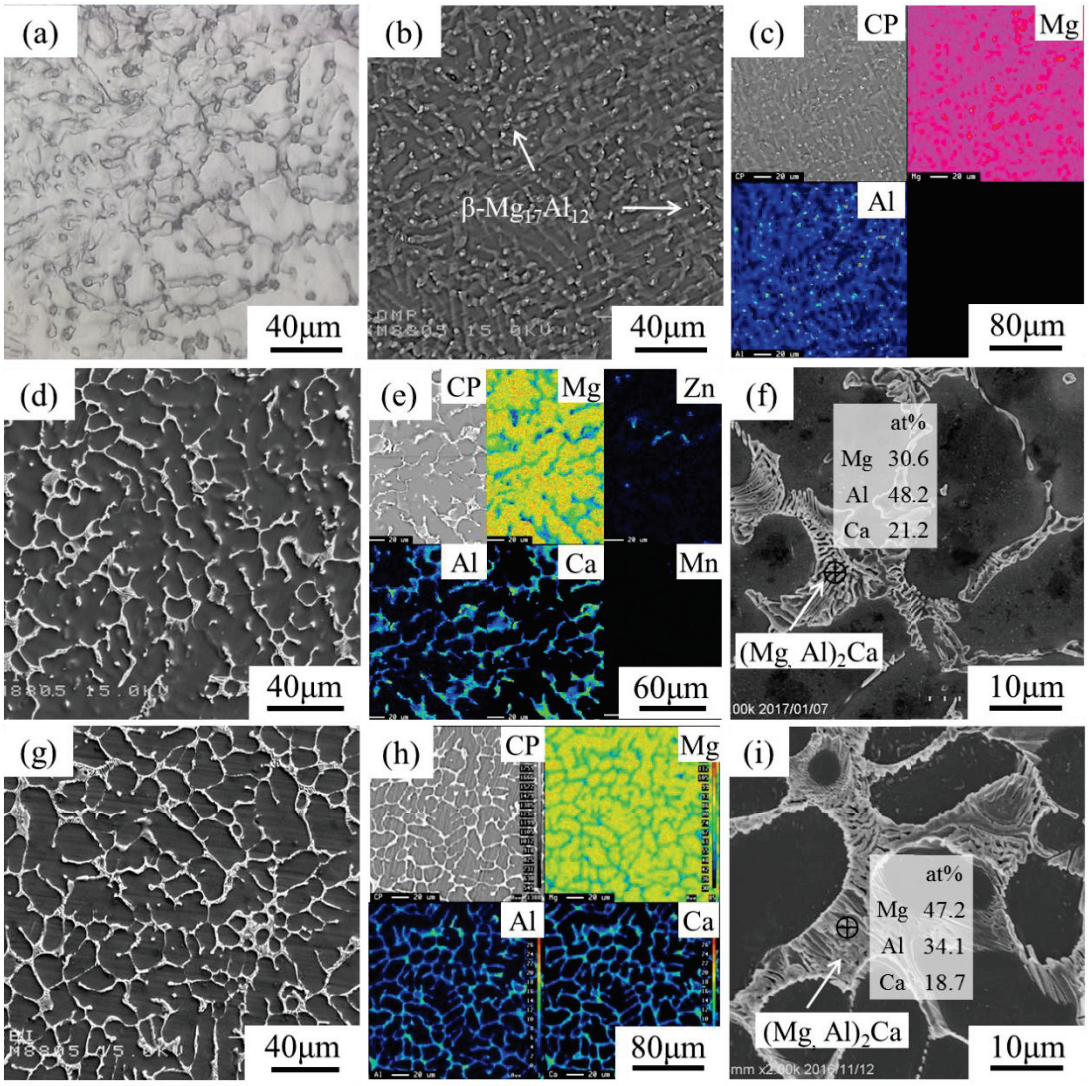

Fig. 4-8 Microstructure at the as-cast condition, showing of (a) Optical image, (b) SEM micrograph, and (c) WDS mapping of Mg-5Al alloy; (d), (f) SEM micrograph and WDS analysis, and (e) WDS mapping of AZX612 alloy; (g), (i) SEM micrograph and WDS analysis, and (h) WDS mapping of AX53 alloy.

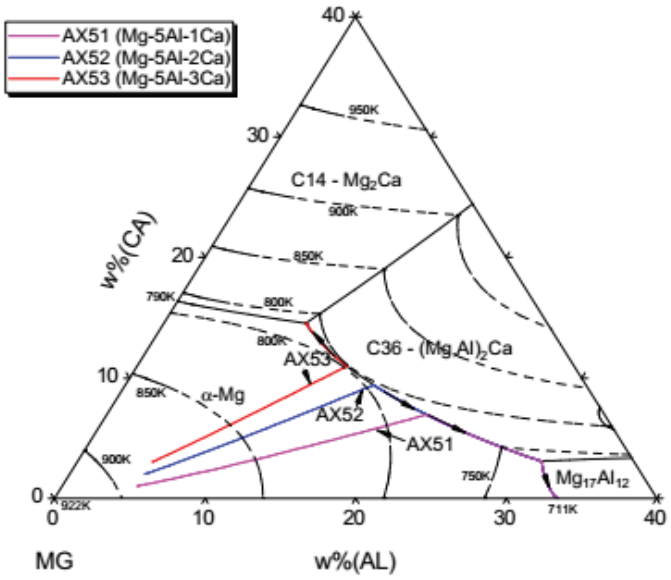

Fig. 4-9 Calculated Mg-Al-Ca liquidus projection and the solidification paths of the experimental Mg-Al-Ca alloys [10].

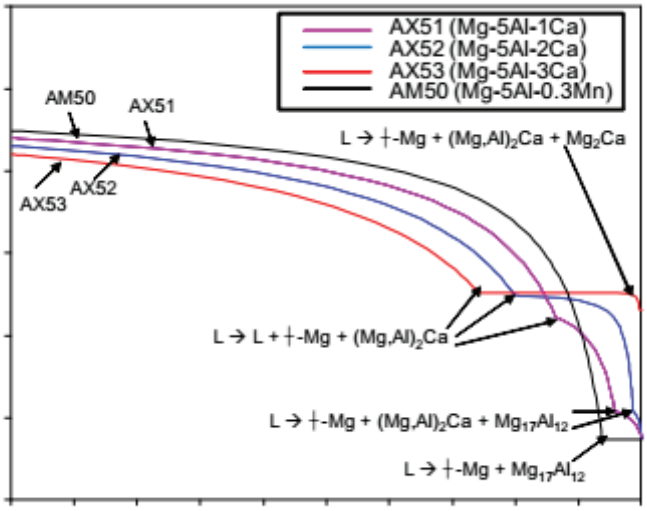

Fig. 4-10 Temperature vs. fraction solid diagram of the Mg-Al-Ca alloys [10].

4.3.3 Microstructures of Mg-Al-Ca alloy composites

Figure 4-11 shows the microstructures of the as-cast Ni-coated VGCF-reinforced AX53 alloy composites. Fig. 4-11a, c and e show the SEM images of the 0.5% Ni@VGCFs/AX53 composites. There are also some $(Mg, Al)_2Ca$ compounds distributed along the grain boundaries. In addition, some cube-shaped Al_3Ni particles with an orthorhombic structure were generated both inside grains and on grain boundaries, because Al-Ni intermetallic compounds prefer to form in the Mg-Al-Ni binary system.[23] However, the Al_3Ni particles were not evenly distributed, especially in the 1.0% VGCF composites (Fig. 4-11b, d and f). There were also areas in which the VGCFs were not evenly dispersed and formed clusters, as shown in Fig. 4-11a and b. Even with the nickel coating on the VGCFs, it was difficult to perfectly disperse the VGCFs using mechanical agitation. The microstructures of the as-cast Ni-coated VGCF-reinforced AZX612 alloy composites are similar with AX53 composites, as shown in Fig. 4-12. $(Mg, Al)_2Ca$ compounds distributed along the grain boundaries, while some cube-shaped Al_3Ni particles formed both inside grains and on grain boundaries.

The distributions of the grain sizes in the composites, as well as the average grain sizes were calculated and shown in Fig. 4-13. With an increase in the amount of Ni-coated VGCFs, the grain size of the composite decreased, along with the range of the grain distribution. This indicated that Ni-coated VGCFs have an effect on the grain refinement of the Mg-Al-Ca alloys. On one hand, this was because, as heterogeneous nuclei, the VGCFs promoted nucleation during the magnesium alloy crystallization. On the other hand, a large amount of dispersively distributed VGCFs impeded the grain growth.

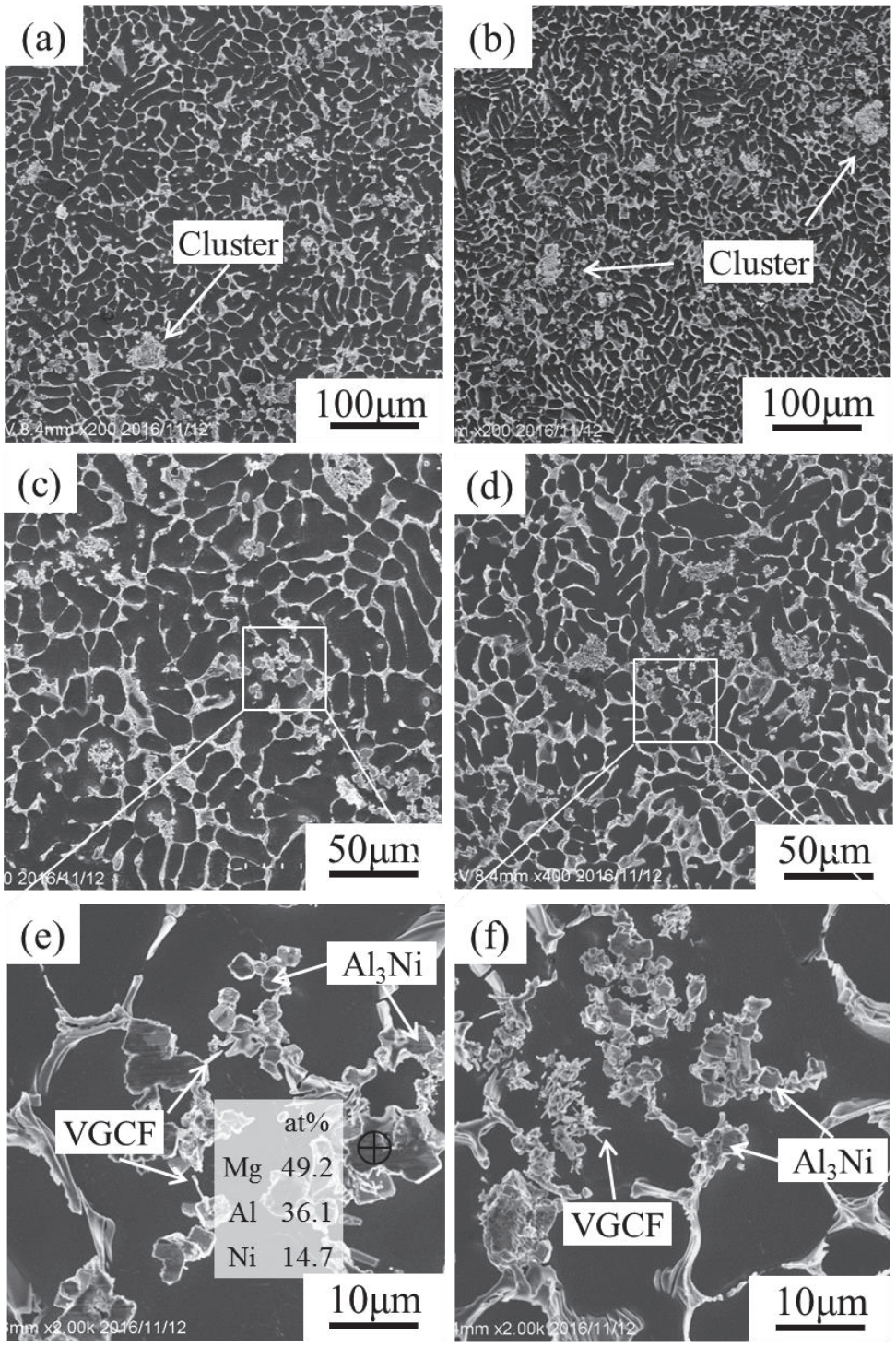

Fig. 4-11 Microstructures and WDS analysis of as-cast (a), (c), (e) 0.5%Ni@VGCFs/AX53, and (b), (d), (f) 1.0%Ni@VGCFs/AX53.

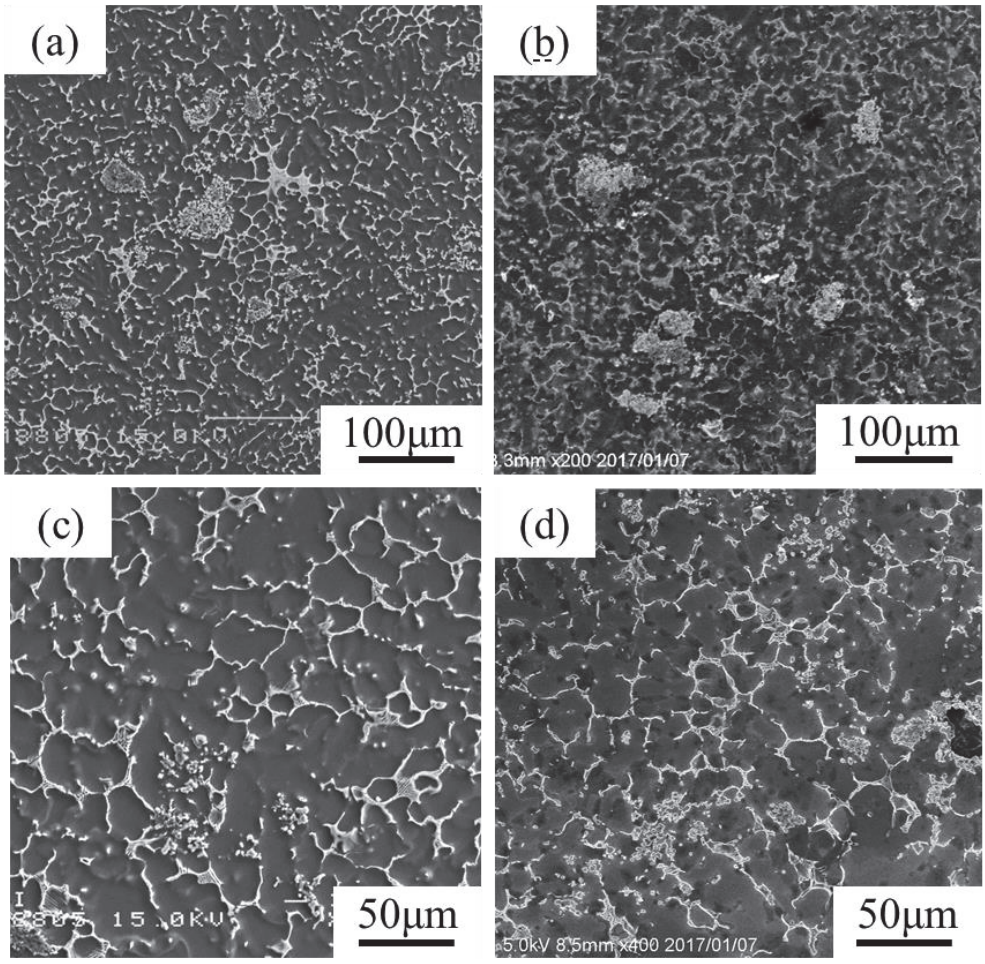

Fig. 4-12 Microstructures of as-cast (a), (c) 0.5%Ni@VGCFs/AZX612, and (b), (d) 1.0%Ni@VGCFs/AZX612.

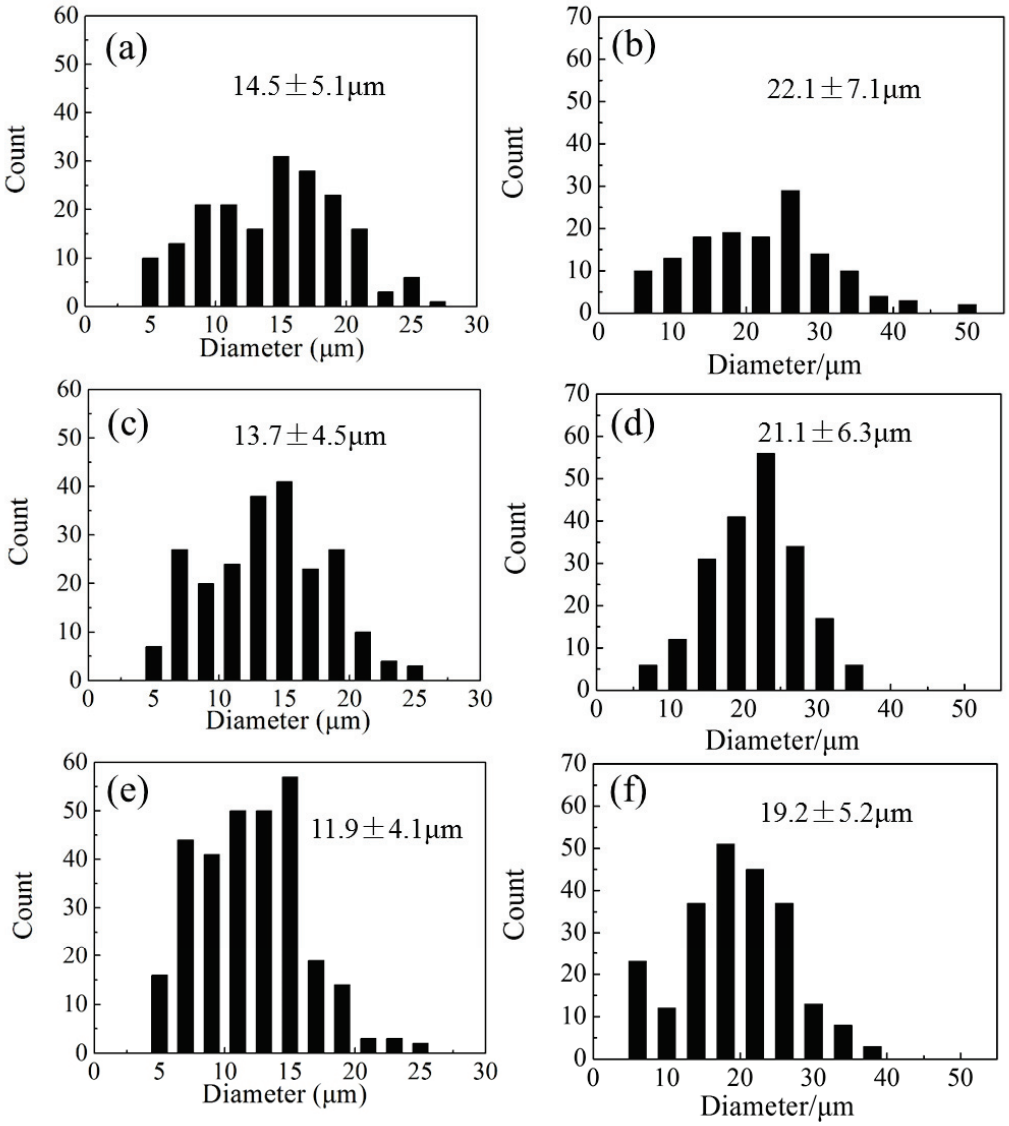

Fig. 4-13 Distribution of grain sizes and average grain sizes of (a) AX53, (c) 0.5%Ni@VGCFs/AX53, (e) 1.0%Ni@VGCFs/ AX53, (b), AZX612, (d) 0.5%Ni@VGCFs/AZX612, and (f) 1.0%Ni@VGCFs/AZX612.

4.3.4 Wetting and dispersion behavior of compo-casting process

Figure 4-14 shows the wetting and dispersion of the Ni-coated VGCFs in metal melts. The preliminary mix of the Ni-coated VGCFs into the SSM was facilitated by compo-casting process. The primary solid particles already formed in the SSM increased the melt viscosity and mechanically entrapped the reinforcements in the SSM. During this process, the Ni-coated VGCFs existed mostly in the form of clusters. Then, the slurry was again heated to a fully liquid state and mechanically mixed, which further dispersed the Ni-coated VGCF clusters. Moreover, according to our previous work,[22] a nickel coating on graphite improves the wettability of a magnesium alloy through the dissolution of nickel into the liquid magnesium alloy. With nickel coatings diffused into the metal, a homogeneous VGCF distribution and high bond strength with the matrix were obtained. In addition, Al_3Ni intermetallic compounds formed during casting.

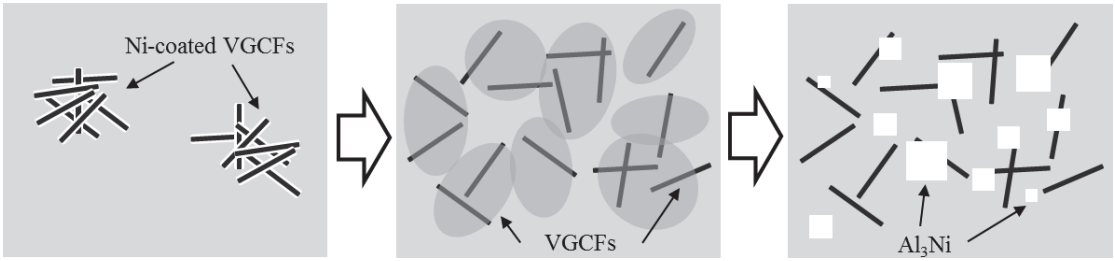

a. Preliminary mix of Ni-coated VGCFs into semi-solid metal.

b. Dispersion of VGCFs with nickel coating diffusing into the melt during agitation.

c. Al_3Ni phase formation during casting.

Fig. 4-14 Schematic of the wetting and dispersion of Ni-coated VGCFs in metal melts.

4.4 Summary

(1) Nickel-coated VGCFs were prepared using an electroless plating process, with the nickel homogeneously deposited on the VGCFs.

(2) Microstructure of Mg-5Al alloy consisted of β-$Mg_{17}Al_{12}$ intermetallic phase in the α-Mg matrix. With the additions of calcium, the Mg-Al-Ca alloy exhibited a dendritic microstructure with calcium-containing phases along the grain boundaries which suppressed the formation of the $Mg_{17}Al_{12}$ phases. With increasing Ca/Al ratio, the volume fraction of the second phase in the as-cast Mg-Al-Ca alloys increases, and the main second phase is $(Mg, Al)_2Ca$ with a coarse lamellar structure.

(3) Nickel-coated VGCFs were prepared using an electroless plating process, with the nickel homogeneously deposited on the VGCFs. Ni-coated VGCF-reinforced Mg-Al-Ca composites were fabricated using the compo-casting method. The preliminary mix of the Ni-coated VGCFs into the semi-solid metal was facilitated by compo-casting process. With the nickel coating diffused into the metal, the dispersion of VGCFs was promoted. Al_3Ni compounds formed both inside the grains and on the grain boundaries. The addition of Ni-coated VGCFs could refine the grain of the Mg-Al-Ca alloy.

References

1) Show Denko Co., Ltd., Material Safety Data Sheet, (2007) p. 1.
2) M. Endo, Y. A. Kim, T. Hayashi, K. Nishimura, K. Miyashita, and M. S. Dresselhaus: Carbon **39** (2001) 1287–1297.
3) L. Wang, H. Choi, J. M. Myoung, and W. Lee: Carbon, **47** (2009) 3427–3433.
4) A. M. K. Esawi, K. Morsi, A. Sayed, M. Taher, and S. Lanka: Applied Science and Manufacturing, **42** (2011) 234–243.
5) G. Sasaki, F. Kondo, K. Matsugi, and O. Yanagisawa: Trans Tech Publications. **561** (2007) 729–732.
6) Z. F. Xu, Y. B. Choi, K. Matsugi, D. C. Li, and G. Sasaki: Mater. Trans. **50** (2009) 2160–2164.
7) J. M. Ting, and M. L. Lake: J. Mater. Res. **10** (1995) 247–250.
8) T. Imanishi, K. Sasaki, K. Katagiri, and A. Kakitsuji: Trans. Jpn. Soc. Mech. Eng. A, **75** (2009), 27–33.
9) R. Ninomiya, T. Ojiro, and K. Kubota: Acta Metall. Mater. **43** (1995) 669–674.
10) A.A. Luo, M.P. Balogh, and B.R. Powell: Metall. Mater. Trans. A **33** (2002) 567–574.
11) A. Suzuki, N.D. Saddock, J.W. Jones, and T.M. Pollock, Scr. Mater. **51** (2004) 1005–1010.
12) L. Han, H. Hu, and D.O. Northwood: Mater. Lett. **62** (2008) 381–384.
13) S. Naher, D. Brabazon, and L. Looney: J. Mater. Process. Technol. **143** (2003) 567–571.
14) M. C. Flemings: Metall. Trans. **22A** (1991) 957−981.
15) S. Naher, D. Brabazon, and L. Looney: J. Mater. Process. Technol. **166** (2004) 430−439.
16) Z. Fan: Int. Mater. Rev. **47** (2002) 49−85.
17) F. Delannay, L. Froyen, and A. Deruyttere: J. Mater. Sci. **22** (1987) 1–16.
18) H. Chen, and A. T. Alpas: Wear, **192** (1996) 186–198.
19) T. Rajan, R. Pillai, and B. Pai: J. Mater. Sci. **33** (1998) 3491–3503.
20) Y. M. Ryu, E. P. Yoon, and M. H. Rhee: J. Mater. Sci. Lett. **19** (2000) 1103–1105.

21) J. Rams, A. Urena, and M.D. Escalera: Composites **38** (2007) 566–575.

22) Y. Yao, Z. Xu, K. Sugio, Y. Choi, S. Kang, R. Fu, and G. Sasaki: Mater. Trans. **56** (2015) 1693-1697.

23) H. Wang, L. Liu, and F. Liu: Mater. Des. **50** (2013) 463–466.

Chapter 5

Mechanical Properties of VGCF-Reinforced Mg-Al-Ca Alloy Composites

5.1 Introduction

Currently, the most widely used magnesium alloys are based on the Mg-Al system, such as, AZ91 and AM60[1, 2]. At temperatures above 125 ℃, Mg-Al alloys undergo excessive creep deformation even at moderate stress levels, which makes them not suitable for use at elevated temperatures[3, 4]. The poor creep resistance of Mg-Al alloys is generally considered to be associated with the formation of the $Mg_{17}Al_{12}$ phase. The poor thermal stability of $Mg_{17}Al_{12}$ phase and its discontinuous precipitation can result in substantial grain boundary sliding at elevated temperatures. Possible approaches to improving creep resistance in magnesium alloys include: suppressing the formation of $Mg_{17}Al_{12}$ phase; pinning grain boundary sliding; and slowing diffusion in the magnesium matrix. To cover the deficiencies in mechanical properties of magnesium, especially at elevated temperatures, efforts have been made to develop creep resistant magnesium alloys, and magnesium matrix composites are prospecting candidates due to their promising superior properties.

Calcium is a promising elemental addition to develop Mg–Al alloys for high-temperature applications. The calcium addition encourages the formation of Ca-containing thermally stable intermetallic compounds and suppresses the formation of unstable β-$Mg_{17}Al_{12}$. Thus, calcium addition significantly improves the high temperature strength, creep resistance, and oxidation resistances.[5-8]

Recently, much work has been devoted to investigate the Mg-based composites reinforced with carbon nanotubes[9-13]. The addition of carbon nanotubes to Mg improves its tensile strength and elongation. VGCFs possess attractive mechanical, electrical, and thermal properties with similar carbon structure to carbon nanotubes.[14, 15] VGCFs have attracted much attention in various fields, and have been particularly considered as an ideal candidate for reinforcement in multifunctional composites and engineering applications. Recent studies of carbon nanofibers into light metal matrix composites are mainly for the enhancement of the mechanical properties1[16, 17], also for the modified electrical conductivity[18, 19], thermal conductivity and coefficient of thermal expansion[20, 21]. To enhance the strength and rigidity of the matrix, VGCFs can be used to reinforce Mg-Al-Ca alloy, which are supposed to give them satisfactory

mechanical properties at both room and elevated temperatures.

In this study, the effects of Ni-coated VGCFs on the microstructure and mechanical properties of magnesium alloy are investigated, and the strengthening mechanism of Ni-coated VGCFs reinforced Mg-Al-Ca alloy composites is discussed.

5.2 Experimental methods

5.2.1 Hardness test

The hardness of the as-cast magnesium alloys and composites was measured in a Vickers hardness tester. The values reported for Vickers hardness represented the average of five separate measurements taken at randomly selected points using a load of 100 g for 10 s.

5.2.2 Tensile tests

Plate tensile specimens with a thickness of 2 mm and gauge length of 18 mm (Fig. 5-1) were cut from the as-cast magnesium alloys and composites in accordance with ASTM test method E8M-11. Tensile tests were carried out using a universal testing machine with a strain rate of 0.5 mm/min at room temperature, 150 °C and 200 °C. A minimum of four tests were conducted for each composition to obtain an average value. SEM was used to analyze the tensile fracture images.

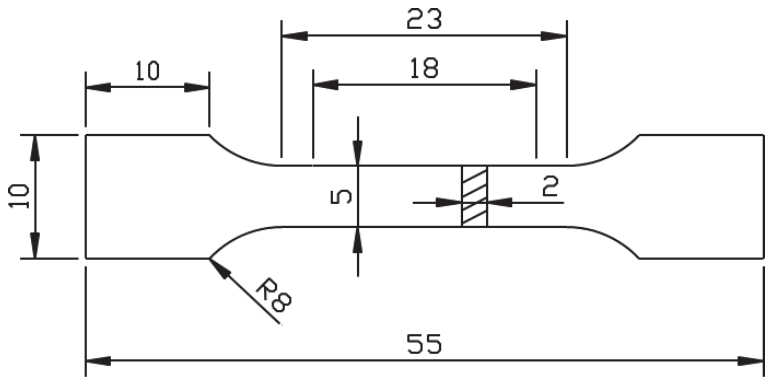

Fig. 5-1 Sketch of tensile specimens (mm).

5.3 Results and discussion

5.3.1 Mechanical properties of Mg-Al-Ca alloys

5.3.1.1 Micro-Vickers hardness of Mg-Al-Ca alloys

The micro-Vickers hardness values of the as-cast Mg-5Al, AZX612 and AX53 alloys are shown in Fig. 5-2. The addition of calcium obviously improved the hardness of the Mg-Al-Ca alloys. Compare to Mg-5Al alloy, the hardness of AZX612 and AX53 alloys increased for 11.1% and 13.8%, respectively. This was attributed to the formation of $(Mg, Al)_2Ca$ compounds, which have higher hardness values than $Mg_{17}Al_{12}$.

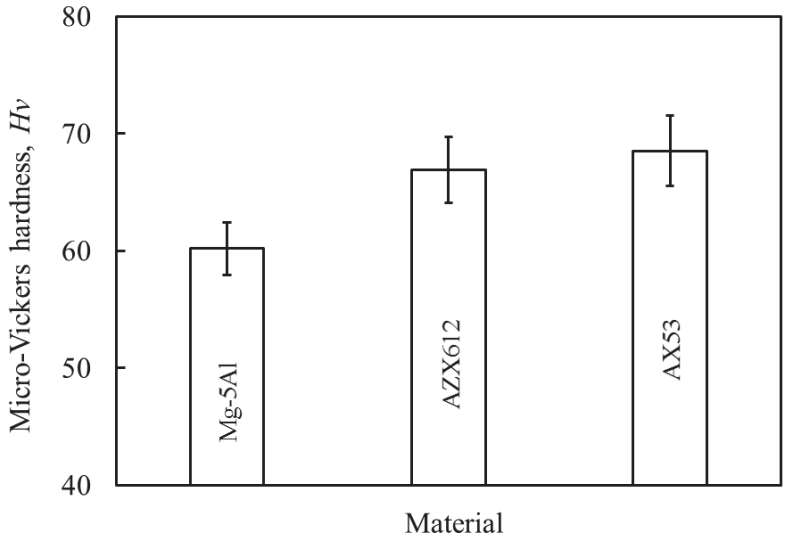

Fig. 5-2 Micro-hardness of as-cast Mg-5Al, AZX612 and AX53 alloys.

5.3.1.2 Tensile properties of Mg-Al-Ca alloys

The stress–strain curves for the as-cast Mg-5Al, AZX612, and AX53 alloys are shown in Fig. 5-3. Their tensile properties are summarized in Table 5-1. It can be observed that the yield strength of the alloys was improved by the addition of calcium. For Mg-5Al alloy, the yield strength was 66 MPa. With 2 wt.% calcium addition, the

yield strength of AZX612 alloy was improved by 48% to 98 MPa. For AX53 alloy, the yield strength increased by 54% to 102 MPa. However, the plasticity of the alloy was significantly reduced with the addition of calcium. The total elongations of AZX612 and AX53 alloys were decreased to 2.8% and 1.4%, respectively, from 5.2% for Mg-5Al alloy. The ultimate tensile strength (UTS) of AZX612 alloy increased to 156 MPa from 146 MPa for Mg-5Al alloy. However, the UTS of AX53 alloy decreased to 141 MPa with a reduced elongation. The addition of calcium tends to makes the alloy brittle.

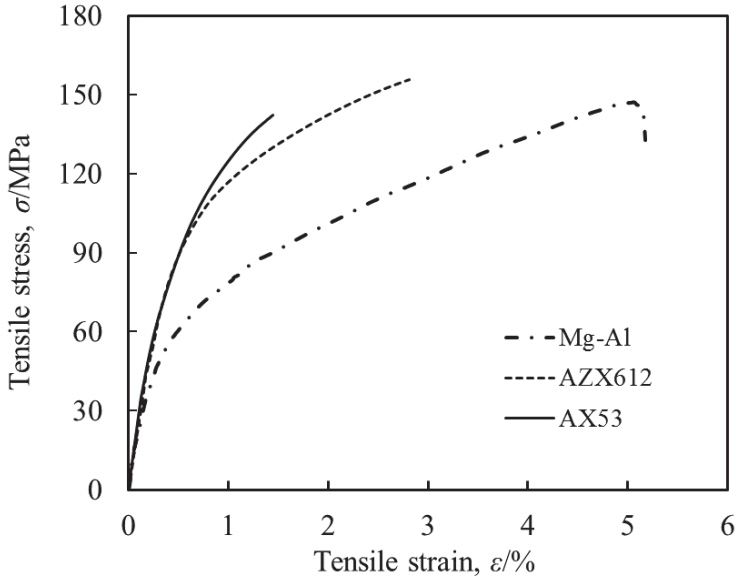

Fig. 5-3 Tensile stress–strain curves of as-cast Mg-5Al, AZX612, and AX53 alloys.

Tab. 5-1 Tensile properties of as-cast Mg-5Al, AZX612, and AX53 alloys.

Material	Yield stress $\sigma_{0.2}$ (MPa)	UTS σ_b (MPa)	Elongation δ (%)
Mg-5Al	66	146	5.2
AZX612	98	156	2.8
AX53	102	141	1.4

The fracture surfaces of the magnesium alloys are shown in Fig. 5-4. The fracture surface of the Mg-5Al alloy shows the presence of many dimples (Fig. 5-4a, b). This indicates that the fracture mechanism is ductile fracture. For the AZX612 and AX53 alloys, the fracture analysis revealed that the mechanism was brittle fracture. As shown in Fig. 5-4c and d, the fracture surface of the AZX612 alloy shows intergranular fracture feature with the presence of some cleavage surface and tearing ridge, which was taken as typical brittle fracture features. As shown in Fig. 5-4e and f, the fracture surface of the AX53 alloy shows typical intergranular fracture feature. It is characterized by equiaxed facets that are correlated with the grain size, and no dimple is observed. This is attributed to the continuous network-shaped distribution of the brittle $(Mg, Al)_2Ca$ phase along the grain boundaries. The fracture is controlled by defects in the material. Figure 5-5a shows the presence of shrinkage cavities, which could form from solidification shrinkage in the AX53 alloy. Figure 5-5b shows the dendritic arms associated to shrinkage cavities on the fracture surface. Micro-cracks near the defects produce and grow along the grain boundaries, which leads to the failure of the material. As a result, the elongation reduces with Ca content increasing.

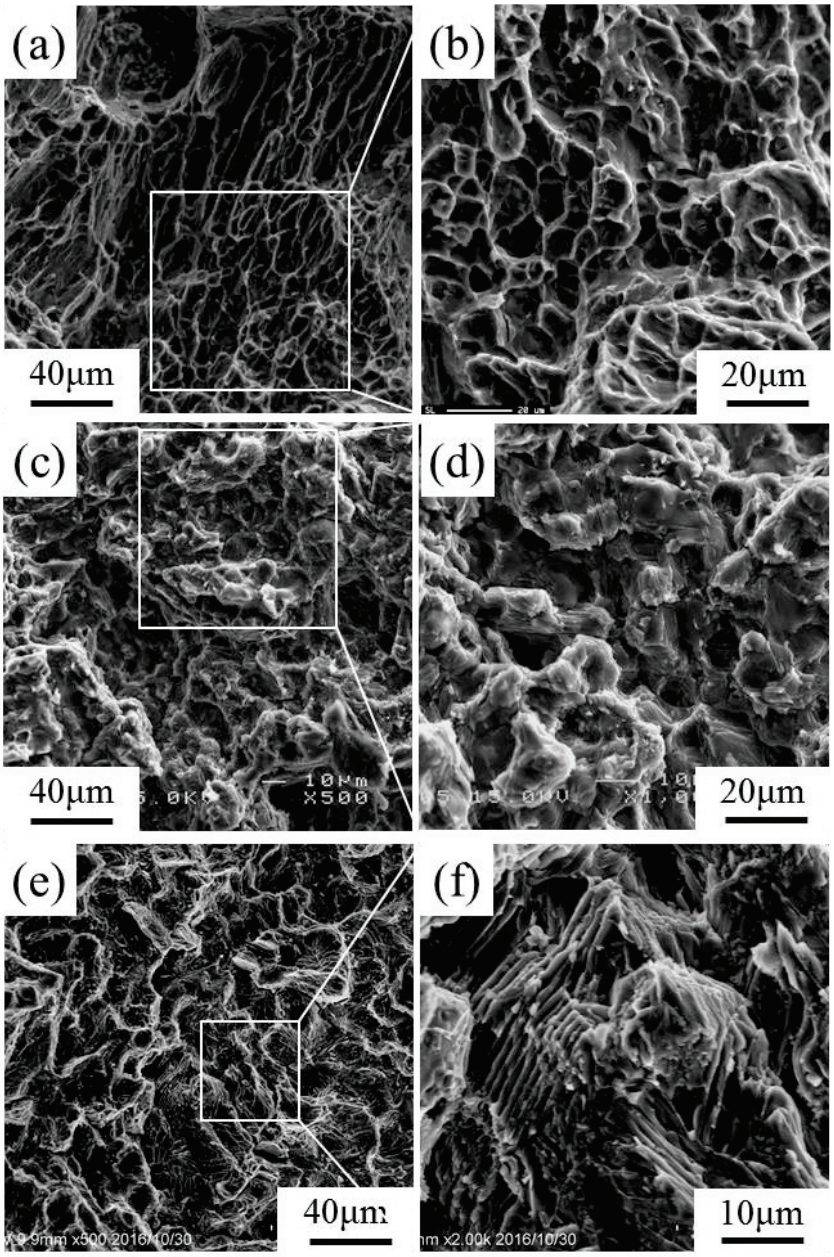

Fig. 5-4 SEM images of fracture surface of (a), (b) Mg-5Al alloy; (c), (d) AZX612 alloy; and (e), (f), AX53 alloy.

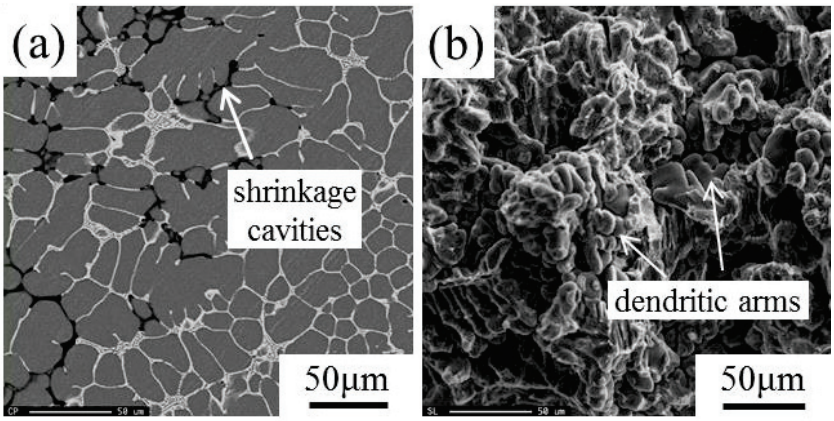

Fig. 5-5 SEM images of (a) defects in AX53 alloy and (b) defects on fracture surface of AX53 alloy.

5.3.1.3 Tensile properties of Mg-Al-Ca alloys at elevated temperatures

Tensile properties of as-cast Mg-5Al, AZX612, and AX53 alloys at elevated temperature are summarized in Tab. 5-2. As shown in Fig. 5-6, compared with the Mg-5Al alloy, the yield strength of the alloys at 150 °C and 200 °C is significantly increased as the Ca content increases. The yield stress of AZX612, and AX53 alloys was decreased slowly from room temperature to 200°. The stress–strain curves up to 200° are governed by work-hardening. Therefore, thermal stability of AZX612 and AX53 alloys is maintained up to 200°. The ultimate tensile strength of AX53 alloy at 200 ℃ is larger than that of ZAX612 alloy, which is opposite at room temperature and 150 ℃. At elevated temperatures, the addition of Ca increases the tensile strength of the alloy. The elongation at 150 ℃ and 200 ℃ also shows a clear downward trend with increase of the Ca content. Compared the properties of the alloys at different temperature, with higher Ca content, with the increase in temperature, the smaller the intensity reduction. The tensile strength and yield strength of AZX612 alloy from room temperature to 200 ℃ decreased, by 37MPa and 13MPa, while that of the AX53 alloy decreased by only 11 MPa and 11 MPa. This result further shows that Ca on Mg-Al based alloy is a useful high-temperature strengthening elements.

Tab. 5-2 Tensile properties of as-cast Mg-5Al, AZX612, and AX53 alloys at elevated temperature.

Material	150℃			200℃		
	$\sigma_{0.2}$ (MPa)	σ_b (MPa)	δ (%)	$\sigma_{0.2}$ (MPa)	σ_b (MPa)	δ (%)
Mg-5Al	52	119	12.2	-	-	-
AZX612	90	149	9.7	85	119	12.3
AX53	94	142	4.4	91	130	7.3

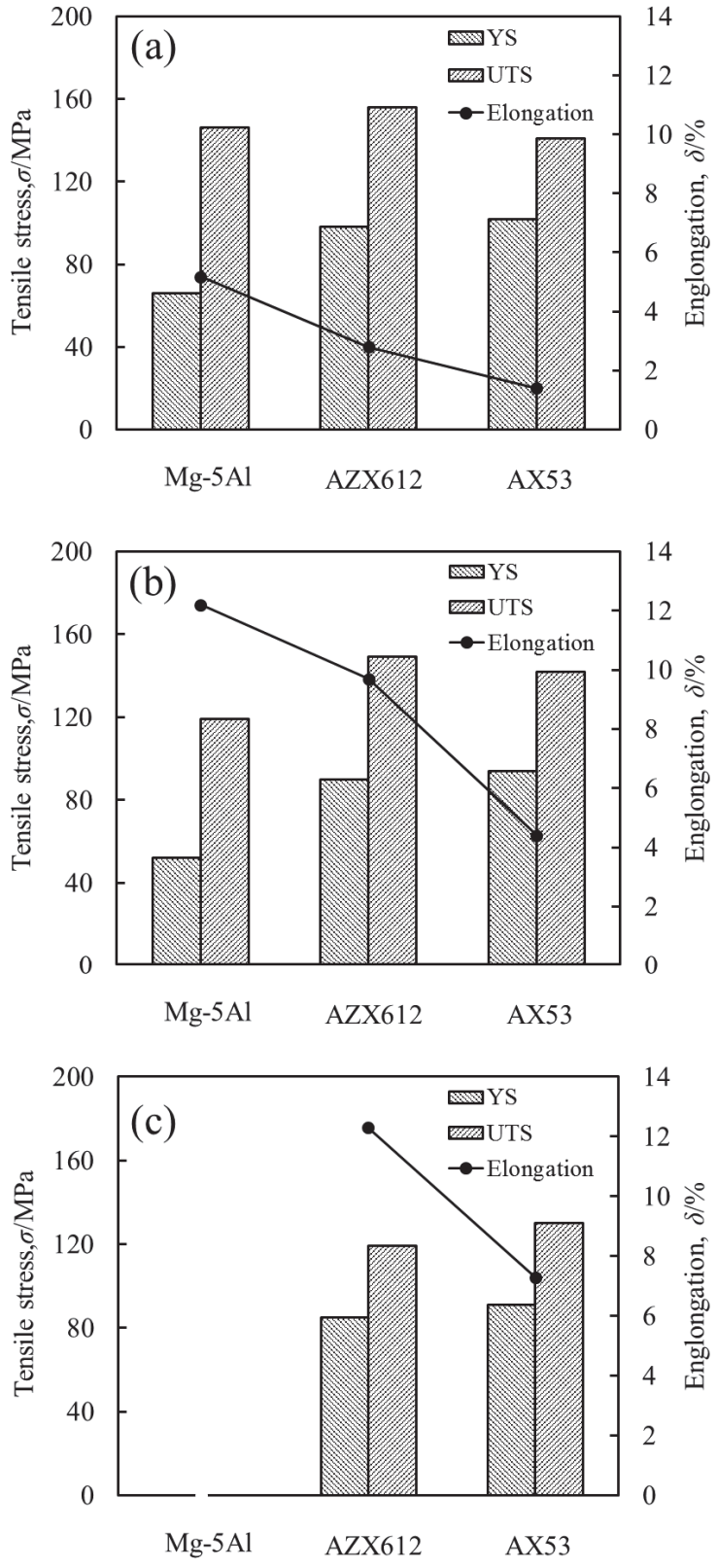

Fig 5-6 Tensile properties of as- cast Mg-Al-Ca alloys at (a) room temperature, (b) 150 °C, and (c) 200 °C.

5.3.1.4 Effects of Ca addition for Mg-Al alloy

The addition of calcium in Mg-Al alloy forms $(Mg, Al)_2Ca$ phase and suppresses the formation of the $Mg_{17}Al_{12}$ phase. However, the reticular distribution along grain boundaries of the $(Mg, Al)_2Ca$ phase is harmful to mechanical properties. As a result, when Ca content increases, the elongation at room temperature is impaired, which also affect the ultimate tensile strength.

The mechanical properties of Mg-5Al alloy decrease rapidly at temperatures above 150 ℃, as shown in Fig. 5-6. This is attributed to the main strengthening phase $Mg_{17}Al_{12}$ in Mg-5Al alloy, which has a low melting point (437 ℃) and poor thermal stability.[22] $Mg_{17}Al_{12}$ phase can readily coarsen and soften at the temperatures exceeding 120–130 ℃, and does not serve to pin the grain boundaries, while magnesium alloys undergo creep mainly by grain-boundary sliding. In addition, $Mg_{17}Al_{12}$ has a cubic crystal structure incoherent with the hcp magnesium matrix, which leads to the fragility of $Mg/Mg_{17}Al_{12}$ interface.[23] All of the above lead to the poor elevated temperature tensile properties of Mg-5Al alloy.

Addition of Ca to Mg-5Al alloy formed $(Mg, Al)_2Ca$ precipitation in the alloy. $(Mg, Al)_2Ca$ has much high melting point and thermal stability, which is at the level between that of Al_2Ca and Mg_2Ca.[24] Al_2Ca has a higher melting point (1079 °C) than that of Mg_2Ca (715 °C). On the other hand, the amount of $Mg_{17}Al_{12}$ reduces after Ca addition. As a result, sliding of grain boundaries and growth of cracks were effectively prevented at elevated temperatures. The reduction of tensile strength of Mg-Al-Ca alloys with temperature increasing declines. The obvious elevated temperature strengthening effect was obtained by calcium addition. However, large amount of reticular $(Mg, Al)_2Ca$ formed along grain boundaries when excessive Ca was added cuts apart the alloy matrix, which results in the decrease or a little change of elevated temperature tensile strength and elongation with Ca content increasing.

Some researchers have indicated that the $(Mg, Al)_2Ca$ intermetallic compounds are brittle. The tensile strength and elongation of the AZ91 magnesium alloy at ambient temperature were reduced by the Ca addition, but this produced elevated temperature strengthening.[22] Masoumi et al. [25] reveal that the presence of the $(Mg, Al)_2Ca$ phase

was the main cause of the intergranular fracture in the Mg–Al–Ca alloy. The coarse $(Mg, Al)_2Ca$ compound is more brittle and easily broken than the fine Mg_2Ca compound.[26] Hot extruded Mg–Al–Ca alloys show high unlimited tensile strength and elongation.[27] The application of hot extrusion cracked the secondary phase along the grain boundaries in the as-cast alloy, which were dispersedly distributed by the fine spherical secondary phases along the extrusion direction. Watanabe et al. [28] found out that, by hot extrusion, the ductility of Mg-6Al-2Ca alloy at room temperature was high compared with other magnesium alloys containing Ca. The ductility was enhanced at elevated temperature, and climb controlled dislocation creep could be a dominant deformation process. Jing et al. [29] indicated that hot extrusion results in significant increase of tensile properties for AJC421 (Mg–4Al–2Sr–1Ca) alloy at ambient and elevated temperature of 175 °C. However, the creep resistance is obviously deteriorated after extrusion deformation. The steady-state creep rate of as-extruded AJC421 at 175 °C/70 MPa is about three orders of magnitude higher than that of their corresponding as-cast samples. To increase applications of these magnesium alloys in the automotive industry, sufficient high temperature strength, creep resistance and inexpensive production for magnesium alloys are required.

5.3.2 Mechanical properties of Mg-Al-Ca composites

5.3.2.1 Micro-Vickers hardness of VGCFs/Mg-Al-Ca composites

The micro-Vickers hardness values of the AX53 alloy, 0.5%Ni@VGCFs and 1.0%Ni@VGCFs composites are shown in Fig. 5-7. Compared to AX53 alloy, the average hardness values of the 0.5% and 1.0% Ni-coated VGCFs/AX53 composites increased by approximately 7% and 10%, respectively. The hardness of the magnesium composites increased with the increasing content of Ni-coated VGCFs in Mg-Al-Ca alloys.

The dependence of the hardness on the grain size is generally well-established, and can be described by the Hall–Petch relation [30] for hardness:

$$Hv = H_0 + k_H d^{-1/2} \quad (1)$$

where H_0 and k_H are the appropriate constants associated with the hardness measurements. However, as shown in Fig. 5-8, the k_H slope for AX53 alloy are226 Hv $\mu m^{1/2}$, which is much larger than that of some magnesium alloys. The improved hardness of the composites was attributed not only to the refined grain, but also to the introduction of Al_3Ni particles and VGCFs. Because Al_3Ni is inherently much harder than magnesium,[31] the presence of Al_3Ni intermetallic compounds caused a higher resistance to the localized deformation of the matrix during indentation.

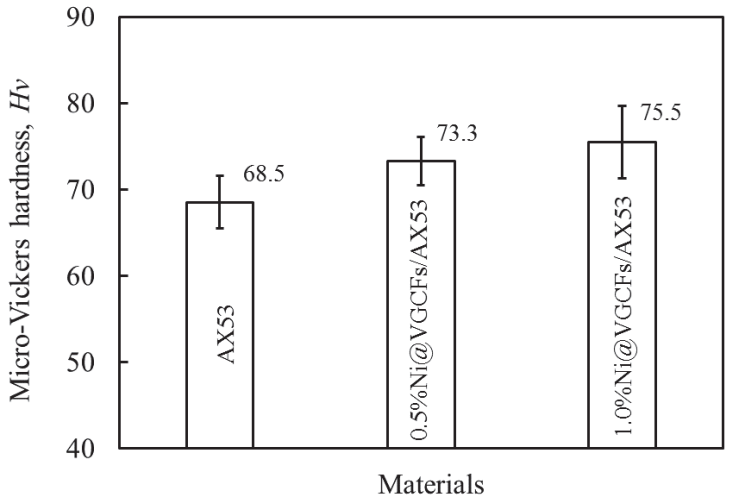

Fig. 5-7 Microhardness of as-cast AX53, and 0.5%Ni@VGCFs, 1.0%Ni@VGCFs composites.

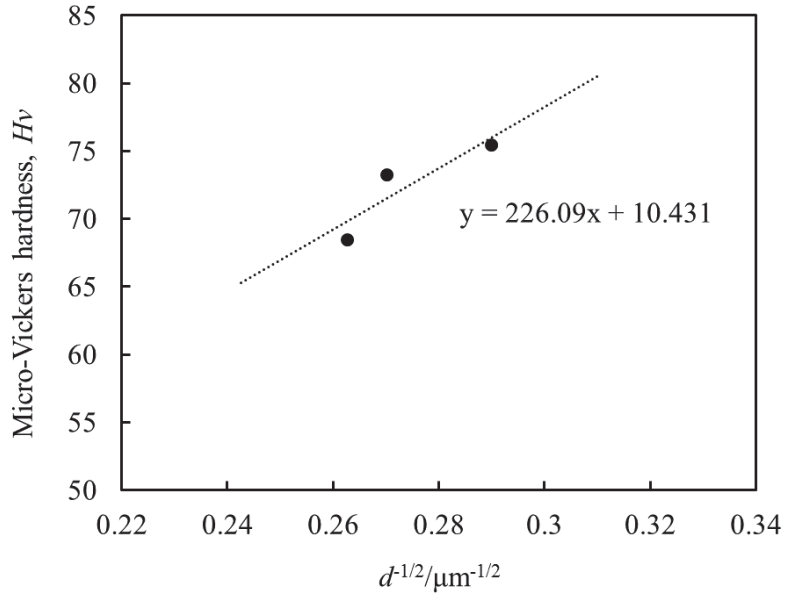

Fig. 5-8 Effect of grain size on hardness of as-cast AX53 alloy and composites.

5.3.2.2 Tensile properties of VGCFs/Mg-Al-Ca composites

The stress–strain curves for the as-cast AX53, 0.5%Ni@VGCFs/AX53, and 1.0%Ni@VGCFs/AX53 are shown in Fig. 5-9. Their tensile properties are summarized in Table 5-3. The addition of 0.5 % VGCFs improved the 0.2 % yield stress, UTS, and elongation of the AX53 matrix by 6%, 14% and 43%, respectively. The increase in the tensile property was attributed to the overall effect derived from the refined grain and introduction of both VGCFs and Al_3Ni intermetallic compounds. The 0.2% yield stress was slightly improved because of the small amount of introduced Ni-coated VGCFs. Moreover, the increase in the UTS of the composite was achieved with increased total elongation, which could mainly be attributed to the strain hardening during a larger strain. However, with the addition of 1.0% VGCFs, the elongation of the composite dropped even lower than that of the AX53 matrix alloy with a similar UTS.

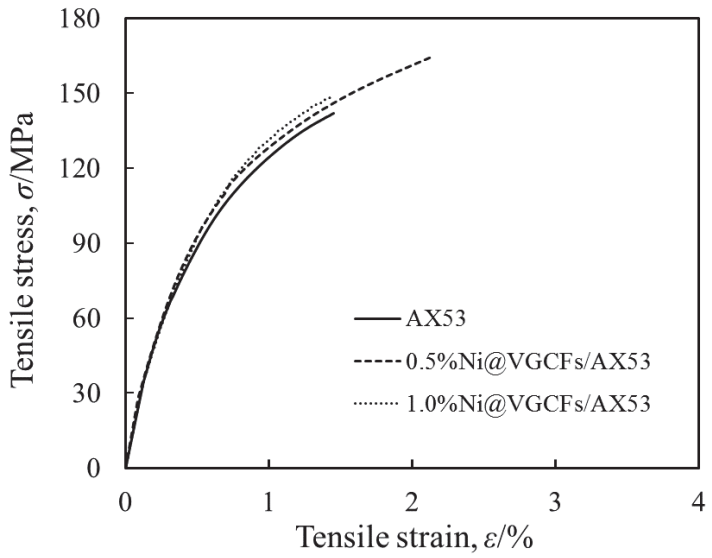

Fig. 5-9 Tensile stress–strain curves of as-cast AX53, 0.5%Ni@VGCFs/AX53, and 1.0%Ni@VGCFs/AX53.

Tab. 5-3 Tensile properties of as-cast AX53, 0.5%Ni@VGCFs/AX53, and 1.0%Ni@VGCFs/AX53.

Material	$\sigma_{0.2}$ (MPa)	σ_b (MPa)	δ (%)
AX53	102	141	1.4
0.5%Ni@VGCFs/AX53	108	162	2.0
1.0%Ni@VGCFs/AX53	112	145	1.3

The fracture surfaces of the composites essentially revealed brittle fracture, as shown in Fig. 5-10a and e. With the addition of Ni-coated VGCFs to the matrix alloy, the grains were refined, and the defects decreased, as shown in Fig. 5-10b. The increased total elongation of the composite could be attributed to the decrease in the defects and presence of VGCFs and Al_3Ni intermetallic compounds on the grain boundaries, which could increase the resistance to crack propagation. Moreover, according to the load transfer reinforcement mechanism,[32] VGCFs well bonded with the magnesium matrix could generate elastic deformation to fit the deformation of the matrix during stretching. Because of the high interface bonding strength, their interface could seldom separate, and there were few pulled-out VGCFs, as shown in Fig. 5-10c. In addition, the improved mechanical properties of the composite could be attributed to grain refinement, which could be explained by the Hall–Petch model.[33] However, as shown in Fig. 5-10d, clusters of Ni-coated VGCFs were clearly observed. These clusters increased the defects of the specimens, which led to the deterioration of the mechanical properties of the composites. For the 1.0% Ni@VGCFs/AX53, when a relatively larger amount of VGCFs was added to the Mg matrix, it contained more VGCF clusters (Fig. 5-10f). These clusters prevented effective bonding between the Mg and VGCFs and led to minute cracks in the matrix. These cracks inevitably led to the failure of the material with low strength.

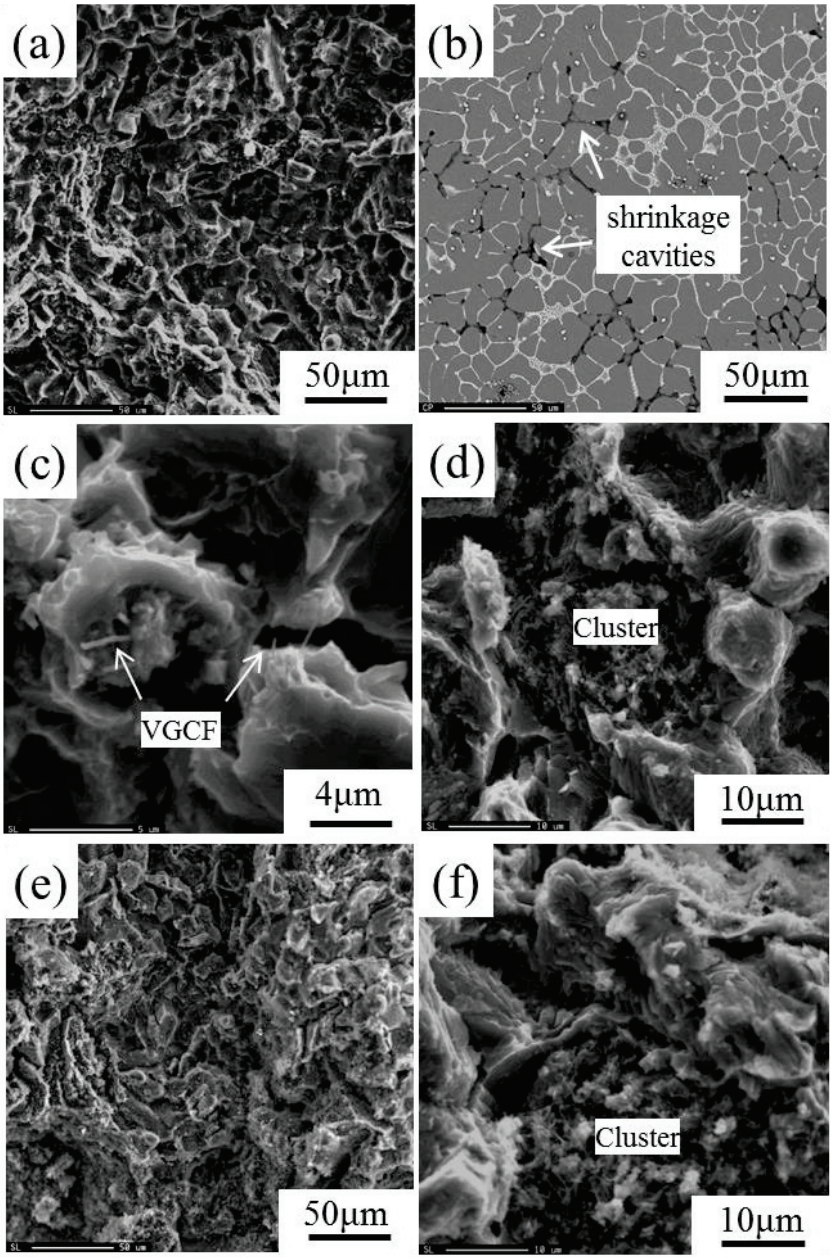

Fig. 5-10 SEM images of (a), (c), (d) fracture surface of 0.5%Ni@VGCFs/AX53, along with (b) shrinkage cavities in 0.5%Ni@VGCFs/AX53 and (e), (f) fracture surface of 1.0%Ni@VGCFs/AX53.

5.3.2.3 Tensile properties of VGCFs/Mg-Al-Ca composites at elevated temperature

The tensile testing results of Mg-Al-Ca composites reinforced with Ni-coated VGCFs at elevated temperature are shown in Table 5-4. Compared with the AX53 alloy, the yield strength, ultimate tensile strength, and elongation of the 0.5% VGCFs composites at 150 °C and 200 °C is slightly increased. The strength and ductility of the composite are improved simultaneously. The addition of VGCFs in AX53 alloys shows some strengthening effect at elevated temperature.

Tab. 5-4 Tensile properties of as-cast AX53 alloy and composites at elevated temperature.

Material	150℃			200℃		
	$\sigma_{0.2}$ (MPa)	σ_b (MPa)	δ (%)	$\sigma_{0.2}$ (MPa)	σ_b (MPa)	δ (%)
AX53	94	142	4.4	91	130	7.3
0.5%Ni@VGCFs/AX53	96	151	5.4	93	139	8.5

5.3.2.4 Strengthening mechanism of VGCFs/Mg-Al-Ca composites

It is important to understand the strengthening mechanism of VGCFs in composites in order to be able to predict the strength. Literature review revealed that few attempts have been made to understand the strengthening mechanism of CNTs in composites.[34] The possible reinforcement mechanisms which might be relevant in CNT/metal composite systems are load transfer, Orowan looping, thermal mismatch and Hall–Petch effect.

Few works have been performed on the strengthening mechanisms of CNTs in magnesium matrix composites. Q.Q Li et al. [35] compared the contributions to the improvement in yield strength of magnesium alloy composites by the three strengthening mechanisms, load transfer, Orowan looping and thermal mismatch. They found out that effective Orowan strengthening and thermal mismatch strengthening take place at low amounts of MWNTs (about 0.1 wt%) and both contribute almost equally to the improvement of the yield strength. Strengthening due to the load transfer of the MWNTs increases linearly and becomes more important than other strengthening effects at higher MWNTs amounts (0.3 wt%). C.D Li et al. [36] reveal that the calculated yield strength by the load transfer mechanism, Orowan mechanism and Hall–Petch relationship are in good agreement with the experimental values.

Here we simply add up in a linear way all the improvements caused by different mechanisms to predict the theoretical yield strength. Based on the previous analysis [35-37], the yield strength of the composites could be expressed as:

$$\sigma_{yc} = \sigma_{ym} + \Delta\sigma_{load} + \Delta\sigma_{Orowan} + \Delta\sigma_{thermal} + \Delta\sigma_{Hall-petch} \quad (2)$$

where σ_{yc} is yield strength of the composite; σ_{ym} is yield strength of the matrix; $\Delta\sigma_{load}$ is the improvement associated with the load transfer effect; $\Delta\sigma_{Orowan}$ is the improvement associated with Orowan strengthening effect; $\Delta\sigma_{thermal}$ is the improvement associated with the increase in dislocation density due to the different thermal expansion coefficients of the matrix and the VGCFs (thermal mismatch); $\Delta\sigma_{Hall-petch}$ is the improvement associated with the decrease of grain size.

For the composites reinforced by short fiber or whisker, the load can be transferred from the matrix to fiber or whisker by a shear stress that develops along the

reinforcement/matrix interface [36, 38]. As a result, the variation in stress generates along the fiber length. The stress on the fiber increases proportionally from the fiber end to reach a maximum value at the mid-region. Thus, the pulling-out and pulling-off of the fiber depends on the fiber length, fiber strength and matrix strength. For the present study, the critical length (l_c) can been defined as [34, 36, 38]:

$$l_c = \sigma_f * d_f/\sigma_{my} \quad (3)$$

where σ_{my} is the yield strength of the matrix, σ_f is the strength of the fiber and d_f is the average diameter of the fibers. The calculated l_c for the VGCFs/Mg-Al-Ca composite is about 4.3 μm. The length (l_f) of VGCF used in this study was 15 μm. This means that the stress on the VGCFs could reach to the fracture strength of the VGCFs.

VGCFs with a larger aspect ratio will assist larger load transfer and hence efficient utilization of reinforcement. For a critical length l_c, the value of σ_f becomes equal to the fracture strength of VGCFs. For fiber lengths $l_f > l_c$, the fracture strength of the composite is given as [34, 39]:

$$\sigma_c = \sigma_f V_f \left(1 - \frac{l_c}{2l_f}\right) + \sigma_{my}(1 - V_f)$$

The relation between the volume fraction (V_f) and weight fraction (W_f) of the VGCFs of a composite is given by:

$$V_f = \frac{W_f/\rho_f}{(W_f/\rho_f) + (1 - W_f)/\rho_m} = \frac{W_f \rho_m}{W_f \rho_m + (1 - W_f)/\rho_f}$$

where ρ_f and ρ_m are the reinforcing phase density and matrix density.

Orowan looping also plays an important role in the strengthening mechanism, which results from restricted movement of the dislocations caused by the incorporation of nanofillers. Assumed that the VGCFs are distributed uniformly, the Orowan strengthening effect is given by [35, 36]:

$$\Delta\sigma_{Orowan} = 0.8bMG_m\sqrt{\frac{2V_f}{\pi d_f^2}}$$

where G_m is the shear modulus of the Mg matrix (1.66×10^4 MPa); b is the value of the Burgers vector of the matrix (3.21×10^{-10} m for Mg); M is the Taylor factor (3.0 for Mg).

There is a significant mismatch in coefficient of thermal expansion between CNT and the matrix, and this might be accommodated by extensive dislocation nucleation

around CNT which then leads to hardening of the metal matrix. The hardening due to the thermal mismatch can be expressed as [35]:

$$\Delta\sigma_{thermal} = \alpha \cdot G_m \cdot b \cdot \sqrt{\rho}$$

where α is a geometric constant (1.25 in this case); ρ is the dislocation density and $\rho = \frac{BV_f \Delta CTE \cdot \Delta T}{b(1-V_f)} \cdot \frac{1}{d_f}$, in which B is a geometric constant (4 in this case); ΔCTE is the difference between the coefficient of thermal expansion; ΔT is the difference between the process and test temperature.

The addition of VGCFs leads to the decrease of grain size, which causes the increase of yield strength according to the Hall–Petch relationship [36, 37]. By comparing with monolithic Mg-Al-Ca alloy, the contribution of grain refinement caused by CNTs can be described by the following equation:

$$\Delta\sigma_{Hall-petch} = K(d_c^{-1/2} - d_m^{-1/2})$$

where d_c and d_m are the average grain sizes of the composite and the monolithic Mg-Al-Ca alloy, respectively. K is the Hall–Petch coefficient of Mg alloy, which is given as 0.13 MPa $m^{1/2}$. The value of K is dependent on the number of slip systems. It is higher for HCP metals than for FCC and BCC metals. Since Mg is HCP, the grain size affects the yield strength significantly.

Figure 5-11 shows the theoretic value of yield strength increment according to the strengthening mechanism of load transfer effect from matrix to VGCFs, Orowan looping, thermal mismatch, and grain refinement, respectively. It can be seen that $\Delta\sigma_{load}$ has the maximum contribution in the strengthening of the composites. $\Delta\sigma_{Hall-petch}$ exhibits a minor contribution compared with the other three, since the grain refinement effect for as-cast composites is not so obvious.

Figure 5-12 shows the comparison of theoretical values of the yield strength increment contributed by strengthening mechanisms of load transfer, Orowan looping and thermal mismatch as a function of VGCF weight fraction. It can be seen that $\Delta\sigma_{load}$, $\Delta\sigma_{Orowan}$, and $\Delta\sigma_{thermal}$ mainly depend on the weight fraction of VGCFs, and their values increase with increasing weight fraction. It shows that at low amounts of VGCFs, thermal mismatch strengthening is the most effective mechanism to the improvement of the yield strength. Strengthening due to the load transfer of the VGCFs increases linearly and becomes more important than other strengthening effects at

higher VGCFs amounts (about 0.5 wt%) according to the present model.

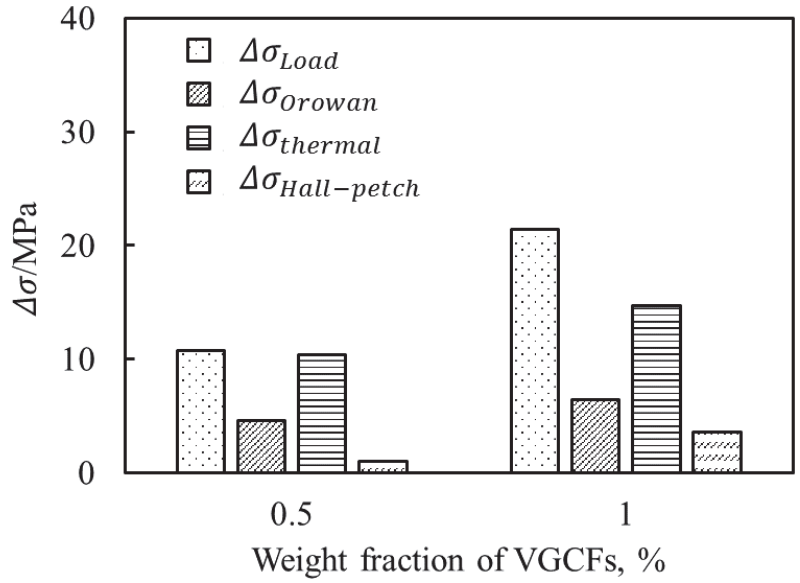

Fig. 5-11 Theoretic value of yield strength increment according to the strengthening mechanism of load transfer effect from matrix to VGCFs, Orowan looping, thermal mismatch, and grain refinement, respectively.

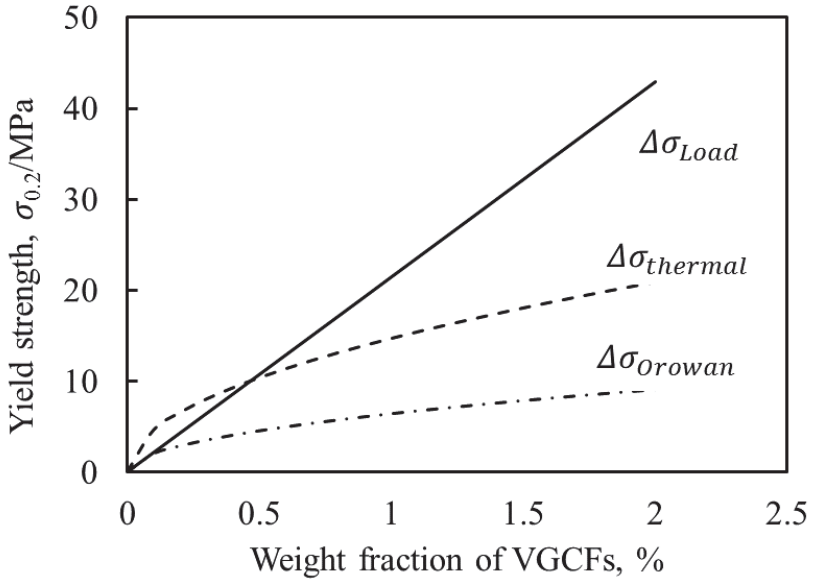

Fig. 5-12 Comparison of theoretical values of the yield strength increment contributed by strengthening mechanisms of load transfer, Orowan looping and thermal mismatch as a function of VGCF weight fraction.

The calculated yield strength of the composites is compared with experimental results in Fig. 5-13. It can be clearly seen that the experimental data is below the theoretical value. The discrepancies of yield strength increased with an increase of the amount of VGCFs. The discrepancy of the detrimental variation trend may be attributed to the aggravation of VGCFs cluster in the matrix with increasing the amount of VGCFs. This suggests that the dispersion of VGCFs can still be improved to produce a stronger composite. The uniform distribution of VGCFs play a significant role for Orowan mechanism. Besides the dispersion of VGCFs, if interfacial shear stresses efficiently transfer load from the elastically softer metal matrix to the stronger VGCF to strengthening, a good interfacial bonding between the VGCFs and the metal matrix is required.

Due to the limitations of all reinforcement mechanisms, such as the evidence for these reinforcement mechanisms and the applicability of the mechanism for VGCF, further understanding is clearly necessary. The behavior of VGCFs in the metal matrix needs to be studied and characterization of such composites by different methods is required.

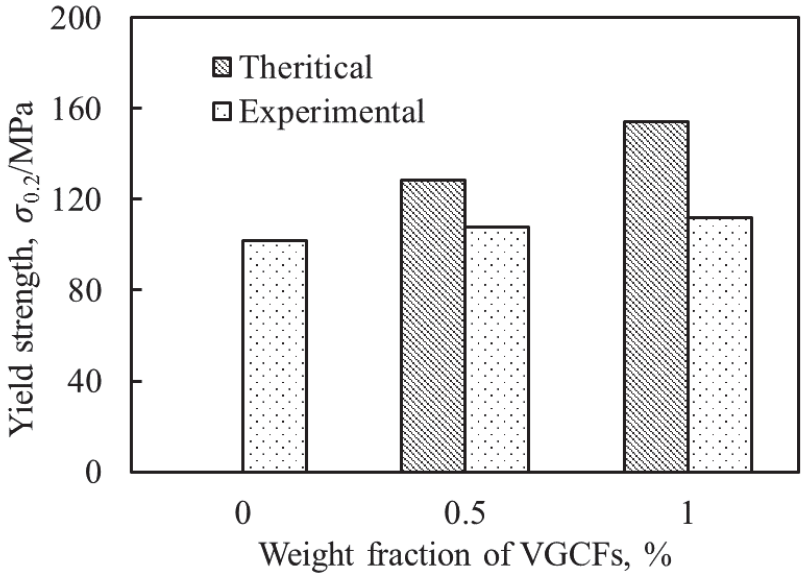

Fig. 5-13 Comparison between theoretical and experimental yield strength.

5.3.2.5 Ductility of VGCFs/Mg-Al-Ca composites

From the tensile test results, one notable observation is that the elongation at failure, i.e. the ductility, increased (as much as 40%) together with the strength. The increased total elongation of the composite could be attributed to the decrease in the defects and presence of VGCFs and Al_3Ni intermetallic compounds on the grain boundaries, which could increase the resistance to crack propagation.

Increased ductility has also been found in CNT reinforced Mg composites before by Goh.[9] Their explanation for this is the activation of prismatic slip planes in the Mg matrix by adding CNTs. It implicates a minimum of five independent slip systems which are required to deform a polycrystalline metal plastically (von Mises criterion), therefore resulting in a much higher ductility of the composites. A high activity of the basal slip system and the initiation of prismatic slip at room temperature were observed under TEM.

5.4 Summary

(1) The addition of calcium in Mg-Al alloy forms $(Mg, Al)_2Ca$ phase and suppresses the formation of the $Mg_{17}Al_{12}$ phase. With Ca content increasing, the Mg-Al-Ca alloy exhibits a higher yield strength and strain-hardening than the Mg-5Al alloy. However, the reticular distribution along grain boundaries of the $(Mg, Al)_2Ca$ phase results in the impairment of elongation at room temperature, which also affect the ultimate tensile strength.

(2) The obvious elevated temperature strengthening effect was obtained by calcium addition, since $(Mg, Al)_2Ca$ has much high melting point and thermal stability. The reduction of tensile strength of Mg-Al-Ca alloys with temperature increasing declines. However, with Ca content increasing, reticular $(Mg, Al)_2Ca$ formed along grain boundaries results in the decrease of elongation or a little change of tensile strength at elevated temperature.

(3) With a 0.5 wt% addition of Ni-coated VGCFs, an increase in the UTS of the composite was achieved, along with an increase in the total elongation, which could mainly be attributed to the strain hardening during a larger strain. However, for the 1.0% VGCF-reinforced AX53 alloy composites, the elongation dropped, which led to a low strength similar to that of the AX53 matrix alloy. The addition of VGCFs in AX53 alloys shows some strengthening effect at elevated temperature. The strength and ductility of the composite are improved simultaneously.

(3) The contributions of load transfer, Orowan strengthening, thermal mismatch and Hall-Petch effect were simply added up to predict the potential yield strengths by adding different weight fractions of VGCFs to the composites. In this model, load transfer and thermal mismatch strengthening are the main mechanism to the improvement of the yield strength. The experimental result of yield strength was compared to the theoretical value. It showed that the dispersion still needs to be improved to produce a stronger material.

References

1) M. K. Kulekci: The International Journal of Advanced Manufacturing Technology, **39** (2008) 851-865.
2) A. K. Dahle, Y. C. Lee, M. D. Nave, P. L. Schaffer, and D. H. StJohn: Journal of Light Metals, **1** (2001) 61-72.
3) A. A.Luo: Mater. Sci. Forum **419** (2003) 57-66.
4) M. K. Kulekci: The International Journal of Advanced Manufacturing Technology **39** (2008) 851-865.
5) R. Ninomiya, T. Ojiro, and K. Kubota: Acta Metall. Mater. **43** (1995) 669-674
6) A. A. Luo, M. P. Balogh, and B. R. Powell: Metall. Mater. Trans. A **33** (2002) 567-574.
7) L. Han, H. Hu, and D.O. Northwood: Mater. Lett. **62** (2008) 381-384.
8) S.W. Xu, N. Matsxumoto, and K. Yamamoto: Mater. Sci. Eng. A **509** (2009) 105-110.
9) C. S. Goh, J. Wei, L. C. Lee, and M. Gupta: Mater. Sci. Eng., A **423** (2006) 153-156.
10) C. S. Goh, J. Wei, L. C. Lee, and M. Gupta: Nanotechnology **17** (2006) 7-12.
11) E. Carreno-Morelli, J. Yang, E. Couteau, K. Hernadi, J. W. Seo, C. Bonjour, L. Forro, and R. Schaller: Phys. Status Solidi A **201** (2004) R53-R55.
12) Y. Shimizu, S. Miki, T. Soga, I. Itoh, H. Todoroki, T. Hosono, K. Sakaki, T. Hayashi, Y. A. Kim, M. Endo, S. Morimoto, and A. Koide: Scripta Mater. **58** (2008) 267-270.
13) F. J. Sun, C. S. Shi, K. Y. Rhee, and N. Q. Zhao: J. Alloys Compd. **551** (2013) 496-501.
14) Show Denko Co., Ltd., Material Safety Data Sheet, (2007) p. 1.
15) M. Endo, Y. A. Kim, T. Hayashi, K. Nishimura, K. Miyashita, and M. S. Dresselhaus: Carbon **39** (2001) 1287–1297.
16) L. Wang, H. Choi, J. M. Myoung, and W. Lee: Carbon, **47** (2009) 3427–3433.
17) A. M. K. Esawi, K. Morsi, A. Sayed, M. Taher, and S. Lanka: Composites Part A **42** (2011) 234–243.

18) G. Sasaki, F. Kondo, K. Matsugi, and O. Yanagisawa: Trans Tech Publications. **561** (2007) 729–732.

19) Z. F. Xu, Y. B. Choi, K. Matsugi, D. C. Li, and G. Sasaki: Mater. Trans. **50** (2009) 2160–2164.

20) J. M. Ting and M. L. Lake: J. Mater. Res. **10** (1995) 247–250.

21) T. Imanishi, K. Sasaki, K. Katagiri, and A. Kakitsuji: Trans. Jpn. Soc. Mech. Eng. A, **75** (2009), 27–33.

22) Q. D. Wang, W. Z. Chen, X. Q. Zeng, Y. Z. Lu, W. J. Ding, Y. P. Zhu, X. P. Xu, and M. Mabuchi: J. Mater. Sci. **36** (2001) 3035-3040.

23) Y. Z. Lü, Q. D. Wang, X. Q. Zeng, W. J. Ding, C. Q. Zhai, and Y. P. Zhu: Mater. Sci. Eng., A **278** (2000) 66-76.

24) Luo, A.A., Recent magnesium alloy development for elevated temperature applications. International Materials Reviews, 2004.

25) M. Masoumi and H. Hu: Mater. Sci. Eng., A **528** (2011) 3589–3593.

26) S. W. Xu, N. Matsumoto, K. Yamamoto, S. Kamado, T. Honma, and Y. Kojima: Mater. Sci. Eng., A **509** (2009) 105–110.

27) L. Zhang, K. K. Deng, K. B. Nie, F. J. Xu, K. Su, and W. Liang: Mater. Sci. Eng., A **636** (2015) 279–288.

28) H. Watanabe, M. Yamaguchi, Y. Takigawa, and K. Higashi: Mater. Sci. Eng., A **454** (2007) 384–388.

29) J. Bai, Y. S. Sun, F. Xue, S. Xue, J. Qiang, and W. J. Tao: Scr. Mater. **55** (2006) 1163-1166.

30) Y. S. Sato, M. Urata, H. Kokawa, K. Ikeda: Mater. Sci. Eng., A **354** (2003) 298-305.

31) H. Chen and A.T. Alpas: Wear **192** (1996) 186–198.

32) J. L. Tsai and T. C. Lu: Compos. Struct. **90** (2009) 172–179.

33) W. S. Miller and F. J. Humphreys: Scr. Metal. Mater. **25** (1991): 33–38.

34) S. C. Tjong: Mater. Sci. Eng., R **74** (2013) 281-350.

35) Q. Q. Li, A. Viereckl, C. A. Rottmair, and R. F. Singer: Compos. Sci. Technol. **69** (2009) 1193-1199.

36) C. D. Li, X. J. Wang, W. Q. Liu, K. Wu, H. L. Shi, C. Ding, X. S. Hu, and M. Y.

Zheng: Mater. Sci. Eng., A **597** (2014) 264-269.

37) Q. H. Yuan, X. S. Zeng, Y. Liu, L. Luo, J. B. Wu, Y. C. Wang, and G. H. Zhou: Carbon, **96** (2016) 843-855.

38) Z. Y. Liu, B. L. Xiao, W. G. Wang, and Z. Y. Ma: Carbon, **50** (2012) 1843-1852.

39) A. Kelly, and W. R. Tyson: J. Mech. Phys. Solids, **13** (1965) 329-350.

Chapter 6

Conclusions

The final purpose of the present research is to develop the VGCFs reinforced Mg-Al-Ca alloy composites with satisfactory mechanical properties by the cost-effective fabrication process, in order to face the elevated temperature application. In this study, the effect of nickel coating on wetting behavior of magnesium alloys and graphite sheet was investigated. Ni-coated VGCFs reinforced Mg-Al-Ca alloy composites were fabricated by compo-casting process. The effects of Ni-coated VGCFs on the microstructure and mechanical properties of magnesium alloy were investigated, and the strengthening mechanism of Ni-coated VGCFs reinforced Mg-Al-Ca alloy composites was discussed. The conclusions of this thesis are summarized as follows:

1. The study on the effect of nickel formation on graphite sheet surface for improving wettability with magnesium alloy (Chapter 2).

Prior to the fabrication of VGCF/Mg-Al-Ca composites, the wettability of magnesium alloys with graphite sheet, which has the basal plane of (002) same with that of VGCFs, was studied, and the effect of nickel coating on wetting behavior of magnesium alloys and graphite sheet was investigated. Mg-Al alloys did not wet graphite sheet with the contact angle of about 120°. The droplet of magnesium alloy on Pure Ni spread rapidly. By means of the wetting of Mg-Al-Ca alloys on pure nickel, the mechanism for the wetting behavior between liquid magnesium alloys and solid nickel was proposed. Nickel dissolved into magnesium alloy during contacting. Spreading of the droplet stopped when nickel saturation occurred and Mg_2Ni intermetallic compound began to form. Improvement of wettability of magnesium alloy on Gr-Ni was achieved through the dissolution of nickel into the liquid magnesium alloy at the interface between droplet and substrate. Calcium addition had no effect on the wetting of magnesium alloy on Gr, while it showed negative effect on the Pure Ni, and slightly hindered the spread of magnesium alloy droplet on Gr-Ni.

2. The study on the fabrication of VGCF-reinforced magnesium matrix composites by low pressure infiltration (Chapter 3).

The effect of nickel coating on infiltration behavior of magnesium alloy into VGCF preform was investigated. Fabrication of VGCF-reinforced magnesium alloy composites was carried out by low pressure infiltration. Infiltration pressure for magnesium alloy into porous VGCF preform was determined to be 1 MPa, considering with both the estimated threshold pressure and the compression strength of the preform. Magnesium alloy was successfully infiltrated into nickel coated porous preform, while the magnesium alloy was partially infiltrated into the preform without nickel coating.

3. The study on the fabrication of VGCF-reinforced Mg-Al-Ca alloy composites by compo-casting process (Chapter 4).

Microstructure of Mg-5Al alloy consisted of ß-$Mg_{17}Al_{12}$ intermetallic phase in the α-Mg matrix. With the additions of calcium, the Mg-Al-Ca alloy exhibited a dendritic microstructure with calcium-containing phases along the grain boundaries which suppressed the formation of the $Mg_{17}Al_{12}$ phases. With increasing Ca/Al ratio, the volume fraction of the second phase in the as-cast Mg-Al-Ca alloys increases, and the main second phase is $(Mg, Al)_2Ca$ with a coarse lamellar structure.

Nickel-coated VGCFs were prepared using an electroless plating process, with the nickel homogeneously deposited on the VGCFs. Ni-coated VGCF-reinforced Mg-Al-Ca composites were fabricated using the compo-casting method. The preliminary mix of the Ni-coated VGCFs into the semi-solid metal was facilitated by compo-casting process. With the nickel coating diffused into the metal, the dispersion of VGCFs was promoted. Al_3Ni compounds formed both inside the grains and on the grain boundaries. The present of Al_3Ni compounds and VGCFs disturbed the reticular distribution of $(Mg, Al)_2Ca$ along grain boundaries. The addition of Ni-coated VGCFs could refine the grain of the Mg-Al-Ca alloy.

4. The study on the mechanical properties of VGCF-reinforced Mg-Al-Ca alloy composites (Chapter 5).

With Ca content increasing, the Mg-Al-Ca alloy exhibits a higher yield strength and strain-hardening than the Mg-5Al alloy. However, the reticular distribution along grain boundaries of the $(Mg, Al)_2Ca$ phase results in the impairment of elongation at room

temperature, which also affect the ultimate tensile strength. The obvious elevated temperature strengthening effect was obtained by calcium addition, since $(Mg, Al)_2Ca$ has much high melting point and thermal stability. The reduction of tensile strength of Mg-Al-Ca alloys with temperature increasing declines. However, with Ca content increasing, reticular $(Mg, Al)_2Ca$ formed along grain boundaries results in the decrease of elongation or a little change of tensile strength at elevated temperature.

With a 0.5 wt% addition of Ni-coated VGCFs, an increase in the UTS of the composite was achieved, along with an increase in the total elongation, which could mainly be attributed to the strain hardening during a larger strain. However, for the 1.0% VGCF-reinforced AX53 alloy composites, the elongation dropped, which led to a low strength similar to that of the AX53 matrix alloy. The addition of VGCFs in AX53 alloys shows some strengthening effect at elevated temperature. The strength and ductility of the composite are improved simultaneously.

The contributions of load transfer, Orowan strengthening, thermal mismatch and Hall-Petch effect were simply added up to predict the potential yield strengths by adding different weight fractions of VGCFs to the composites. In this model, load transfer and thermal mismatch strengthening are the main mechanism to the improvement of the yield strength. The experimental result of yield strength was compared to the theoretical value. It showed that the dispersion still needs to be improved to produce a stronger material.

Acknowledgements

I would like to express my sincere gratitude to Professor Gen Sasaki for his great guidance and insight throughout this study. He gave me full support not only on my research, but also on my life and career, which has played an important role in both of my professional and personal development. I am also greatly indebted to Associate Professor Kenjiro Sugio, Assistant Professor Yongbum Choi and Assistant Professor Zhefeng Xu. They gave me so much positive help on the research, the accumulation of the knowledge and my life, and I have learnt so much from them. In addition, I would like to express my heartfelt thanks to Professor Kenji Shinozaki, Professor Atsushi Sugeta and Professor Kazuhiro Matsugi for their suggestions.

Then, I would like to thank Dr. Shaoming Kang, Mr. Hiroyuki Yamashita, Mr. Keigo Terada, and Mr. Kentaro Tashiro for considerable assistance and help in my experiments and my life. Moreover, I would also like to thank all the past and present members of Materials Science Laboratory, in Department of Mechanical System Engineering, Hiroshima University, for their enthusiastic help to both of my life and study.

Last, my thanks would go to my beloved family for their loving considerations and great confidence in me all through these years. I also owe my sincere gratitude to my friends who gave me their help and time in helping me work out my problems during the difficult course of the thesis.

Published Papers in Regards to This Thesis

1. **Y. Q. Yao**, Z. F. Xu, K. Sugio, Y. B. Choi, K. Matsugi, S. M. Kang, R. D. Fu, G. Sasaki*. Fabrication of Vapor-Grown Carbon Fiber-Reinforced Magnesium-Calcium Alloy Composites by Compo-Casting Process. Materials transactions. 2017(58)4: 673-678. (Chapter 2)

2. **Y. Q. Yao**, Z. F. Xu, K. Sugio, Y. B. Choi, S. M. Kang, R. D. Fu, G. Sasaki*. Nickel formation on graphite sheet surface for improving wettability with magnesium alloy. Materials transactions, 2015(56)10:1693-1697. (Chapter 4 & 5)

3. **Y. Q. Yao**, Y. B. Choi, Z. F. Xu, F. Gao, S. M. Kang, R. D. Fu, K. Sugio, G. Sasaki*. Preparation of VGCF reinforced magnesium matrix composites by low pressure infiltration. The Ninth Pacific Rim International Conference on Advanced Materials and Processing (PRICM9), Ed. by T. Furuhara, M. Nishida and S. Miura, The Japan Institute of Metals and Materials, 2016: 901-904. (Chapter 3)

4. **Y. Q. Yao**, Z. F. Xu, K. Sugio, Y. B. Choi, S. M. Kang, R. D. Fu, G. Sasaki*. Effect of Nickel Coating on Graphite for Preparation of Graphite/Magnesium Composite. The 10th Korea-Japan Joint Symposium on Composite Materials, Chonbuk National University, October 29, 2015: 105-106. (Chapter 2)

Presentations

1. **Y. Q. Yao**, Z. F. Xu, Y. B. Choi, K. Sugio, R. D. Fu, and G. Sasaki. Fabrication process of carbon nanofibers reinforced magnesium-calcium alloy composites. 日本金属学会 日本鉄鋼協会 中国四国支部 第36回若手フォーラム2017年2月, 岡山, 日本.

2. **Y. Q. Yao**, Z. F. Xu, Y. B. Choi, K. Sugio, R. D. Fu, and G. Sasaki. Fabrication of Carbon Nanofiber Reinforced Magnesium Matrix Composites by Compo-casting Process 2016年9月 日本金属学会 日本鉄鋼協会 秋期講演大会 大阪, 日本.

3. **Y. Q. Yao**, Y. B. Choi, Z. F. Xu, F. Gao, S. M. Kang, R. D. Fu, K. Sugio, and G. Sasaki. Preparation of VGCF reinforced magnesium matrix composites by low pressure infiltration. The Ninth Pacific Rim International Conference on Advanced Materials and Processing (PRICM9), August 1-5, 2016, Kyoto, Japan.

4. Fabrication Process of Carbon Nanofiber Reinforced Magnesium Matrix Composites 2016年3月 日本金属学会 日本鉄鋼協会 春期講演大会, 東京, 日本.

5. **Y. Q. Yao**, Z. F. Xu, R. D. Fu, K. Sugio, and G. Sasaki. Effect of nickel coating on the wettability of magnesium alloy on graphite sheet. 日本機械学会 第23回機械材料材料加工技術講演会, 2015年11月, 広島, 日本.

6. **Y. Q. Yao**, Z. F. Xu, K. Sugio, Y. B. Choi, S. M. Kang, R. D. Fu, G. Sasaki. Effect of Nickel Coating on Graphite for Preparation of Graphite/Magnesium Composite. The 10th Korea-Japan Joint Symposium on Composite Materials, October 29, 2015, Chonbuk, Korea.

7. **Y. Q. Yao**, Z. F. Xu, Y. B. Choi, R. D. Fu, K. Sugio, and G. Sasaki. Nickel formation on graphite sheet surface for improving wettability with magnesium alloy 日本鉄鋼協会 日本金属学会 秋期講演大会, 2015年9月, 九州, 日本.

8. **Y. Q. Yao**, Z. F. Xu, Y. B. Choi, R. D. Fu, K. Sugio, and G. Sasaki. Wettability of nickel coated graphite sheet by magnesium alloy. 金属第55回鉄鋼第58回中国四国支部講演大会, 2015年8月, 広島, 日本.

9. **Y. Q. Yao**, Z. F. Xu, R. D. Fu, K. Sugio, and G. Sasaki. Nickel formation on graphite sheet surface for improving wettability with magnesium alloy. 軽金属学会 中

国四国支部 講演大会, 2015年7月, 岡山, 日本.

10. **Y. Q. Yao**, G. Sasaki, K. Sugio, Z. F. Xu, and R. D. Fu. Fabrication of carbon nanofiber reinforced magnesium matrix composites. 日本鉄鋼協会 日本金属学会 春期講演大会, 2015年3月, 東京, 日本..

11. **Y. Q. Yao**, G. Sasaki, K. Sugio, and R. D. Fu. Corrosion phenomenon and mechanism of friction stir welded joints of 2060 aluminum alloy. 金属第54回 鉄鋼第57回 中国四国支部講演大会, 2014年8月, 徳島, 日本.